NIST-GCR-95-677

PREDICTING THE IGNITION TIME AND BURNING RATE OF THERMOPLASTICS IN THE CONE CALORIMETER

Donald Hopkins, Jr.

NIST

United States Department of Commerce
Technology Administration
National Institute of Standards and Technology

NIST-GCR-95-677

PREDICTING THE IGNITION TIME AND BURNING RATE OF THERMOPLASTICS IN THE CONE CALORIMETER

Donald Hopkins, Jr.

Department of Fire Protection Engineering
University of Maryland
College Park, MD 20742

September 1995

U.S. Department of Commerce
Ronald H. Brown, *Secretary*
Technology Administration
Mary L. Good, *Under Secretary for Technology*
National Institute of Standards and Technology
Arati Prabhakar, *Director*

Notice

This report was prepared for the Building and Fire Research Laboratory of the National Institute of Standards and Technology under grant number 60NANB2D1266. The statement and conclusions contained in this report are those of the authors and do not necessarily reflect the views of the National Institute of Standards and Technology or the Building and Fire Research Laboratory.

Predicting the Ignition Time and Burning Rate of Thermoplastics in the Cone Calorimeter

by

Donald Hopkins, Jr

Thesis submitted to the Faculty of the Graduate School
of The University of Maryland in partial fulfillment
of the requirements for the degree of
Master of Science
1995

Advisory Committee:

Dr. James G. Quintiere, Chairman/Advisor
Dr. James A. Milke
Dr. John A. Rockett

ABSTRACT

Title of Thesis:	Predicting the Ignition Time and Burning Rate of Thermoplastics in the Cone Calorimeter.
Name of degree candidate:	Donald Hopkins, Jr.
Degree and Year:	Master of Science in Fire Protection Engineering, 1995
Thesis directed by:	Dr. James G. Quintiere, Professor, Department of Fire Protection Engineering

Ignition and burning rate data are developed for Nylon 6/6, Polyethylene, and Polypropylene in a Cone Calorimeter heating assembly. The objective is to examine a testing protocol that leads to the prediction of ignition and burning rate for thermoplastics from Cone data. The flame heat flux is not measured, but is inferred from Cone data. The constancy of the flame heat flux for thermoplastics in the Cone calorimeter is due to the geometry of the flame. The burning rate model is shown to yield good accuracy in comparison to measured transient values.

Ignition and burning rate data are developed for Redwood and Red Oak in a Cone Calorimeter heating assembly. Measurements of the flame plus external heat flux are presented. The data is intended to be used for future work to develop a testing protocol and burning rate model for charring materials.

Predicting the Ignition Time and Burning Rate of Thermoplastics in the Cone Calorimeter

by

Donald Hopkins, Jr

Thesis submitted to the Faculty of the Graduate School
of The University of Maryland in partial fulfillment
of the requirements for the degree of
Master of Science
1995

Advisory Committee:

Dr. James G. Quintiere, Chairman/Advisor
Dr. James A. Milke
Dr. John A. Rockett

ACKNOWLEDGEMENTS

I would like to express my deepest thanks and appreciation to Dr. James Quintiere, whose guidance and support made this research possible and enabled me to continue my education.

I would also like to thank the National Institute for Standards and Technology for their financial support of this project.

In addition, I would like to thank Dr. Thomas Ohlemiller for his suggestions and advice, Darren Lowe and Randy Shields for their assistance in gathering necessary equipment, and Marc Janssens for donating the wood samples.

Also, I wish to thank my advisory committee and the faculty and staff of the Department of Fire Protection Engineering for the unending support given throughout this project.

TABLE OF CONTENTS

LIST OF TABLES

LIST OF FIGURES

CHAPTER 1 INTRODUCTION

Predicting the way a fire will behave under realistic conditions can be a challenging task. In order to examine the effects of fire on it's surroundings and the hazard posed to occupants, information about the heat release rate, total energy, and flame spread characteristics of the fire need to be known. Subsequently, it is desirable to have a means of determining fire growth and spread in terms of measurable material properties. A general model for predicting the burning rate of materials is needed to accomplish this.

Quintiere [1] developed a one-dimensional model which includes charring, vaporization, extinction, flame and heat conduction effects. However, unsteady solutions for the burning rate were not determined. Quintiere and Iqbal [2] developed a model that solves the one-dimensional unsteady heat transfer equations during the pre-heating and gasification periods using an integral method. They assume a polynomial profile for the temperature within the solid to satisfy the heat transfer boundary conditions. However, the effects of flaming are not included in the solution.

The objective of this research is to develop transient burning rate models which utilize data obtained from the Cone Calorimeter [3]. The models will be dependent on the class of material; namely, thermoplastic, charring, dripping, and laminated. It is intended to first succeed for thermoplastic-like materials; materials approximated by constant surface temperature vaporization, which are large enough to be considered one dimensional in behavior.

The ultimate goal of the research is to incorporate the burning rate models into fire growth simulations [e.g. 4, 5, 6, 7] to provide more accurate predictions and assessment of hazard. It is first necessary to succeed at developing a technique which utilizes Cone Calorimeter data to predict the transient burning rate, at least for thick

thermoplastics and charring materials. The technique presented herein has been examined by Quintiere and Rhodes [8] for Black Polycast Polymethylmethacrylate (PMMA). The model is based on the formulation outlined by Quintiere [1] and implemented by Quintiere and Iqbal [2] for non-flaming pyrolysis of a thermoplastic. Further validation of the technique using Nylon 6/6, Polyethylene, and Polypropylene is attempted in the present study. The primary objective is to see if the method used by Quintiere and Rhodes [8] for PMMA is general for thermoplastic-like materials burning in the Cone Calorimeter. Furthermore, data is presented for charring materials; namely, Redwood and Red Oak to present insight into the extension of the current model to deal with charring materials.

CHAPTER 2 OVERVIEW OF THESIS

2.1 Introduction

The Cone Calorimeter is a commonly used device utilized to measure the mass loss rate per unit area ($\dot{m}''$) and the heat release rate per unit area ($\dot{Q}''$) for a given constant external radiative heat flux. The ratio of the mass loss rate and the heat release rate gives the instantaneous heat of combustion (ΔH_c) relative to the gaseous fuel produced during flaming combustion. It has been shown that the heat of combustion is generally constant for a material undergoing flaming combustion. The heat of combustion is measurable and is not expected to be scale dependent, i.e. change as a larger area of fuel is burned. Similarly the thermal and chemical properties of a decomposing material are also independent of scale, with the exception of multi-dimensional effects involving seams, joints, etc.. Conversely, the heat flux per unit area ($\dot{q}''$) to a materials surface is dependent on scale and on test conditions in the Cone Calorimeter. Subsequently, it can be shown that under one dimensional burning conditions,

$$\dot{m}'' = f(\dot{q}'', \text{thermo}-\text{chemical properties}) \tag{2.1}$$

and,

$$\dot{Q}'' = \dot{m}''\Delta H_c. \tag{2.2}$$

Equation (2.1) symbolically represents a model involving the surface heat flux and the needed properties. A specific model for a vaporizing non-charring thermoplastic model is examined. Experimentally, three materials are examined, namely; Nylon 6/6, Polyethylene, and Polypropylene. In addition, Redwood and Red Oak are examined experimentally to lay the foundation for a model to examine the behavior of charring materials.

2.2 Burning Rate Experiments

The burning rate experiments were conducted to measure the mass loss rate, ignition time, and surface temperature for both the thermoplastic and wood materials tested. A cone heater assembly with a continuous mass loss measurement was used for all of the experiments. Experiments were conducted until steady burning was reached. In addition, measurements of the flame plus external heat flux to the surface was measured for the wood samples using a 3 mm diameter heat flux gage. This was not done for the thermoplastic materials. However, previously Rhodes [9] measured the surface heat flux for PMMA in the Cone Calorimeter and concluded that the flame heat flux (convection plus radiation) is constant for a thermoplastic-like material burning in the Cone Calorimeter. The flame heat flux can be deduced from the steady burning rate data for the thermoplastics in which Equation (2.1) becomes,

$$\dot{m}'' = \frac{\dot{q}''}{L} \tag{2.3}$$

where, $\dot{q}''$ is the net surface heat flux,

and, L is the effective heat of gasification.

At steady burning, the incident flame heat flux is deduced from the net surface heat flux in equation (2.3). The gage measurement for the thermoplastic materials would have only provided a second means of determining the flame plus external heat flux to the material surface. The current results verify that the flame heat flux for a thermoplastic-like material burning in the Cone Calorimeter is approximately constant. However, due to charring and the associated change in flame height for wood burning in the Cone Calorimeter, the constancy of the flame heat flux does not appear to be one of the attributes of the burning behavior.

2.3 Application of Models

The data obtained from the experiments was examined in conjunction with ignition and burning rate models designed to yield the needed thermo-chemical properties, i.e. the thermal conductivity, density, specific heat, and heat of gasification. The properties are model dependent, but are not void of physical significance.

The experimental and modeling details will be reviewed and their results presented. A recommended testing protocol for thermoplastics is presented in Chapter 5. The method used to elucidate the needed properties for the wood materials is applied, but currently a model has not been used to attempt to predict the ignition time and burning rate for wood. The results of the wood experiments are presented for aid in the future development of a model for charring materials, which will be based on a solid phase model developed by Quintiere [1].

CHAPTER 3 THERMOPLASTIC EXPERIMENTAL SET-UP, PROCEDURE, AND MEASUREMENTS

3.1 Experimental System

Ignition and burning rate experiments for the thermoplastic materials were performed using a radiant cone heater assembly. The apparatus, shown in Figure 3.1 [9], consisted of a cone heater, a load cell, a methane pilot ignitor, and a data acquisition system. A scanner and a voltmeter were used to monitor thermocouple, heat flux transducer, and load cell measurements. A Hewlet Packard (HP) computer was utilized as the data acquisition system. As data was measured it was transferred to a second computer where it was recorded. The voltage measurements corresponding to temperature, mass, and heat flux were converted to the appropriate metric units prior to their recording. The HP Basic program used for the experimentation is included in Appendix A, although a description of the program is not included in this report.

3.2 Thermoplastic Samples

Three thermoplastic-like materials were selected for evaluation in this study; namely, Nylon 6/6, Polyethylene, and Polypropylene. These materials were selected based on availability from commercial retailers. The samples were nominally 10 cm (4 in.) x 10 cm (4 in.) x 2.5 cm (1 in.) thick. Previously, experiments were carried out by Rhodes [9] using Black Cast Polymethylmethacrylate (PMMA). The current testing and analysis is an attempt to generalize the previous results found for PMMA.

Samples were placed on a standard cone metal holder in the horizontal orientation on a bed of Kaowool. The Kaowool was used to insulate the back side of the specimen to minimize heat loss effects. In order to maintain only one dimensional burning, cardboard was bonded to the sides of the samples to inhibit edge burning effects.

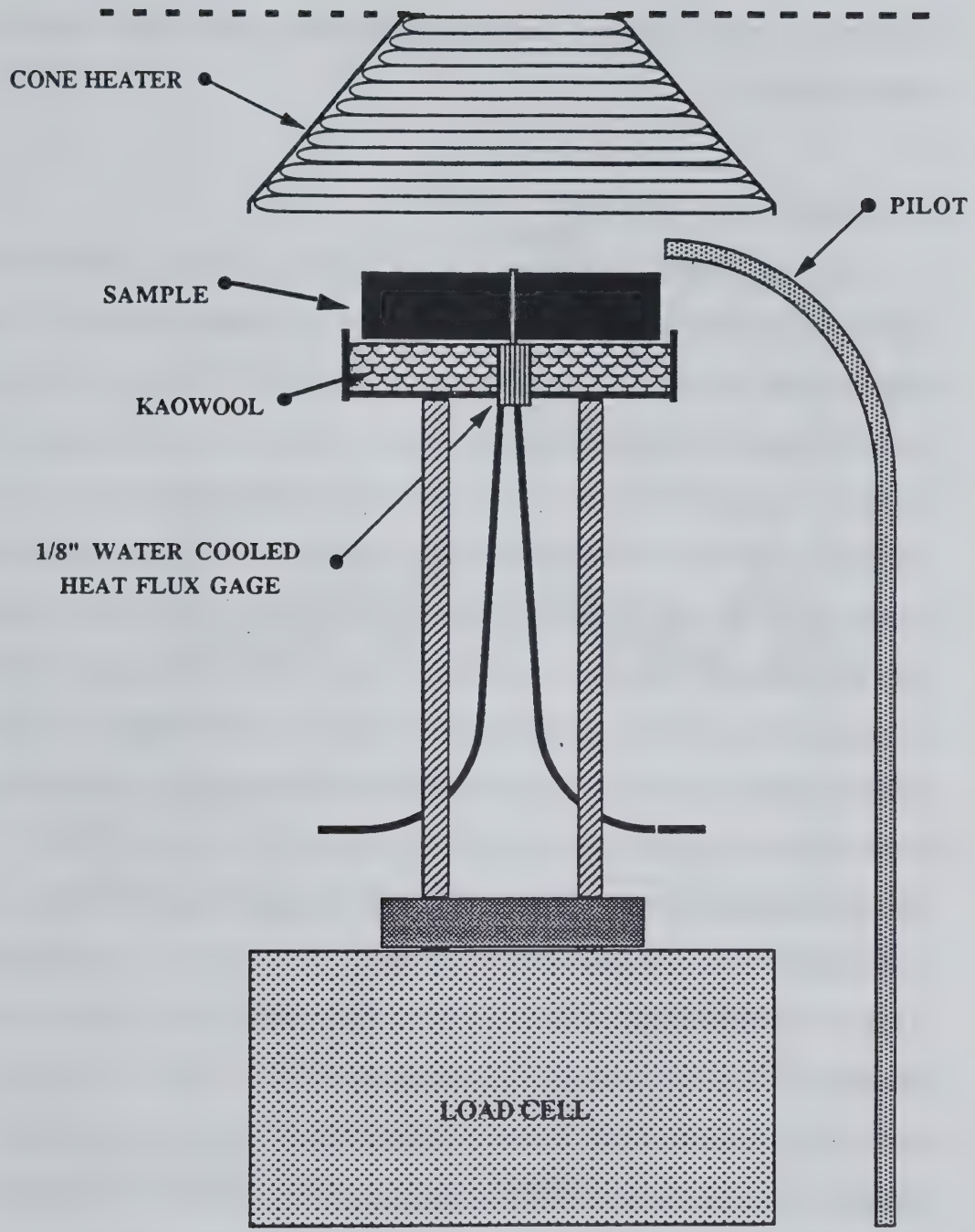

Figure 3.1 Schematic layout of burning rate apparatus.

Furthermore, aluminum foil was wrapped around the edges and the back of the sample to prevent dripping.

3.3 Experimental Procedure

The experimental procedure consisted of exposing a sample, in the horizontal orientation, to a constant external irradiance from the cone heater assembly. The time to piloted ignition was measured and mass loss data recorded for each test. Prior to the onset of each experiment the cone heater needed to be set to the desired constant external irradiance. The initial incident heat flux was determined using a Medtherm 1 inch thermopile type heat flux transducer (Model # 64-5SB-20) situated such that it was in the same location that the center of the sample would be, and so that the face of the gage was 1 inch below the base of the cone heater. The experiment was not started until a constant heat flux recording was obtained for at least a one minute period. The heat flux gage could not be left in place during the experiment. Subsequently, the constancy of the cone heater was ensured by monitoring the temperature of the cone coil. Two thermocouples were located in the cone heater coil. The thermocouple readings were averaged and displayed every two seconds so that the cone heat flux, which corresponds to a given coil temperature, could be monitored. The cone coil temperature was kept constant ($\pm$ 5° C) by manually adjusting the current to the coil using a 220 Volt transformer. This approach allowed for adjustment of the current to compensate for temperature fluctuations induced by flame impingement on the cone coil. Figure 3.2 shows a typical cone temperature variation for Nylon subjected to a 75 kW/m^2 exposure.

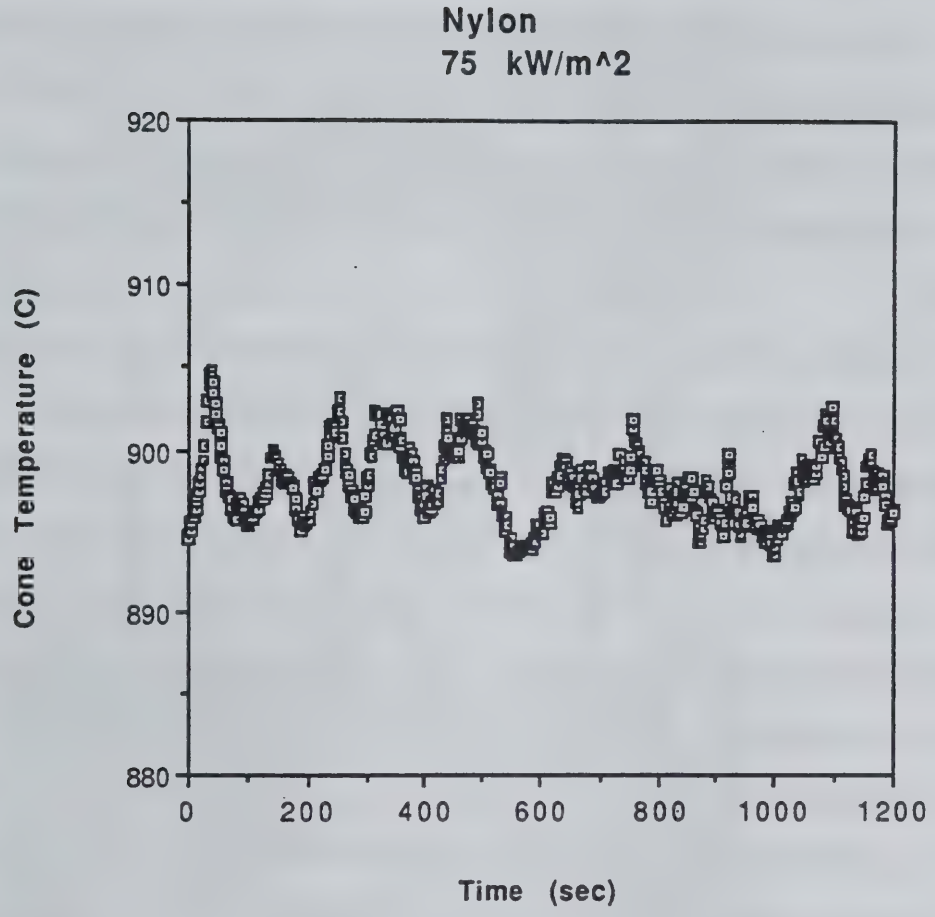

Figure 3.2 Cone heater coil temperature variation with a 75 kW/m^2 external irradiance.

3.3.1 Ignition

The arrangement of the assembly was such that the top of the sample was initially located 1 inch below the base of the cone heater as is done for standard Cone Calorimeter tests [3]. The load cell was oriented between two guide bars to ensure proper placement of the sample underneath the center of the cone heater assembly. A one inch methane flame, located on one edge approximately 1/2 inch above the surface of the sample, was used as a pilot ignition source. Figure 3.3 shows the arrangement of the pilot and the assembly.

Once the cone was set to the desired constant external irradiance and the sample was prepared and situated on the load cell, the load cell was shifted into position underneath the cone. Simultaneously, the data acquisition system was initiated. It should be noted that sliding the sample into place caused some bouncing of the load cell. This effects the mass loss recordings for the first few seconds of the experiment. This is not however expected to have adverse effects on the results since ignition nominally took longer that ten seconds.

The ignition time is defined as the time at which a continuous flame is supported on the material surface. In some instances flashing occurred on the surface of the sample prior to sustained flaming. However, in all cases the ignition time was taken as the time at which flaming was sustained over the entire surface of the specimen. Ignition times for all of the thermoplastic tests for irradiances ranging from 20 kW/m^2 to about 80 kW/m^2 are shown in Appendix B.

In some experiments, a fine wire Type K thermocouple (0.003 in. diameter) was mounted on the thermoplastic material surface to attempt to measure the surface temperature at ignition. The thermocouple wire was placed on the sample surface by heating the wire so that it recessed into the surface of the material. Measurements of the surface temperature were recorded until the onset of burning. Figure 3.4 shows a typical

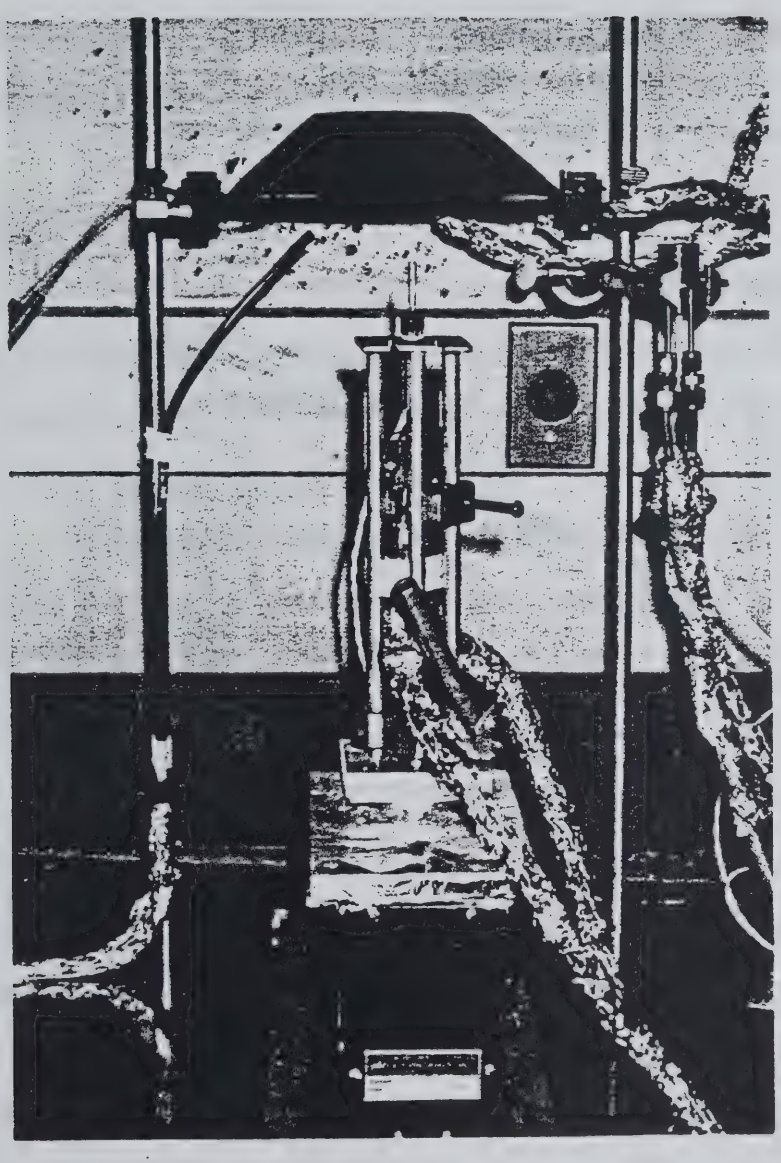

Figure 3.3 Experimental burning rate apparatus.

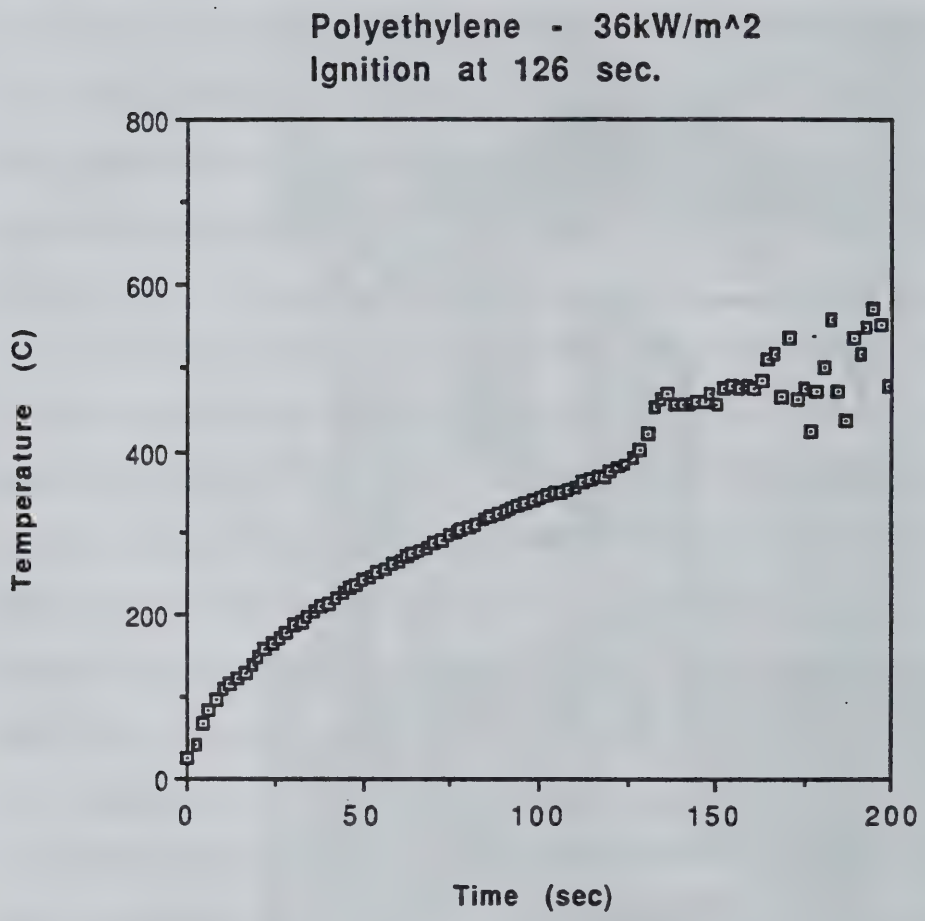

Figure 3.4 Surface temperature of Polyethylene as a function of time with a 36 kW/m^2 external irradiance.

result of the measured surface temperature for the preheating period for Polyethylene exposed to a 36 kW/m^2 external irradiance. The temperature at the onset of the sudden rise in temperature is defined as the ignition temperature (T_{ig}). Results for the surface temperature measurements for the thermoplastic experiments at various external irradiances are shown in Appendix C.

3.3.2 Mass Loss Rate

Experiments to determine the mass loss rate of the materials were performed concurrently with the ignition experiments. The mass loss of the samples was recorded using a load cell. The mass loss readings were recorded every two seconds for approximately a 1200 second period.

The transient mass loss rate is found using a five point least squares fit of the mass loss data. The mass loss rate at some time t_i is given as,

$$\dot{m}'' = \frac{5 \sum_{n=i-2}^{i+2} (m_n t_n) - \sum_{n=i-2}^{i+2} (m_n) \sum_{n=i-2}^{i+2} (t_n)}{5 \sum_{n=i-2}^{i+2} (t_n)^2 - \left[\sum_{n=i-2}^{i+2} (t_n) \right]^2}$$

where, i is a given measured data point,

m is the mass at i,

and, t is the time at i.

Figure 3.5 shows a typical mass loss rate result for Nylon exposed to an 80 kW/m^2 irradiance. Results for Nylon at other exposures, Polyethylene, and Polypropylene are shown in Appendixes D, E, and F, respectively.

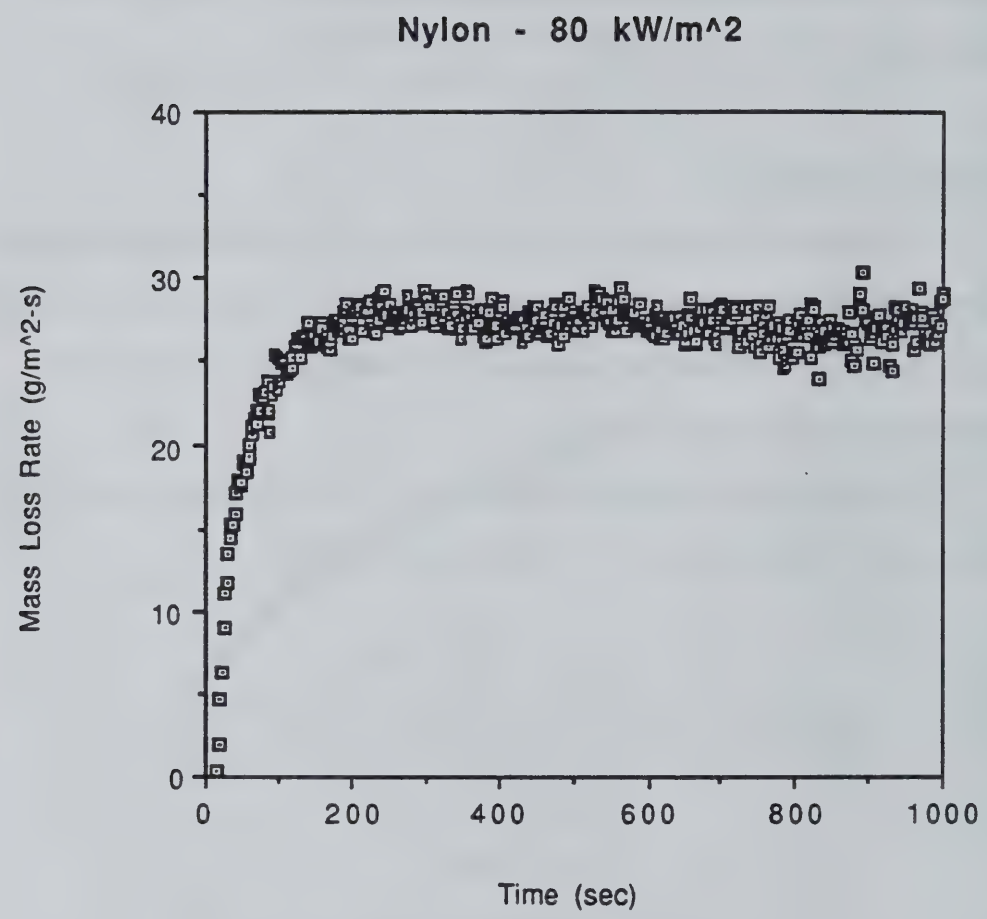

Figure 3.5 Transient mass loss rate of Nylon with an 80 kW/m^2 external irradiance.

3.4 Calibration

Calibration of the load cell, thermocouples, and 2.5 cm (1 inch) heat flux gage was necessary before any experiments were conducted and only occasionally once testing began. The methods used to calibrate each of the instruments are discussed below.

3.4.1 Load Cell

The load cell was calibrated by first adjusting the weight of the sample holder and insulation to approximately zero. At this point, standard weights between 1 and 100 gram were added to the load cell and the voltage readings were recorded. The relationship between weight and voltage was found to be linear, with a calibration constant of 582.0 g/V. Because only mass loss rate is desired, only the difference in mass is necessary. Therefore, small fluctuations in the zero weight did not affect the results. At the start of each day, the load cell was checked for accuracy using 1 and 2 gram weights. Furthermore, in some instances the mass of the sample was measured using a scale and the results compared to that indicated by the load cell. No significant errors were found for the mass loss measurements.

3.4.2 Heat Flux Gauge

The 2.5 cm (1 inch) heat flux gauge was initially calibrated using the standard NIST heat lamp calibration box. It was tested with water at room temperature and again with water at 46 °C. No notable differences in the calibration constant were observed. Although the water temperature did not affect the calibration constants, it did affect the zero reading. Unlike the mass loss, the heat flux measurement must be zero when there is no incident heat flux. The hot water resulted in an initial negative heat flux measurement due to convection between the sensor and the atmosphere. The heat flux

measurement was calibrated to be zero, under no external irradiance, before each experiment in order to obtain consistent results. Besides the zero flux measurement, the 1 inch gage did not require calibration before each of the experiments because it was positioned such that it did not get disturbed or touched. The calibration constant for the 1 inch heat flux meter was determined to be 5235 kW/m^2 V.

3.4.3 Thermocouples

The thermocouples used to measure the coil temperature and surface temperature were calibrated before any testing began. This was done by placing them in an ice bath and also in boiling water for a prolonged period of time. Temperature readings were found to be accurate within ± 2 °C. The thermocouples in the coil did not require additional calibration as the absolute temperature was not necessary. The thermocouples for the surface were calibrated against each other before each experiment.

Although the experiments yielded extraneous results for some tests, no major calibration errors were found. Inconsistencies in the results are likely to be due to factors other than calibration errors.

CHAPTER 4 MODEL FOR THERMOPLASTICS

The model used for this analysis is based on the formulation of Quintiere [1] as presented by Quintiere and Iqbal [2]. The model is one-dimensional and assumes that surface vaporization occurs at a specified temperature, T_v. The model can be extended to include an analysis for charring materials, but at the present time only thermoplastic (non-charring) materials will be considered. The model will be briefly described below.

4.1 Preheating to Ignition

The one-dimensional unsteady heat conduction equation applies to the preheating period. Constant properties are assumed such that the governing equation is,

$$\frac{\partial T}{\partial t} = \alpha \frac{\partial^2 T}{\partial y^2} \tag{4.1}$$

with a constant initial temperature ,

$$T = T_0 \text{ @ } t = 0. \tag{4.2}$$

Furthermore, considering convection at the surface (y = 0) and radiative heat loss,

$$-k \frac{\partial T}{\partial y}\Big|_{y=0} = \dot{q}'' \equiv \varepsilon \dot{q}''_{ext} - h_c (T - T_0) - \varepsilon \sigma T^4 \tag{4.3}$$

An approximate integral solution is applied to formulate a solution to the above problem. Therefore, the solution to Equation (4.1) comes from integrating the equation between zero and some penetration depth, δ , where at $y = \delta$,

$$T = T_0$$

and,

$$\frac{\partial T}{\partial y} = 0. \tag{4.4}$$

A quadratic profile is assumed for T such that the three conditions given by equations (4.3) and (4.4) are satisfied:

$$T - T_0 = \frac{\dot{q}''\delta}{2k}\left(1-\frac{y}{\delta}\right)^2 \tag{4.5}$$

Applying the above boundary condition and integrating equation (4.1) from 0 to δ yields,

$$\frac{d}{dt}\left(\dot{q}''\delta^2\right) = 6\alpha\dot{q}'' \tag{4.6}$$

If $\dot{q}''$ is assumed to be constant, which is a reasonable assumption for large external irradiances, then equation (4.6) yields,

$$\delta \cong \sqrt{6\alpha t} \tag{4.7}$$

A more complete solution to the above problem has been shown by Abu-Zaid and Atreya [10] to yield;

$$\delta = \sqrt{\frac{12\alpha t}{e_4}} \tag{4.8}$$

where e_4 was shown to vary between 1.6 at 15 kW/m^2 and 1.9 at 50 kW/m^2. Taking the asymptote as 2.0 yields equation (4.7). Since the solution presented here is approximate, the accuracy sacrificed by using equation (4.7) is assumed to be acceptable, although the error will be greatest, about 10%, at low external irradiances.

Substituting the equation for δ from equation (4.7) into equation (4.5) at y = 0 produces,

$$T_{ig} - T_0 = \frac{\dot{q}''\delta}{2k} = \frac{\dot{q}''}{2k}\sqrt{6\alpha t_{ig}} \tag{4.9}$$

Solving equation (4.9) for t_{ig} gives,

$$t_{ig} = \frac{2}{3}(k\rho c)\frac{(T_{ig}-T_0)^2}{(\dot{q}'')^2} \tag{4.10}$$

This approach also gives a method for determining the surface temperature as a function of time. This is done implicitly by selecting T_s, calculating the corresponding net heat flux, and using equation (4.10) to determine the time. This result also allows for the determination of a critical flux for ignition, $\dot{q}''_{cr}$, by extrapolating ignition data for $(tig)^{-1/2}$ to zero. At this intercept,

$$\dot{q}''_{ext}=\frac{1}{\varepsilon}\left[h_c(T_{ig}-T_0)+\varepsilon\sigma T_{ig}^4\right] \equiv \dot{q}''_{cr} \tag{4.11}$$

The critical flux for ignition is determined using equations (4.4) and (4.10). Once the critical flux is found, the temperature at the critical flux can be determined using equation (4.11).

4.2 Burning Rate

The governing equations for the gasification period can be derived in integral form by selecting the appropriate control volumes (CV_1 and CV_2) for the vaporization plane and the solid, as shown in Figure 4.1 [2]. The governing equations for the burning rate follow from equation (4.1) which governs conduction to the material below the vaporizing plane at a fixed temperature. Subsequently, at y = 0,

$$T = T_v \tag{4.12}$$

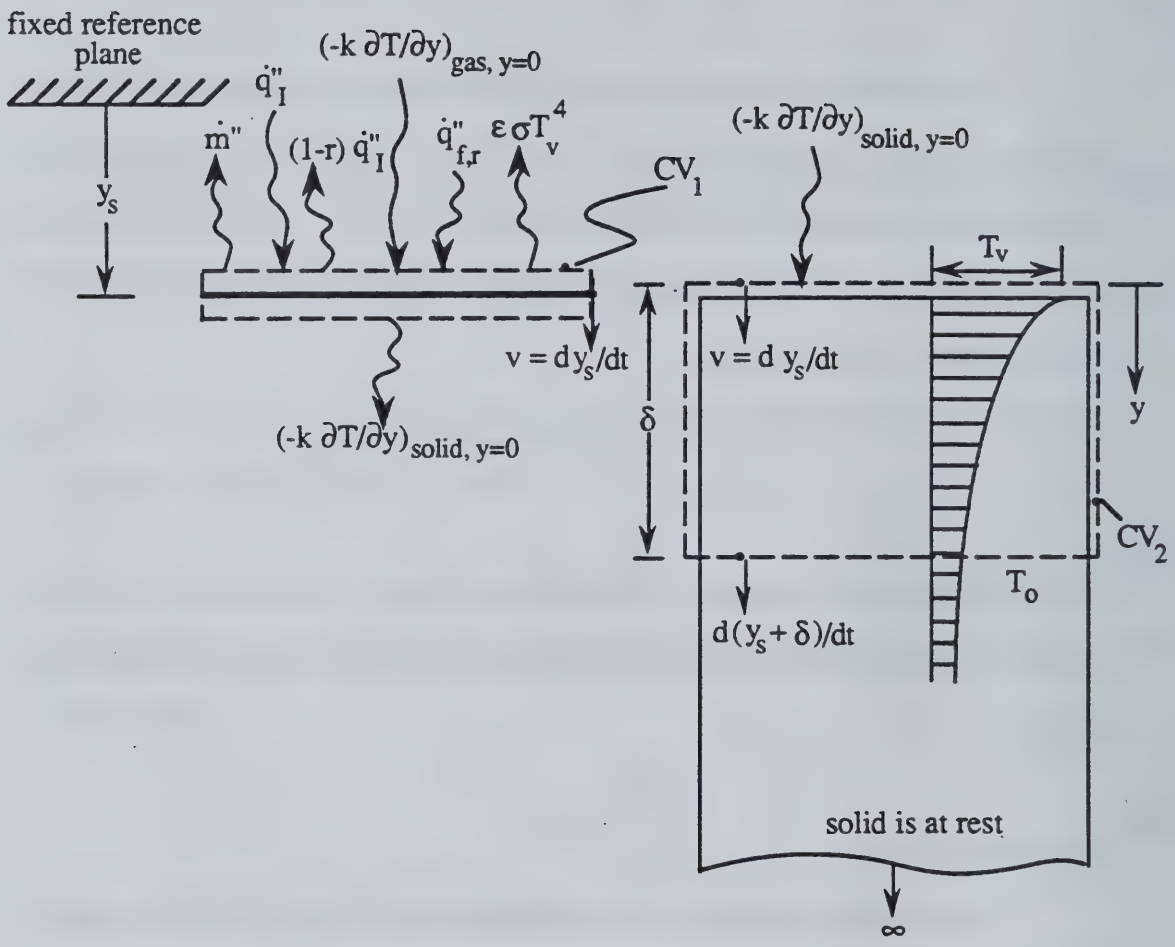

Figure 4.1 Heat and mass transfer processes for a thermoplastic-like solid fuel. CV1 is around the vaporizing interface. CV2 is bounded by the interface and thermal penetration depth, δ.

and,

$$-k\frac{\partial T}{\partial y} = \dot{q}'' - \dot{m}''\Delta H_v \tag{4.13}$$

where, $\dot{m}''$ is the mass loss rate per unit area,

ΔH_v is the heat of vaporization,

and $\dot{q}''$ is the net surface heat flux.

It should be noted that the net surface heat flux, $\dot{q}''$, is different for the gasification period in equation (4.13) than for the preheating period as defined in equation (4.4). The net surface heat flux for the gasification period is,

$$\dot{q}'' = \varepsilon\dot{q}''_{ext} + \dot{q}''_{fl} - \varepsilon\sigma T_v^4 \tag{4.14}$$

where $\dot{q}''_{fl}$ is the flame heat flux, which is defined as,

$$\dot{q}''_{fl} = \varepsilon\dot{q}''_{fl,r} + \dot{q}''_{fl,c} \tag{4.15}$$

Where, $\dot{q}''_{fl,r}$ is the flame incident radiant heat flux, and $\dot{q}''_{fl,c}$ is the convective flux, from a stagnation film model [1], and can be shown to be,

$$\dot{q}''_{fl,c} = \frac{h_c}{c_g}\left(\frac{\xi}{e^{\xi}-1}\right)\left[Y_{ox,\infty}(1-\chi_r)\frac{\Delta H_c}{r} - c_g(T_v - T_0)\right] \tag{4.16}$$

where, $\xi = \dfrac{\dot{m}''c_g}{h_c}$,

$\left(\dfrac{\xi}{e^{\xi}-1}\right)$ is the mass transfer "blocking factor" that is 1 for $\dot{m}''$ ->0,

$Y_{ox,\infty}$ is the ambient mass fraction of oxygen,

χ_r is the flame radiative fraction,

ΔH_c is the heat of combustion,

r is the stoichiometric fuel to oxygen mass ratio,

c_g is the gas phase specific heat at constant pressure.

An alternate way of expressing this is,

$$\dot{q}''_{fl,c} = h_c\left(\frac{\xi}{e^{\xi}-1}\right)(T_{fl}-T_v) \tag{4.17}$$

where T_{fl} is an effective flame temperature.

Assuming a quadratic profile for the temperature, which satisfies the boundary conditions supplied by equations (4.2) and (4.12),

$$\frac{T-T_0}{T_v-T_0} = \left(1-\frac{y}{\delta}\right)^2 \tag{4.18}$$

and substituting the profile into equation (4.13) yields,

$$\dot{m}''\Delta H_v = \dot{q}'' - \frac{2k}{\delta}(T_v-T_0) \tag{4.19}$$

where the last term represents transient conduction heat loss into the solid. Integrating equation (4.1) from y = 0 to y = δ, as was done for the ignition analysis, and substituting in the profile from equation (4.18) yields,

$$\frac{1}{3}\frac{d\delta}{dt} + \frac{\dot{m}''}{\rho} = \frac{2\alpha}{\delta} \tag{4.20}$$

where at ignition, $T = T_v$ and $\delta = \sqrt{6\alpha t} = \delta_{ig}$. (4.20a)

If the total flame heat flux is assumed to be constant, or if the dependence of the burning rate on the blocking factor is ignored, then equation (4.20) can be solved exactly. It can be shown that,

$$t - t_{ig} = \frac{\delta_s^2}{6\alpha}\frac{\Delta H_v}{L}\left[\frac{\delta_{ig} - \delta}{\delta_s} - \ln\left(\frac{\delta_s - \delta}{\delta_s - \delta_{ig}}\right)\right] \tag{4.21}$$

where, $\delta_s = \frac{2k}{c}\frac{L}{\dot{q}''}$, a steady value, (4.22)

and, $L = \Delta H_v + c(T_v - T_0)$, is the heat of gasification. (4.23)

It follows that the steady state mass loss rate is given by,

$$\dot{m}''_s = \frac{\dot{q}''}{L} \tag{4.24}$$

It should be noted that in addition to the flame heat flux, other properties are needed to obtain a solution. These properties need to be derivable in a convenient manner consistent with the burning rate and ignition models. The properties are, ε, ρ, c, k, T_v or T_{ig}, and ΔH_v or L.

4.3 Flame Heat Flux

For the present experiments, only the steady mass loss rate measurements are used to determine the flame heat flux. Rhodes [9] used surface heat flux measurements in addition to the steady mass loss measurements for his study with PMMA. In addition, a simulated sample was used to examine the effect of the flame heat flux. This will be discussed.

4.3.1 Flame Radiation

The emissivity of a flame can be represented as,

$$\varepsilon_f = 1 - e^{-\kappa l_m} \tag{4.25}$$

where, κ is the absorption coefficient,

and l_m is the mean beam length.

According to Orloff and deRis [11] , κ and l_m can be computed from an algorithm for pool fires. For cases where the flame height is greater than twice the diameter of the base, which is the case for all of the thermoplastic-like materials tested, the mean beam length is,

$$l_m = 0.65D \tag{4.26}$$

where D is the diameter of the base, which is 10 cm for the materials tested in the cone heater assembly. This says that the mean beam length is constant for a given diameter when the flame height is greater than twice the diameter. It follows that the flame emissivity is constant and subsequently the radiative flame heat flux is approximately constant for a constant flame temperature because,

$$\dot{q}''_f = \varepsilon_f \sigma T_f. \tag{4.27}$$

In addition, the transmissivity is defined as,

$$\tau = e^{-\kappa l_m} \tag{4.28}$$

Because the mean beam length is constant, it follows that the transmissivity is constant. This suggests that the amount of radiation from the cone heater that reaches the surface is constant for a thermoplastic material. Rhodes [9] found that the transmissivity of PMMA is approximately 0.91, suggesting that the flame is very transparent.

4.3.2 Convective Flame Heat Flux

The convective heat flux, assuming a blocking factor of 1, can be estimated from equation (4.16) considering,

$h_c = 10$ W/m^2 K $\qquad\qquad$ $\Delta H_c/r = 13$ kJ/g

$c_g = 1.0$ J/g K $\qquad\qquad$ $\chi_r = 0.4$

$Y_{ox,\infty} = 0.233$

A maximum $\dot{q}''_{fl,c} = 15$ kW/m^2 is determined since blocking would reduce this value as the burning rate increases.

4.3.3 Total Flame Heat Flux

Assuming the surface emissivity , ε, is approximately 1, equation (4.15) indicates that the total flame heat flux is approximately constant. This constancy has been shown for PMMA by Rhodes [9] and has good utility in aiding in the analysis of Cone Calorimeter data.

Measurements of the flame plus external heat flux were not attempted for the thermoplastics examined due to difficulties encountered in the PMMA experiments. However, it was shown by Quintiere and Rhodes [8] that the flame heat flux for thermoplastic-like materials burning in the Cone Calorimeter is constant. This was accomplished through measurements of the flame plus external heat flux to the material surface during the burning rate experiments and by utilizing a simulated sample methane gas burner. Since the phenomenon of the constant flame heat flux is critical to the analysis presented within for thermoplastics, a brief overview of the procedure using the simulated sample is presented here.

A simulated sample was used to examine the effect of flame heat flux on burning rate. The simulated sample was steel and measured 10 cm x 10 cm x 7.5 cm thick. A

14.3 mm (9/16 inch) hole was located in the center of the sample to allow for heat flux measurements using a 3.175 mm (1/8 inch) heat flux meter. The burner was filled with glass beads and methane was injected through the base. The glass beads insured a steady flow rate of methane through the top surface, with the rate of flow of the gas being controlled by a calibrated flow meter and a regulator.

The methane burner simulated sample was positioned beneath the cone heater in exactly the same position as the thermoplastic samples. The sample was subjected to a 50 kW/m^2 constant external irradiance. Considering that the sample was utilized to examine the effects of flame heat flux in the Cone Calorimeter, the sample was placed under the cone, not in the open environment, since the assembly tends to induce a specific airflow which influences the burning rate. The sample was exposed to a constant external flux so that flame impingement on the cone coils did not change the heat flux to the surface. As was previously discussed, the cone coil temperature was monitored and could be adjusted using a transformer. Figure 4.2 shows the steady state sensor heat flux measurements for an external exposure of 50 kW/m^2. The results show a constant flame heat flux above the external radiant heat flux. This is approximately 27 kW/m^2 for the methane over a range of energy release rates per unit area of 200 - 600 kW/m^2, which was determined from the methane flow rate and the heat of combustion of methane (50 kJ/g).

The constancy of the flame heat flux may be attributed to the shape of the flame for materials burning in the Cone Calorimeter. Figure 4.3 shows the flame for PMMA burning in the Cone. The long column shape of the flame is typical of all of the thermoplastic-like materials tested. The flame height to effective diameter is on the order of 4.

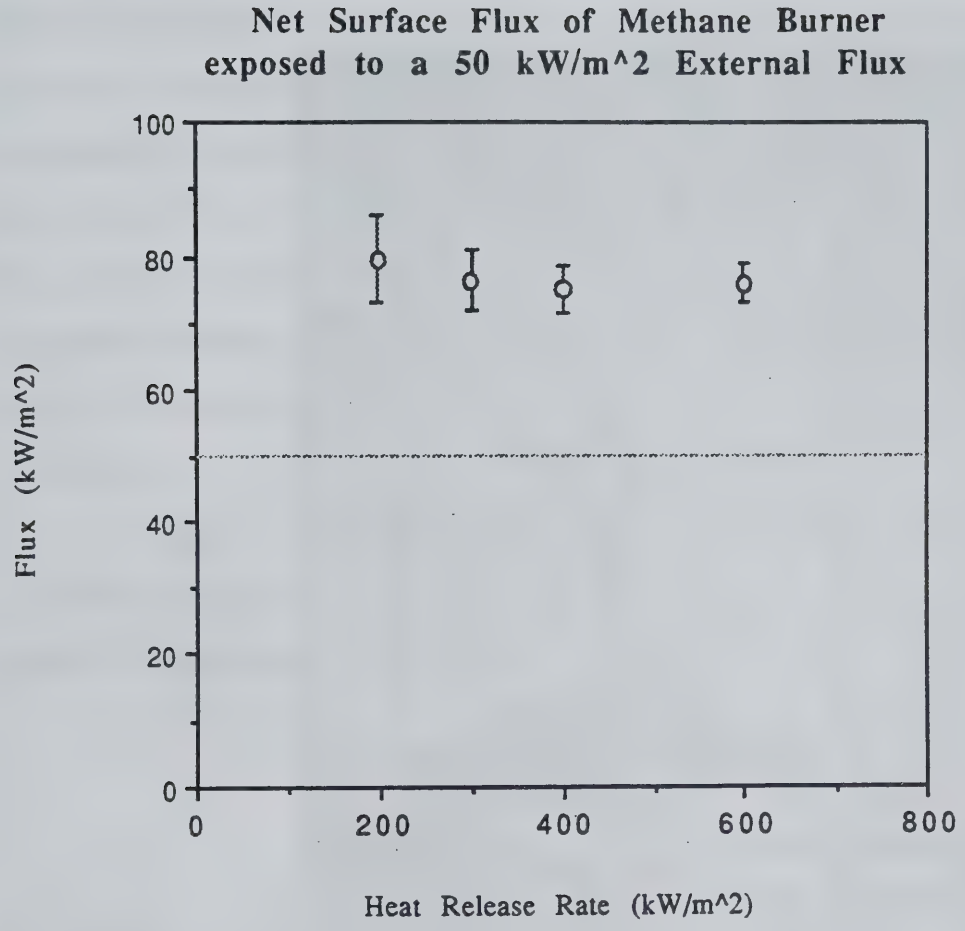

Figure 4.2 Steady state heat flux, measured by sensor, of methane gas burner with a 50 kW/m^2 external irradiance.

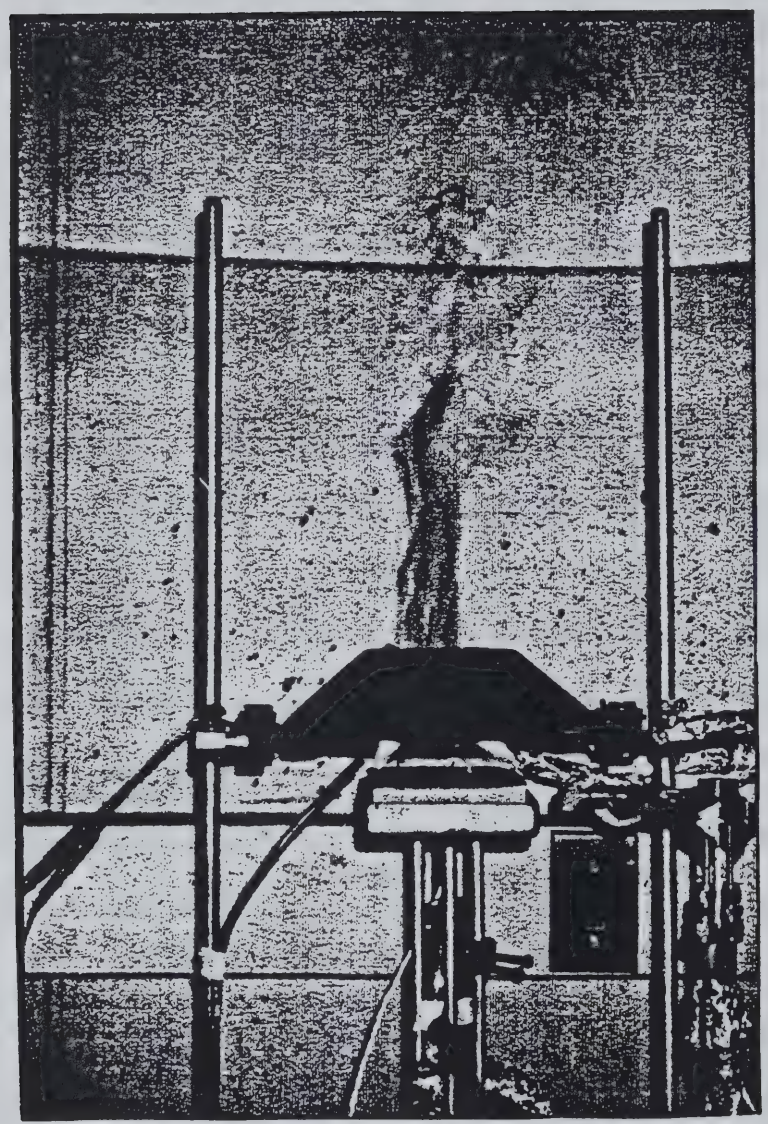

Figure 4.3 Flaming PMMA sample.

CHAPTER 5 ANALYSIS OF THERMOPLASTIC RESULTS

The analysis of the results is done in a manner consistent with the protocol outlined by Quintiere and Rhodes [8] for PMMA. The intent is to see if the protocol is general for all thermoplastic-like materials. Results obtained from the thermoplastic experiments are used to obtain the required properties to utilize the ignition and burning rate models. While most of the necessary properties are deduced from the experimental data, the density is determined by measurement, and the thermal diffusivity, which is assumed to be approximately constant for a given material, is obtained from the literature [12, 13]. The density and the thermal diffusivity for the three thermoplastics are shown in Table 5.1.

The approach used to obtain the needed properties will be demonstrated for Nylon 6/6. The approach is identical for the analysis of the other materials. The properties for all of the materials can be seen in Table 5.3.

Table 5.1

Measured and Literature Properties

Property	Nylon	Polyethylene	Polypropylene	PMMA	Units
α	1.24×10^{-7}	2.228×10^{-7}	6.736×10^{-8}	8.81×10^{-8}	m^2/s
ρ	1169	955	900	1190	kg/m^3

5.1 Ignition

In order to predict the ignition time and the critical flux for ignition, the ignition temperature and the thermal inertia must be determined. Once this is accomplished it is possible to determine the critical flux and the ignition time as a function of the external irradiance.

5.1.1 Ignition Temperature and Thermal Inertia

Figures 5.1 - 5.4 show plots of external irradiance as a function of ignition time for Nylon 6/6, Polyethylene, Polypropylene, and PMMA, respectively. The line through the data represents the best fit of the data below 40 kW/m^2 where the results should be better since for lower heat fluxes ignition takes longer. The best fit line in Figure 5.1 gives an intercept of approximately 14 kW/m^2, which represents the critical flux for ignition for Nylon 6/6. The values for the critical flux for ignition, $\dot{q}''_{cr}$, for the other materials are shown in Table 5.3. Using the value for the critical flux, equation (4.11) can be used to determine the ignition temperature, T_{ig}, given $T_0 = 20$ °C, $h_c = 10$ W/m^2-K (determined from an analysis for natural convection over a flat plate), and $\varepsilon = 1.0$. This yields an ignition temperature for Nylon 6/6 of $T_{ig} = 380$ °C. While this value is lower than the measured ignition temperature for Nylon, it will be shown that the deduced value yields good results when used in the model. Table 5.2 shows a comparison of the measured and calculated ignition temperatures for the materials tested. For all of the materials, the measured ignition temperatures were higher than the deduced values. While this may be an attribute of the modeling procedure, there is also uncertainty in the measured values, especially for Nylon where only one result was obtained.

Using the slope of the line in Figure 5.1, along with equations (4.3) and (4.10)

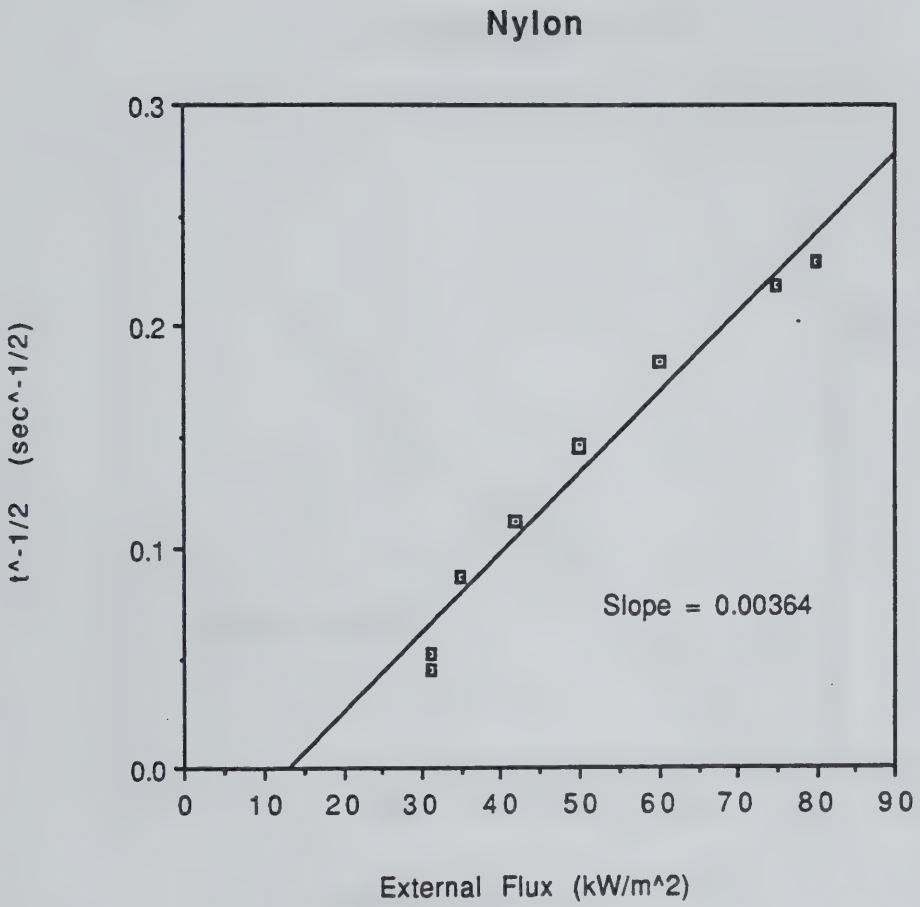

Figure 5.1 Ignition data for Nylon.

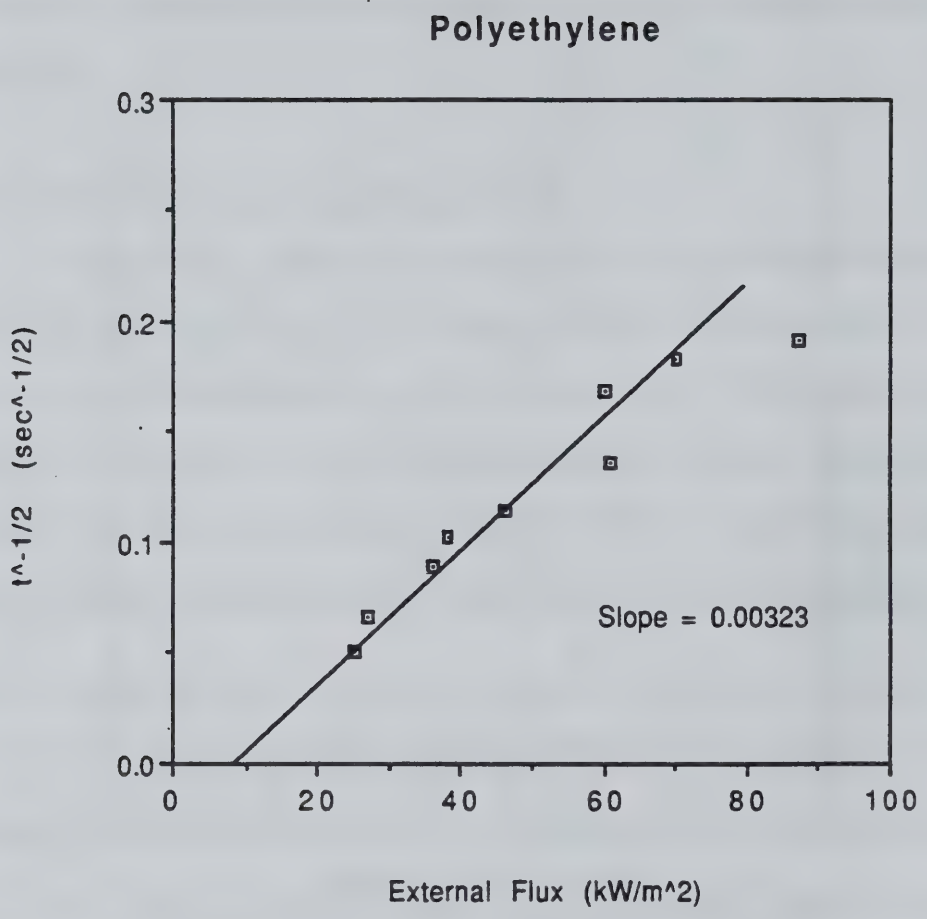

Figure 5.2 Ignition data for Polyethylene.

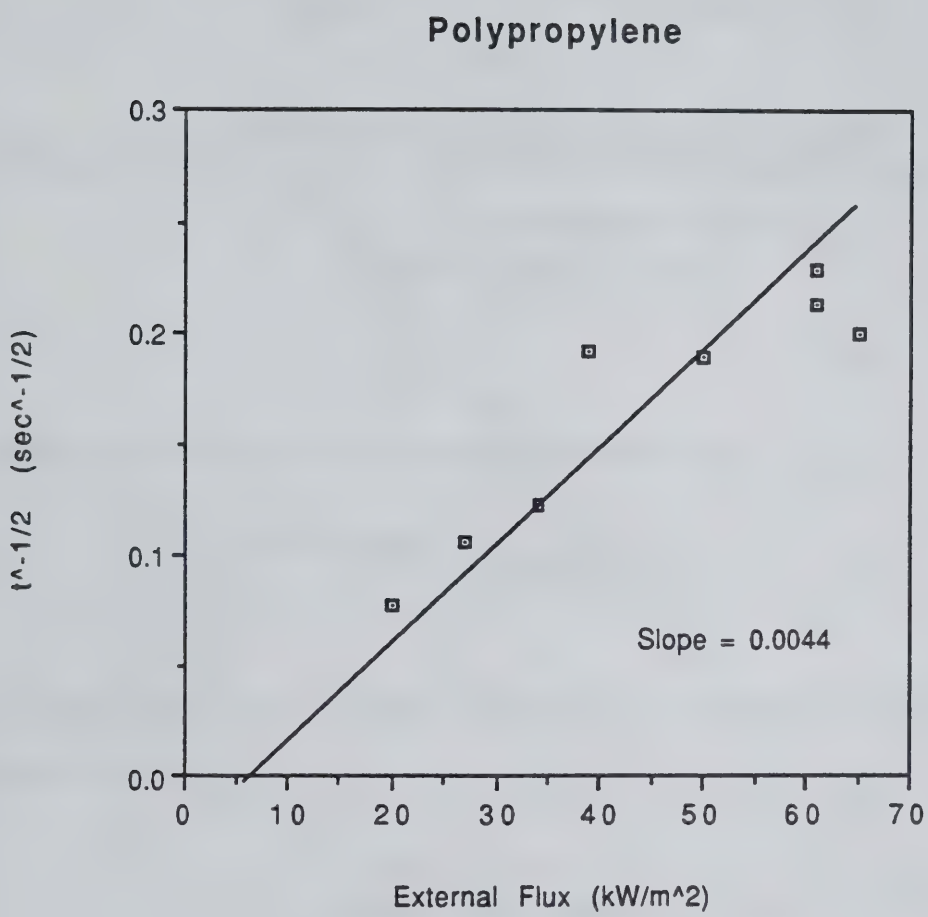

Figure 5.3 Ignition data for Polypropylene.

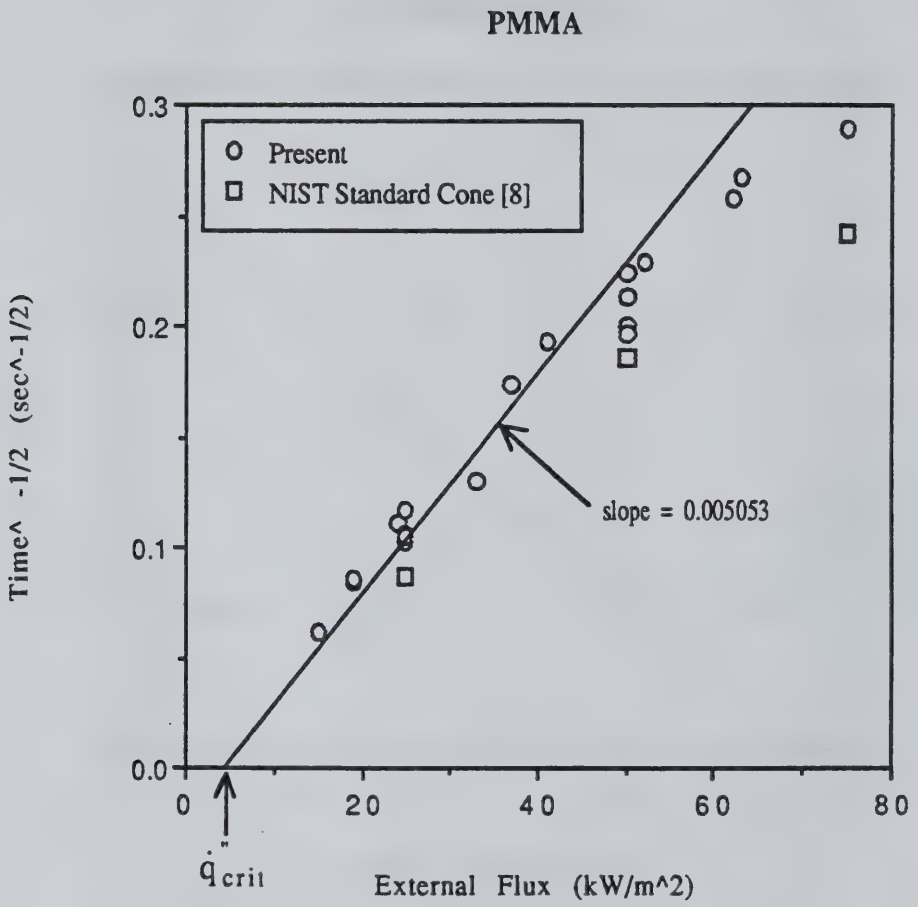

Figure 5.4 Ignition data for PMMA.

the thermal inertia can be calculated as follows:

From equations (4.3) and (4.10),

$$t_{ig}^{-1/2} = \left[\frac{\varepsilon}{\sqrt{\frac{2}{3}k\rho c\,(T_{ig}-T_0)}}\right]\dot{q}''_{ext} - \left[\frac{h_c(T_{ig}-T_0)+\varepsilon\sigma T_{ig}^4}{\sqrt{\frac{2}{3}k\rho c\,(T_{ig}-T_0)}}\right] \qquad (5.1)$$

Subsequently, from equation (5.1), the slope of the line in Figure (5.1) is,

$$\text{Slope} = \left[\frac{\varepsilon}{\sqrt{\frac{2}{3}k\rho c\,(T_{ig}-T_0)}}\right] \qquad (5.2)$$

Equation (5.2) can be solved to determine the thermal inertia,

$$k\rho c = \frac{3}{2}\left(\frac{\varepsilon}{\text{Slope}(T_{ig}-T_0)}\right)^2 \qquad (5.3)$$

Therefore, for Nylon 6/6 , the slope from Figure (5.1) is 0.00364 and subsequently the thermal inertia is,

$$k\rho c = 0.874\ \frac{kJ^2}{m^4 s\ K^2}$$

The values for the thermal inertia, kρc, for the other materials are shown in Table 5.3.

Figures 5.5 - 5.8 show plots of ignition time versus external flux for Nylon, Polyethylene, Polypropylene, and PMMA, respectively, along with the results of the model using the deduced values for the ignition temperature and the thermal inertia as input for equation (4.10).

5.1.2 Thermal Conductivity and Specific Heat

Knowing the thermal inertia, kρc, as was determined above, the density, ρ, and the thermal diffusivity, $\alpha = k/\rho c$, which varies only slightly with temperature, the thermal conductivity, k, and the specific heat, c, can be determined.

For Nylon 6/6 with $\rho = 1169$ kg/m^3 and $\alpha = 1.24 \times 10^{-7}$ m^2/s, the thermal conductivity and the specific heat are,

$$k = 3.29 \times 10^{-4} \text{ kW/m K}$$

and,

$$c = 2.27 \text{ kJ/kg K}$$

Although the thermal diffusivity must be independently determined, the above method gives a means of determining the specific heat and the thermal conductivity. Table 5.3 shows the specific heat and the thermal conductivity for the materials tested.

Table 5.2

Calculated and Measured Ignition Temperatures

Material	Calculated Ignition Temperature (°C)	Measured Ignition Temperature (°C)
Nylon 6/6	380	≈ 500
Polyethylene	300	315 - 330
Polypropylene	210	250 - 360
PMMA	180	250 - 355

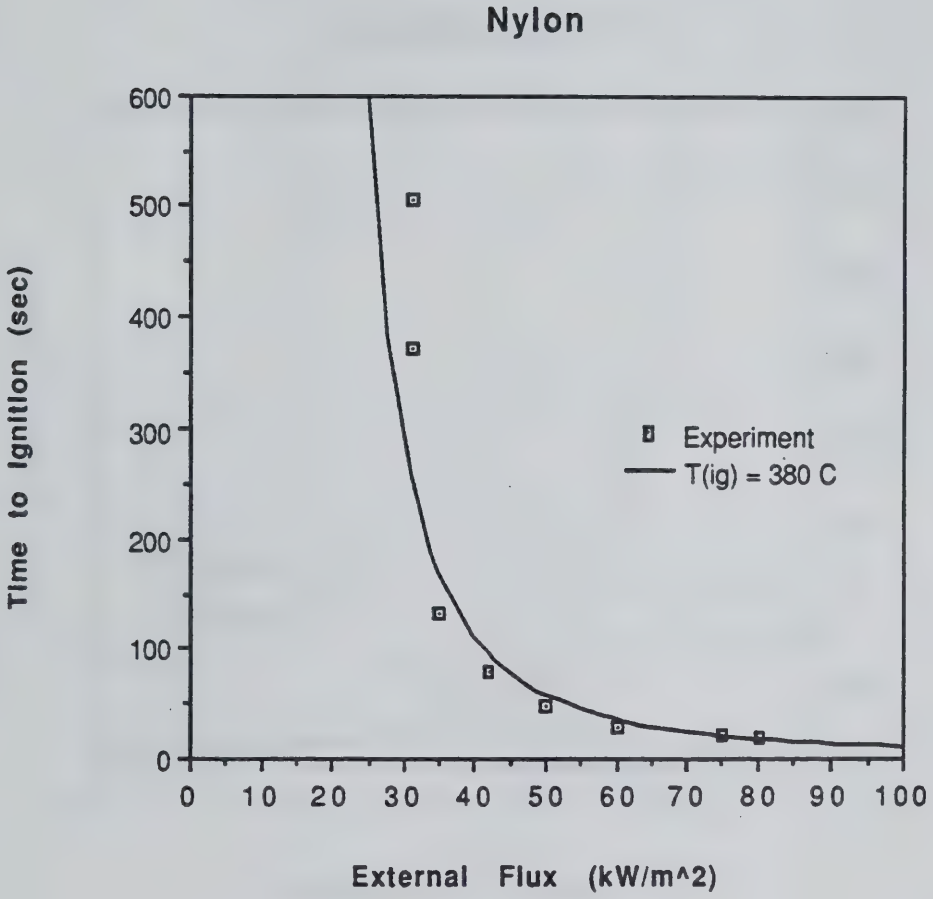

Figure 5.5 Calculated and measured ignition time of Nylon as a function of external irradiance.

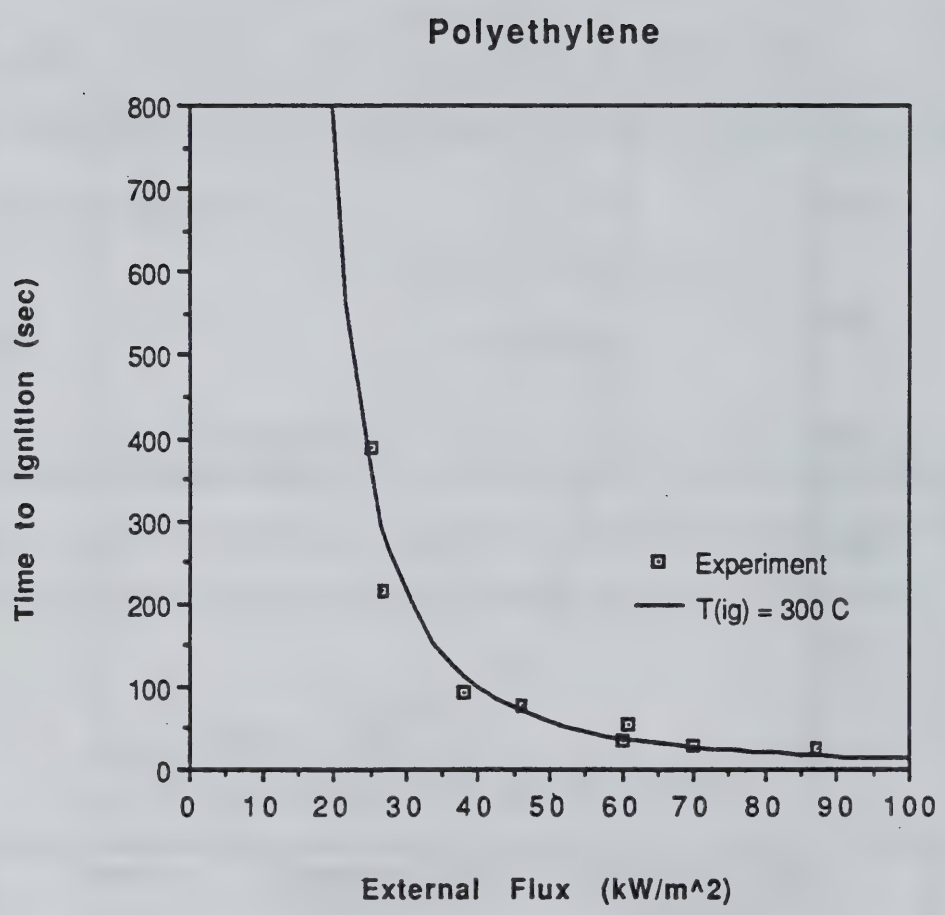

Figure 5.6 Calculated and measured ignition time of Polyethylene as a function of external irradiance.

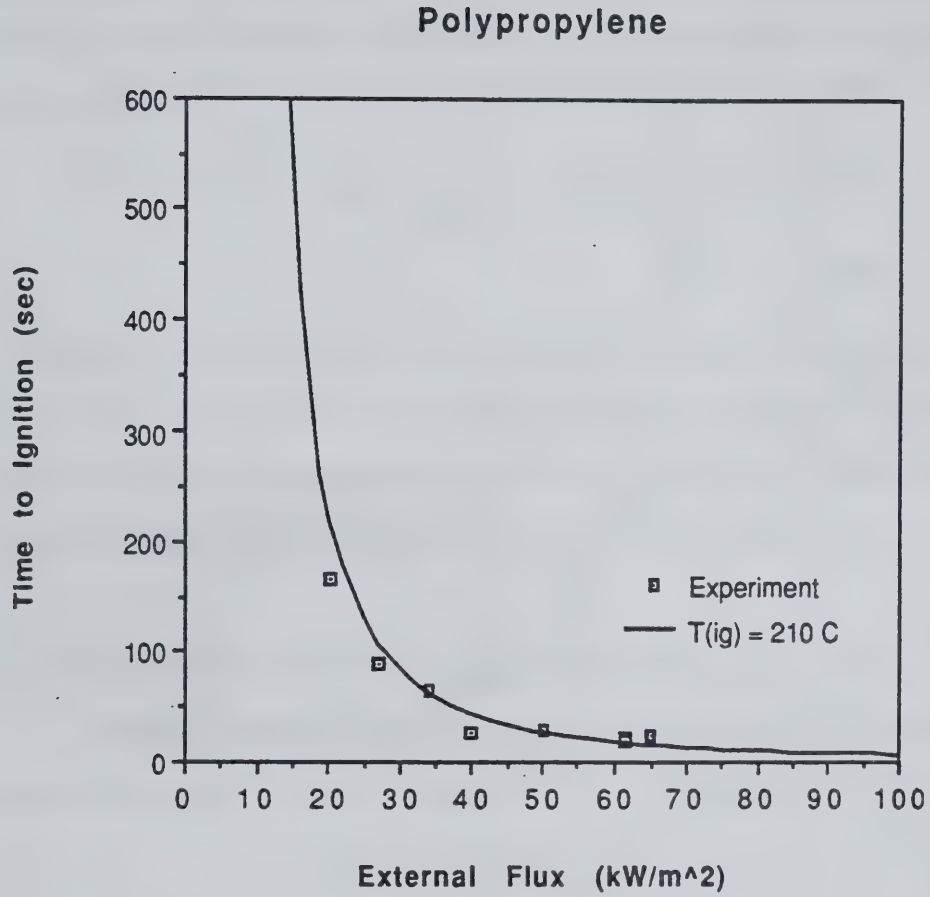

Figure 5.7 Calculated and measured ignition time of Polypropylene as a function of external irradiance.

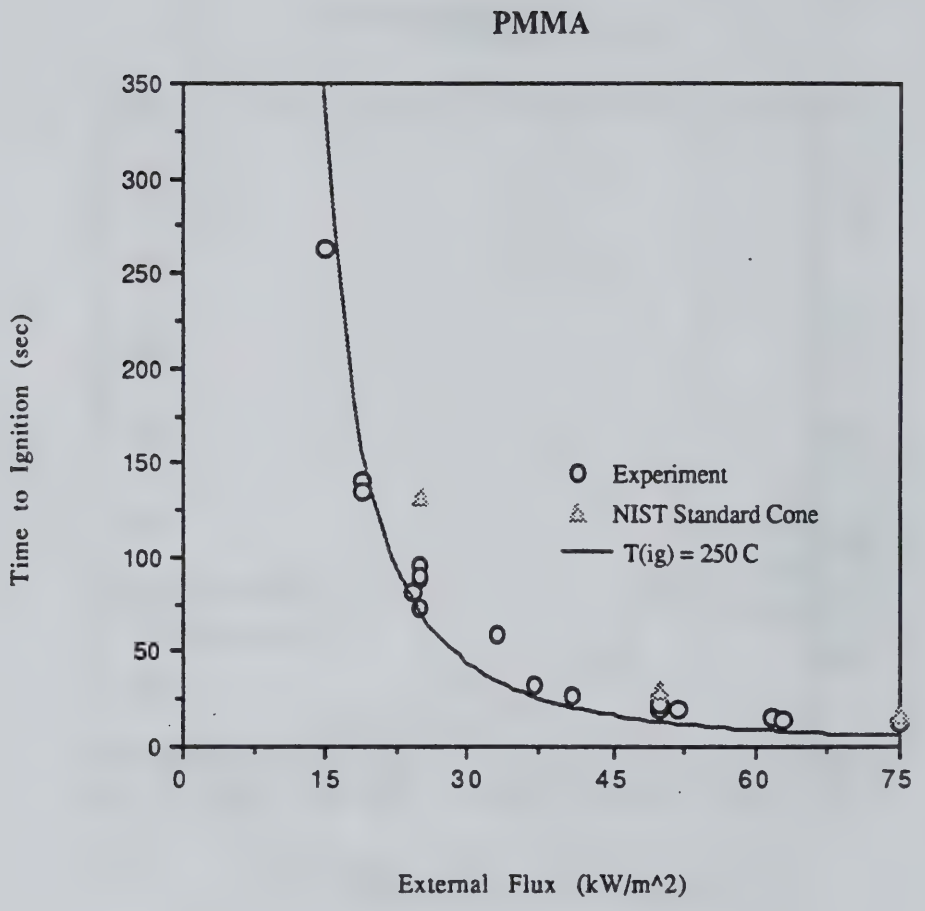

Figure 5.8 Calculated and measured ignition time of PMMA as a function of external irradiance.

5.2 Burning Rate

Since most thermoplastic-like materials approximate vaporizing solids, it is possible to represent the steady-state mass loss data using equation (4.24). Therefore, if the flame heat flux is assumed to be constant, which has been shown to be the case for thermoplastic-like materials burning in the Cone Calorimeter [8], then equation (4.24) can be written as,

$$\dot{m}'' = (\frac{1}{L})\dot{q}''_{ext} + \frac{(\dot{q}''_{g} - \varepsilon\sigma T_{v}^{4})}{L} \tag{5.4}$$

Subsequently, a plot of the steady state mass loss rate data as a function of the external flux has utility in determining the heat of gasification and the total flame heat flux. Figure 5.9 - 5.12 show plots of steady state mass loss rate versus external irradiance for Nylon 6/6, Polyethylene, and Polypropylene, and PMMA, respectively.

5.2.1 Effective Heat of Gasification and Total Flame Heat Flux

Equation (5.4) suggests that the slope of the fit to the data in Figures 5.7 - 5.9 represents the inverse of the heat of gasification, 1/L. Subsequently, for Nylon 6/6,

$$(\frac{1}{L}) = 0.26456\ \frac{g}{kJ}$$

Therefore,

$$L = 3.78\ kJ/g.$$

Furthermore, the intercept of the fit to the data in Figure 5.7 is,

$$\frac{\dot{q}''_{g} - \varepsilon\sigma T_{v}^{4}}{L} \tag{5.5}$$

For Nylon 6/6 this is,

$$\frac{\dot{q}''_{fl} - \varepsilon\sigma T_v^4}{L} = 5.32 \frac{g}{m^2 s}$$

Therefore, for an average vaporization temperature, taken to be the deduced value of the ignition temperature (380 °C), and an emissivity, ε, assumed to be 1.0, the flame heat flux is estimated using equation (5.5). For Nylon the flame heat flux is,

$$\dot{q}''_{fl} = 30.4 \frac{kW}{m^2}$$

Table 5.3 shows the heat of gasification and the flame heat flux for the other materials.

Table 5.3

Deduced Properties

Property	Nylon	Polyethylene	Polypropylene	PMMA	Units
$k\rho c$	0.874	1.834	2.15	2.12	$kJ^2/m^4\ s\ K^2$
k	3.29×10^{-4}	6.39×10^{-4}	3.81×10^{-4}	0.432×10^{-3}	kW/m K
c	2.27	3.0	6.27	4.12	kJ/kg K
T_{ig} (calc)	380	300	210	180	°C
L	3780	3580	3070	2770	kJ/kg
$\dot{q}''_{fl}$	30.4	25.3	14.3	37.0	kW/m^2
$\dot{q}''_{net}$	20.1	19.2	11.2	27.6	kW/m^2

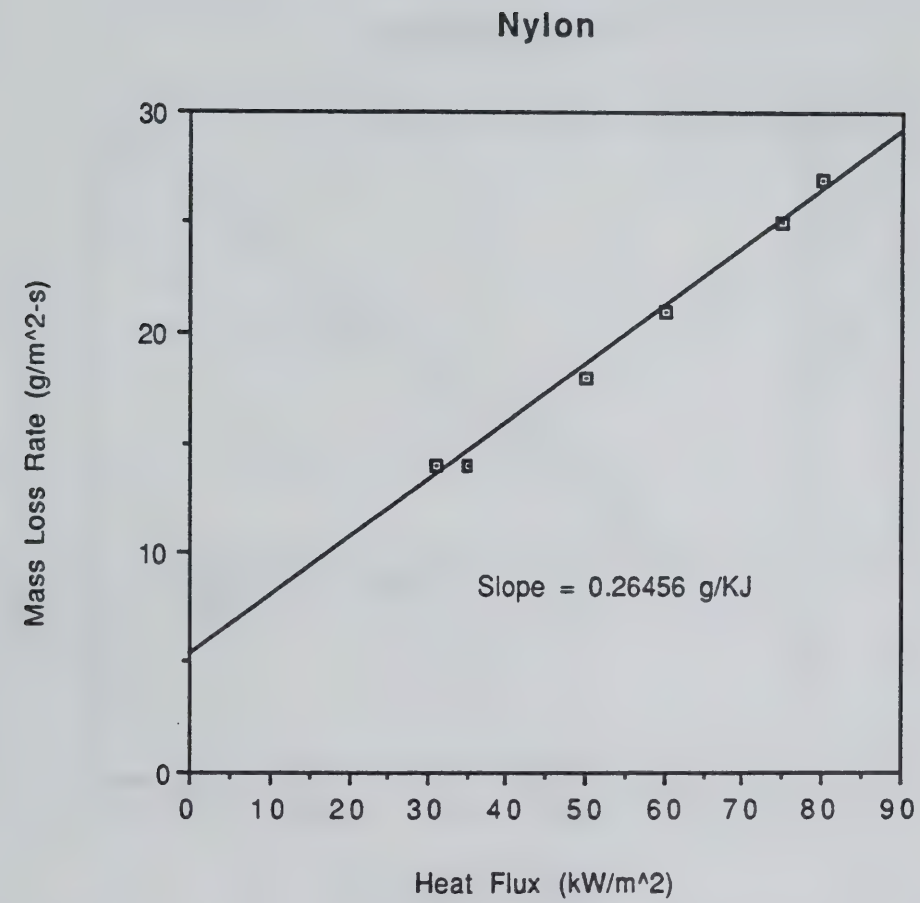

Figure 5.9 Steady state mass loss rate of Nylon as a function of external irradiance.

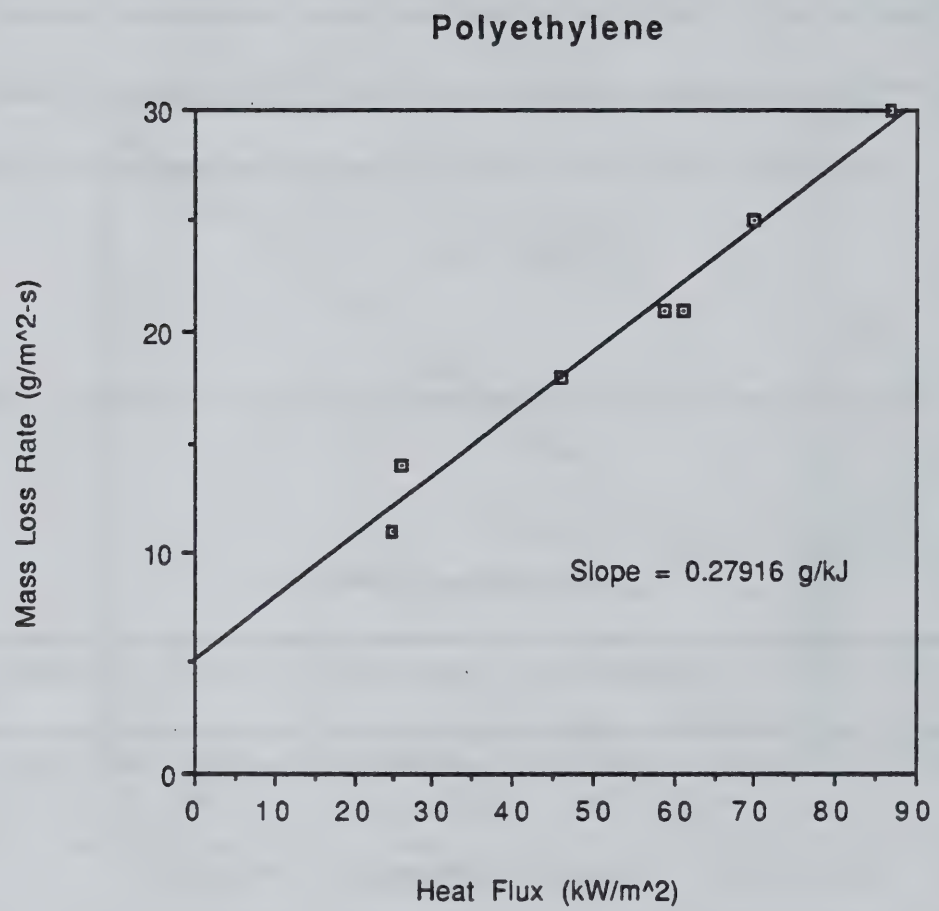

Figure 5.10 Steady state mass loss rate of Polyethylene as a function of external irradiance.

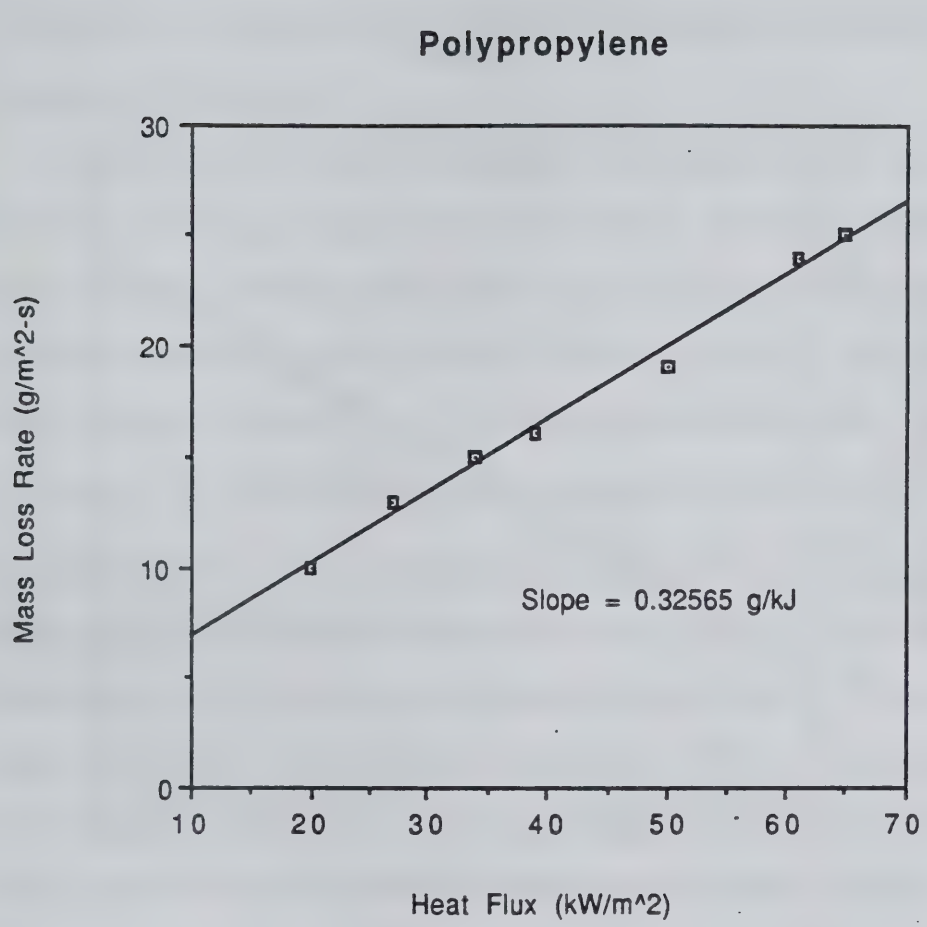

Figure 5.11 Steady state mass loss rate of Polypropylene as a function of external irradiance.

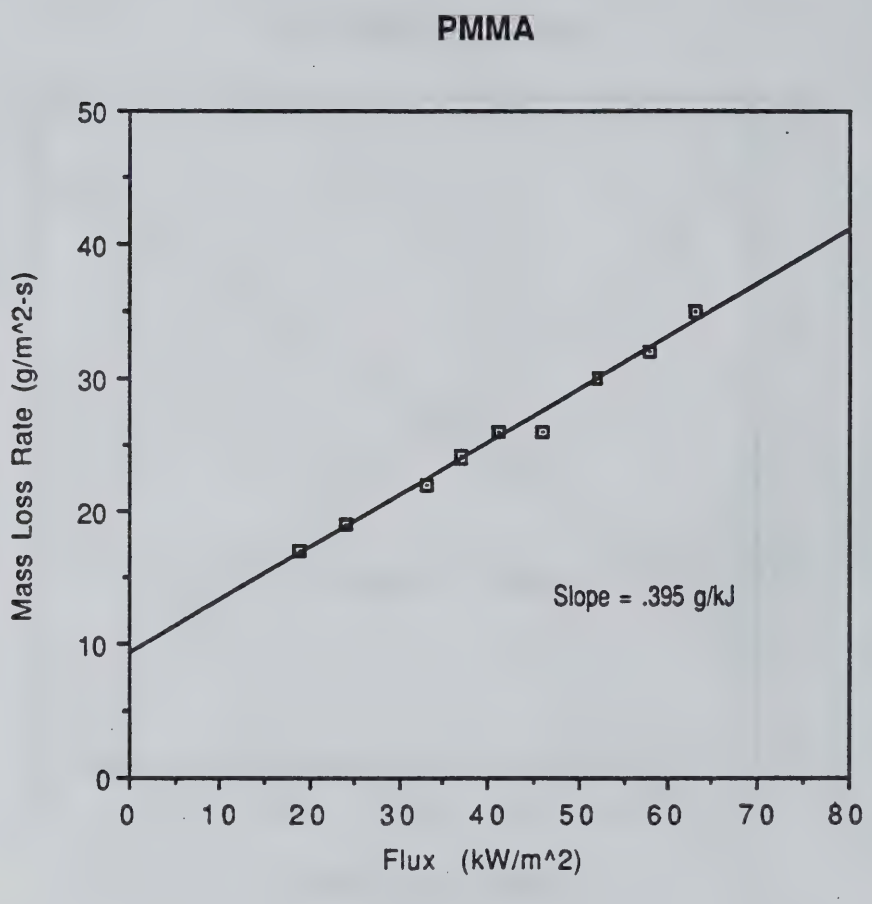

Figure 5.12 Steady state mass loss rate of PMMA as a function of external irradiance.

5.2.2 Transient Mass Loss Rate

The mass loss rate per unit area can be calculated using the properties in Tables 5.1 and 5.3 along with equations (4.19) and (4.21). The convective heat transfer coefficient, h_c, was taken to be 0.01 kW/m^2-K (determined from an analysis for natural convection over a flat plate).

Figures 5.13 - 5.18 show the calculated and experimental mass loss rates for Nylon exposed to range of external irradiances from 31 - 80 kW/m^2. It should be noted that at low external heat fluxes there are discrepancies in the calculated versus the experimental ignition times for Nylon 6/6. This can be seen for the exposure to a 31 kW/m^2 irradiance, shown in Figure 5.13. The reason for the discrepancy is that at low heat fluxes ($\dot{q}''_{ext} < 35$ kW/m^2) a bubble formed on the surface of the Nylon sample, thus preventing the release of pyrolisates. Ignition did not occur in these cases until the bubble over the surface broke. This phenomenon was only seen in the Nylon experiments and only at low external heat flux exposures. Once the Nylon samples ignited they quickly reached a steady state burning rate. While the Nylon was burning small bubbles from the surface could be seen bursting and burning in the air near the sample. With the exception of the erroneous ignition time shown in Figure 5.13, the calculated mass loss rate results for Nylon are in good agreement with the experimental data.

The quick rise to a steady burning rate after ignition, as well as an approximately constant flame height, which is much taller than the top of the cone heater, is indicative of the burning behavior of all three of the thermoplastic materials tested. Polyethylene and Polypropylene both seemed to become a pool of liquid inside of the aluminum foil while the samples were undergoing steady burning. In some instances the material could be seen boiling inside of the flame.

Calculated and experimental mass loss rates for Polyethylene exposed to external

irradiances ranging from 36 - 87 kW/m^2 are shown in Figures 5.19 - 5.23. Fluctuations can be seen in some of the Polyethylene experimental data. The exact reason for the fluctuations is unknown, but it is assumed that they were caused by currents in the lab causing bouncing of the load cell. Despite the fluctuations, the calculated mass loss rate results for Polyethylene appear to be in good agreement with the experimental data.

Calculated and experimental mass loss rates for Polypropylene exposed to external irradiances ranging from 27 - 65 kW/m^2 are shown in Figures 5.24 - 5.30. The calculated mass loss rate results appear to be in good agreement with the experimental data.

Calculated and experimental mass loss rates for PMMA exposed to external irradiances of 25, 50, and 75 kW/m^2 are shown in Figures 5.31 - 5.33, respectively.

It should be noted that in Figures 5.17, 5.21, 5.22, 5.23, 5.28, and 5.30, the mass loss rate rises above the steady value after some duration. This rise in mass loss rate is caused by an increase in temperature of the material associated with the fact that there is only a fraction of the steady state penetration depth remaining and subsequently less material is being heated. Because the sample is insulated with Kaowool on the backside, little or no heat is lost through the back, and consequently the mass loss rate increases. This phenomenon is expected to have been present in all of the experiments, prior to burnout, should the test have been allowed to proceed long enough.

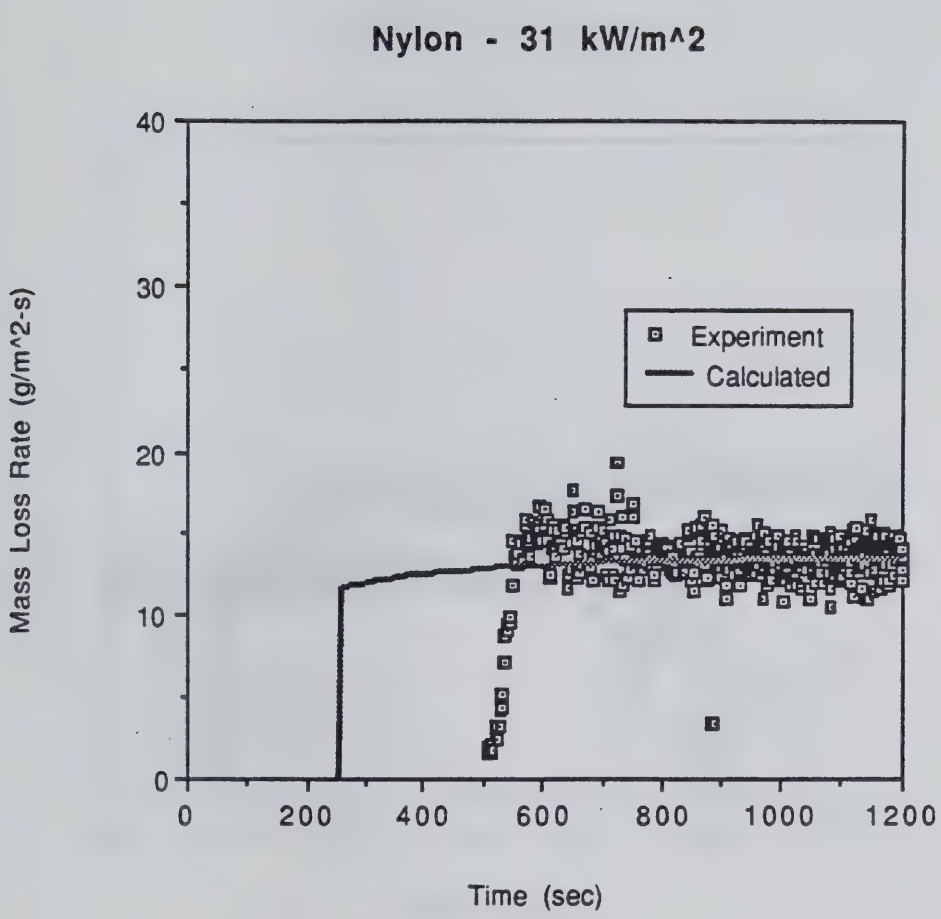

Figure 5.13 Calculated and experimental transient mass loss rate of Nylon with a 31 kW/m^2 external irradiance.

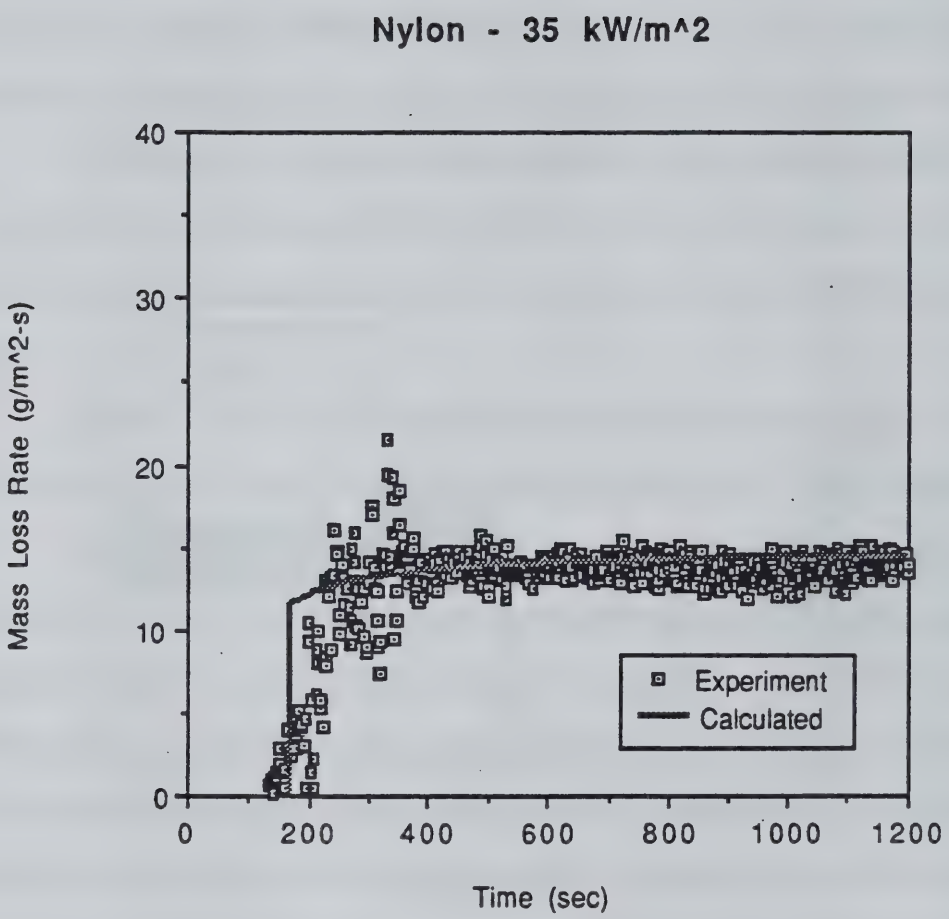

Figure 5.14 Calculated and experimental transient mass loss rate of Nylon with a 35 kW/m^2 external irradiance.

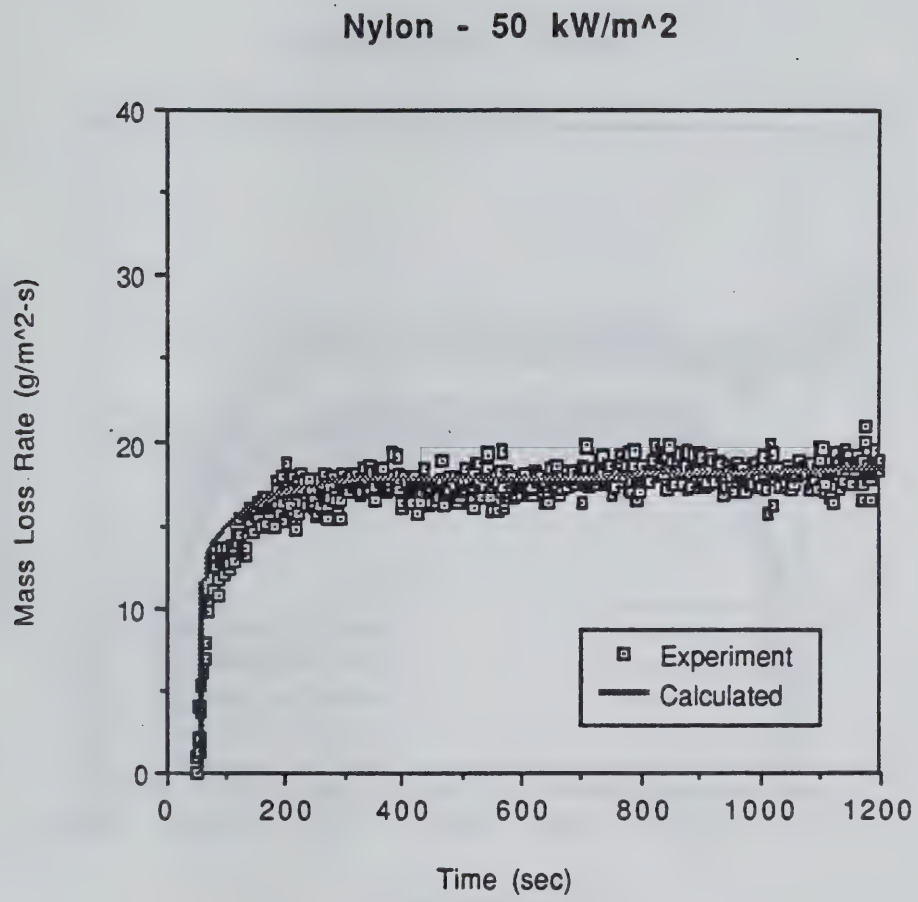

Figure 5.15 Calculated and experimental transient mass loss rate of Nylon with a 50 kW/m^2 external irradiance.

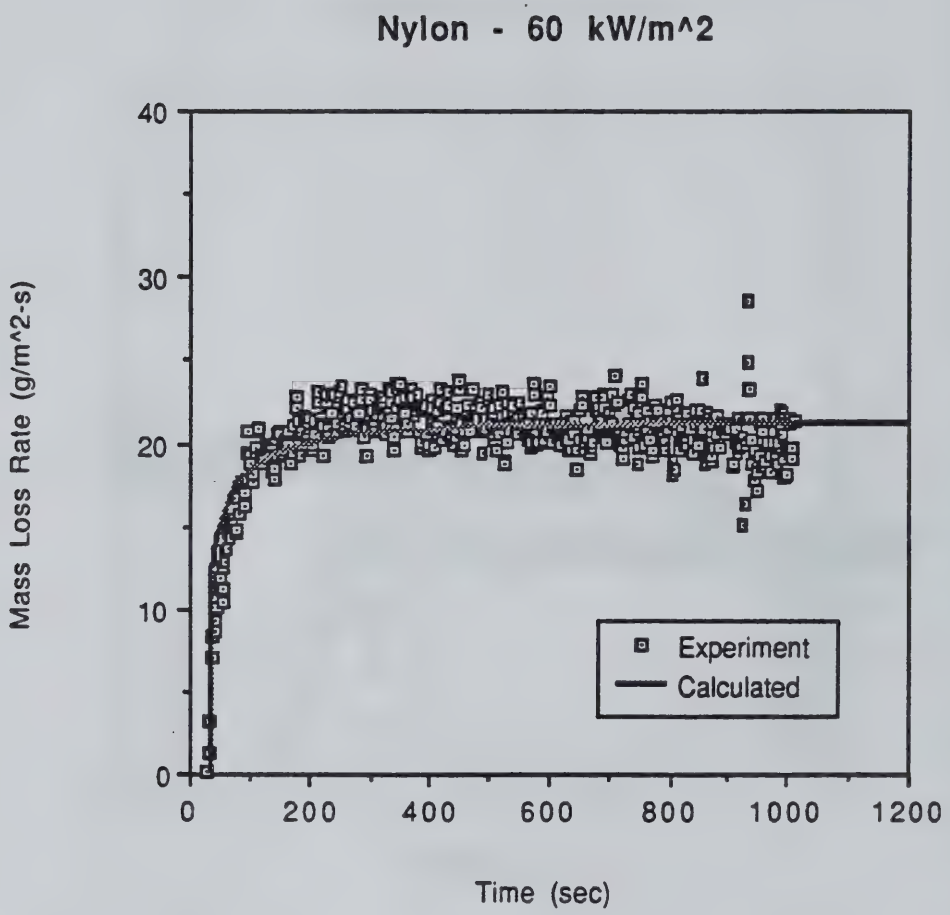

Figure 5.16 Calculated and experimental transient mass loss rate of Nylon with a 60 kW/m^2 external irradiance.

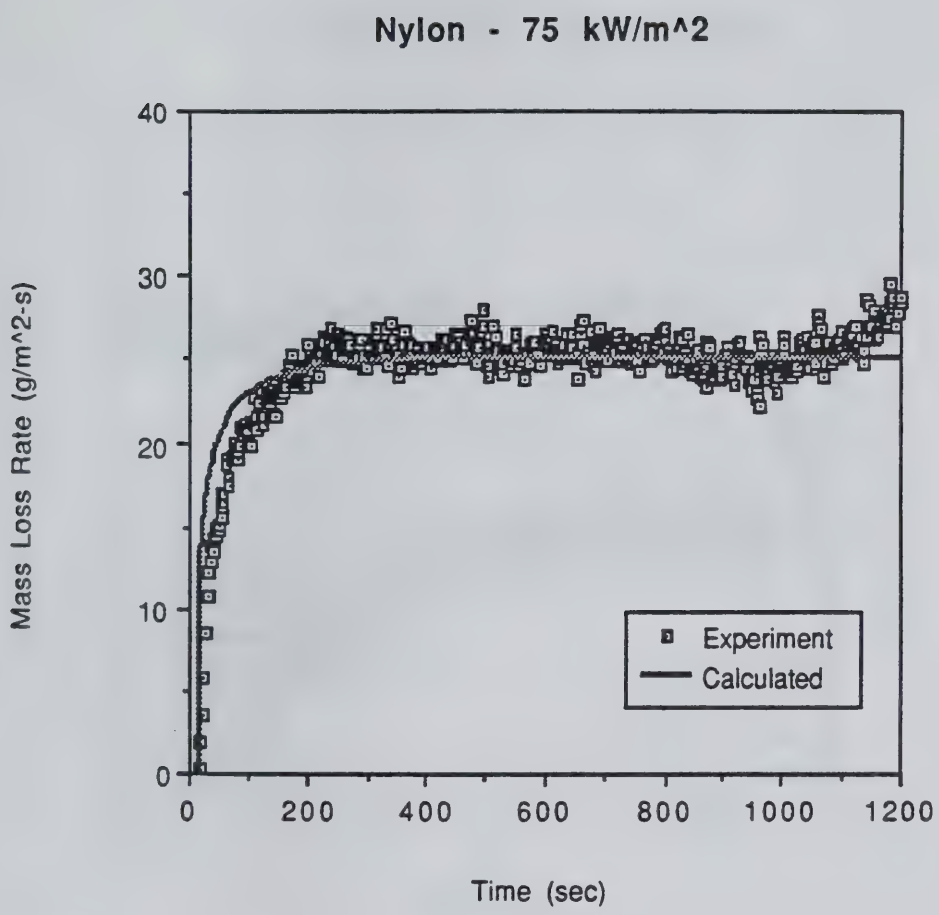

Figure 5.17 Calculated and experimental transient mass loss rate of Nylon with a 75 kW/m^2 external irradiance.

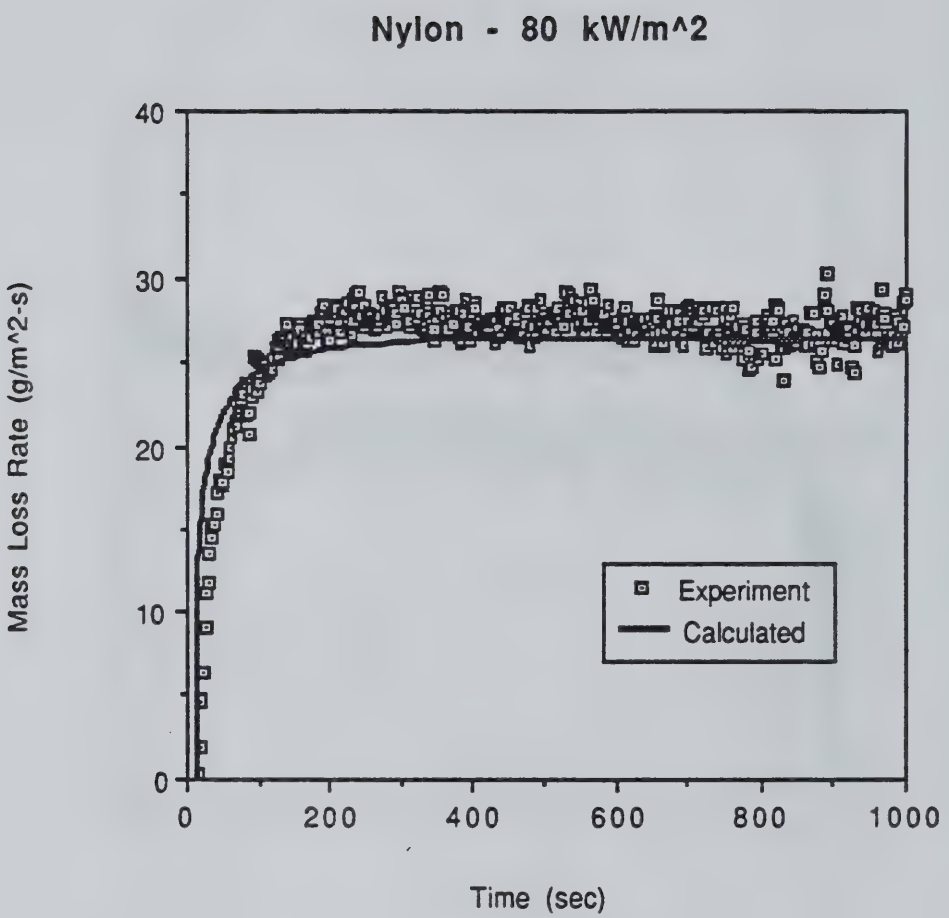

Figure 5.18 Calculated and experimental transient mass loss rate of Nylon with an 80 kW/m^2 external irradiance.

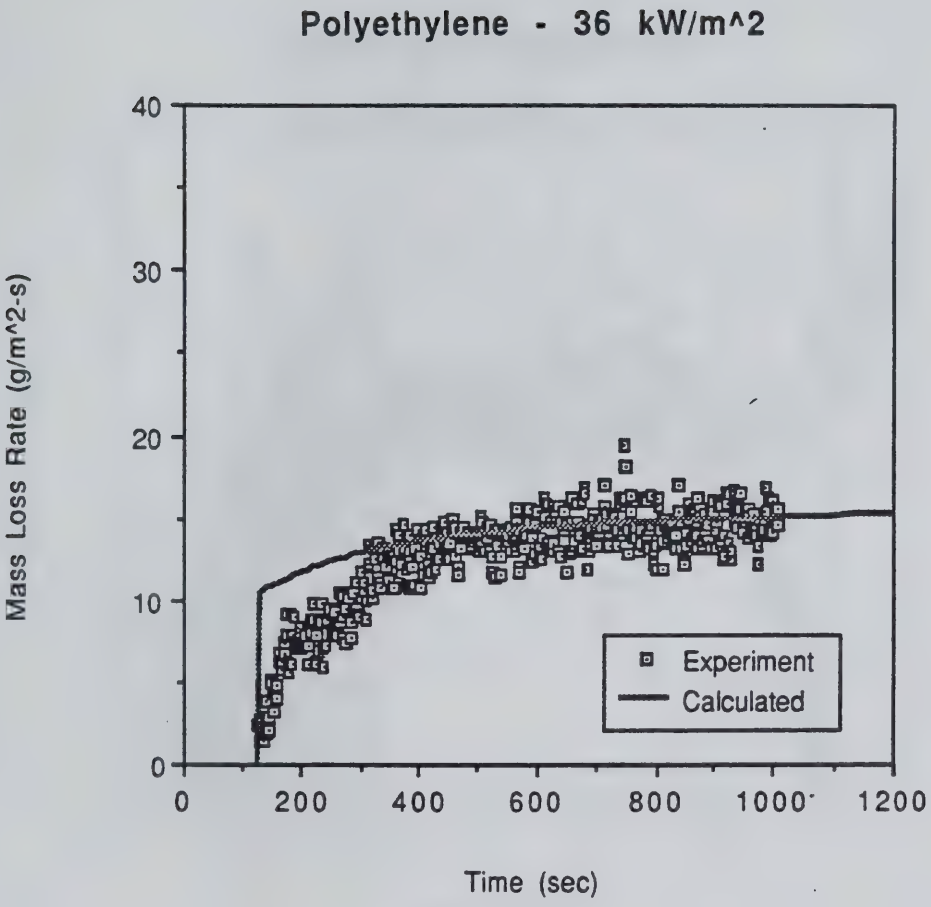

Figure 5.19 Calculated and experimental transient mass loss rate of Polyethylene with a 36 kW/m^2 external irradiance.

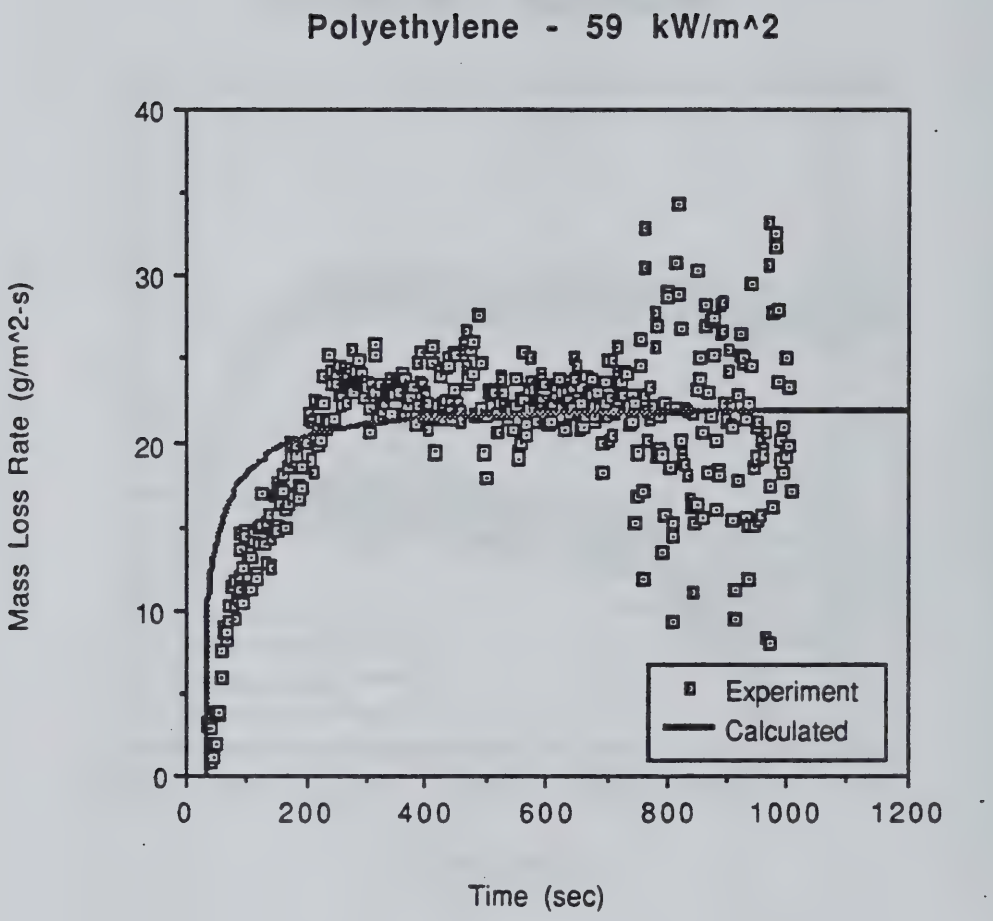

Figure 5.20 Calculated and experimental transient mass loss rate of Polyethylene with a 59 kW/m^2 external irradiance.

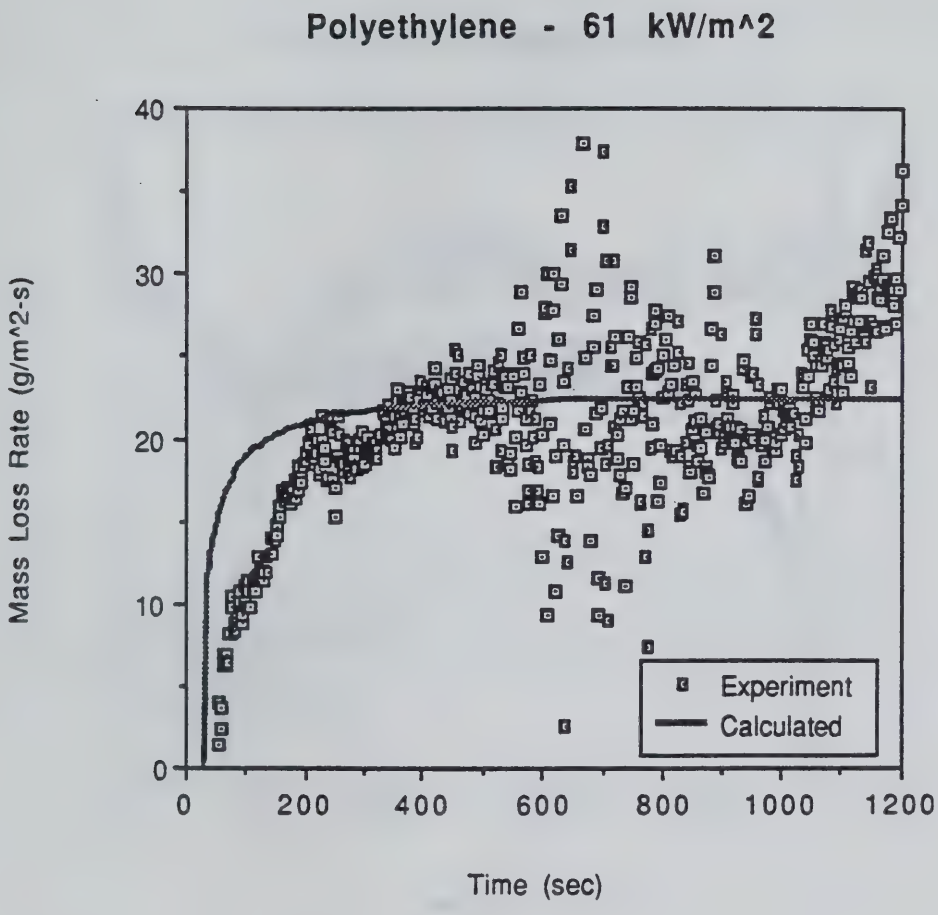

Figure 5.21 Calculated and experimental transient mass loss rate of Polyethylene with a 61 kW/m^2 external irradiance.

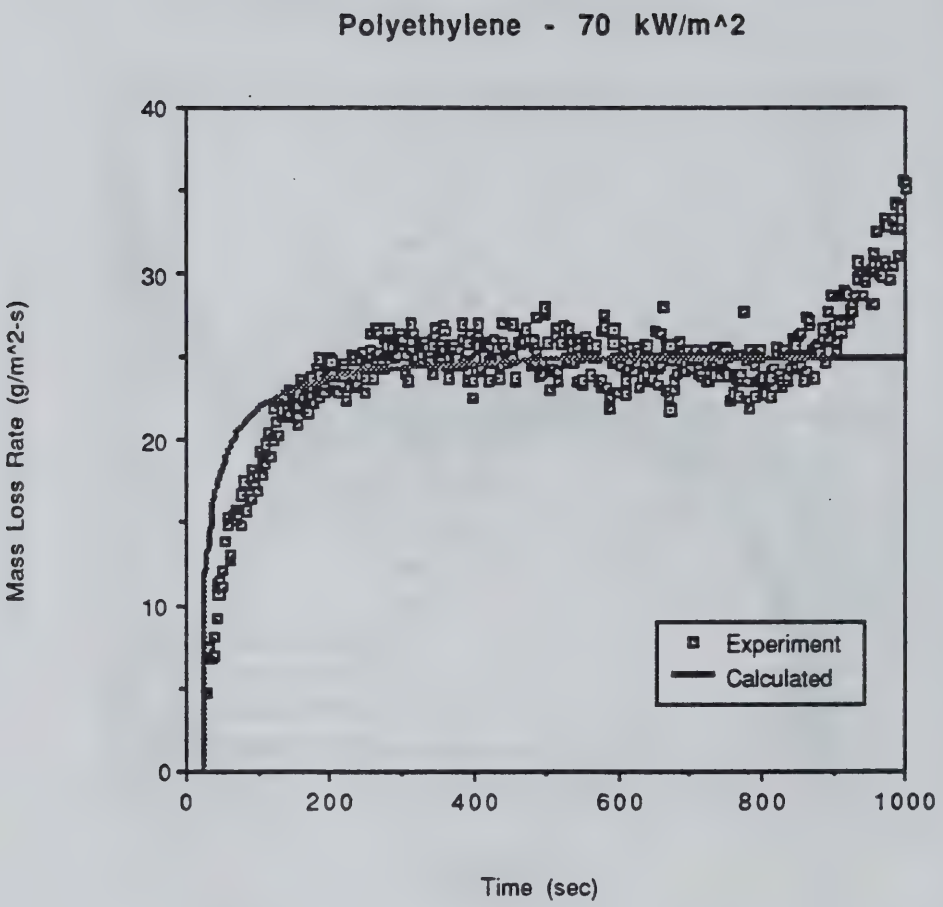

Figure 5.22 Calculated and experimental transient mass loss rate of Polyethylene with a 70 kW/m^2 external irradiance.

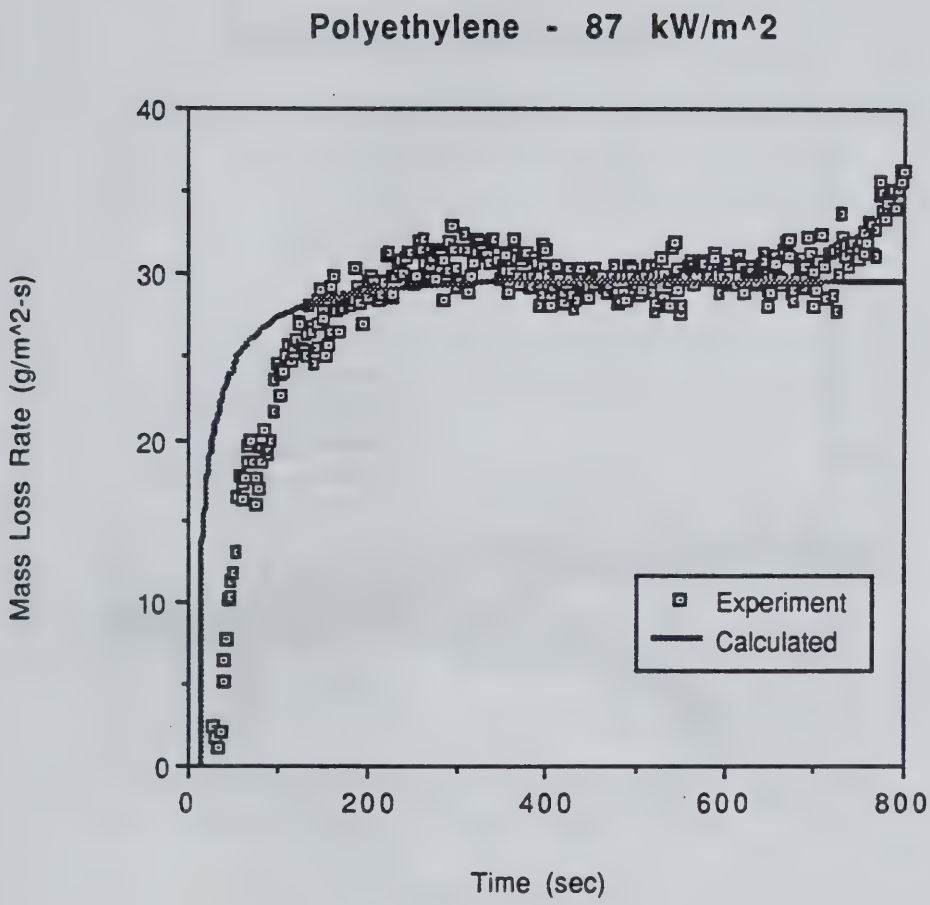

Figure 5.23 Calculated and experimental transient mass loss rate of Polyethylene with an 87 kW/m^2 external irradiance.

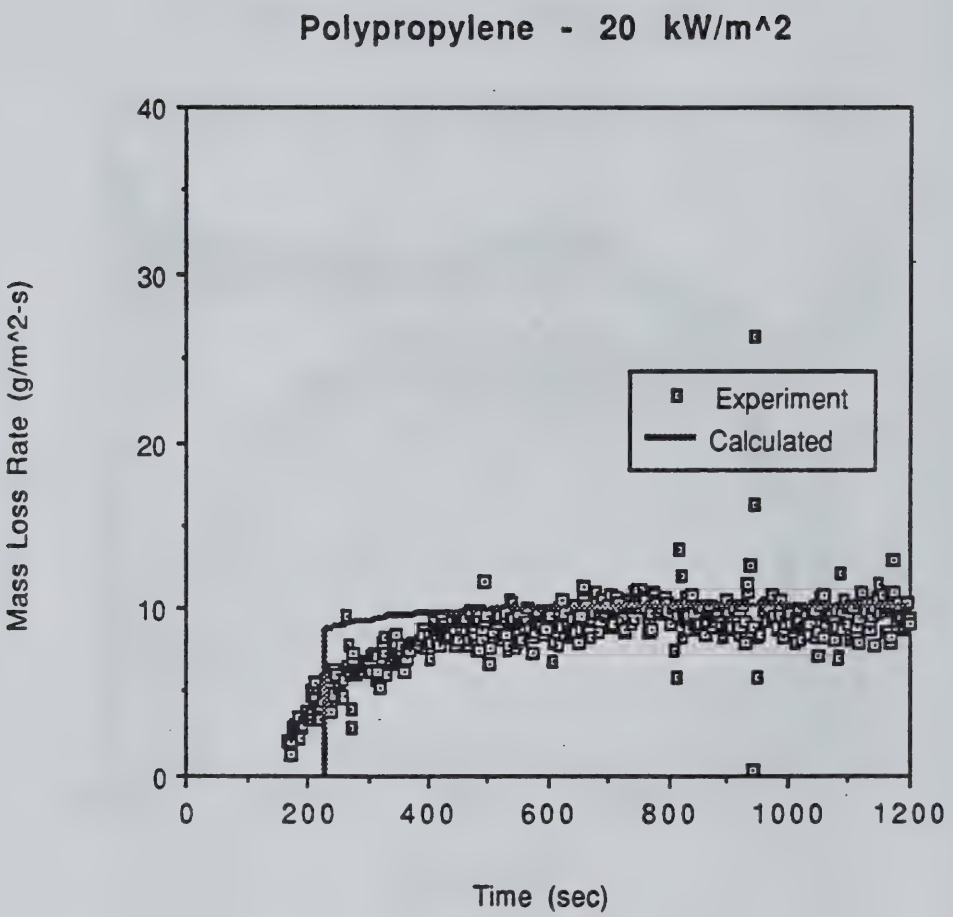

Figure 5.24 Calculated and experimental transient mass loss rate of Polypropylene with a 20 kW/m^2 external irradiance.

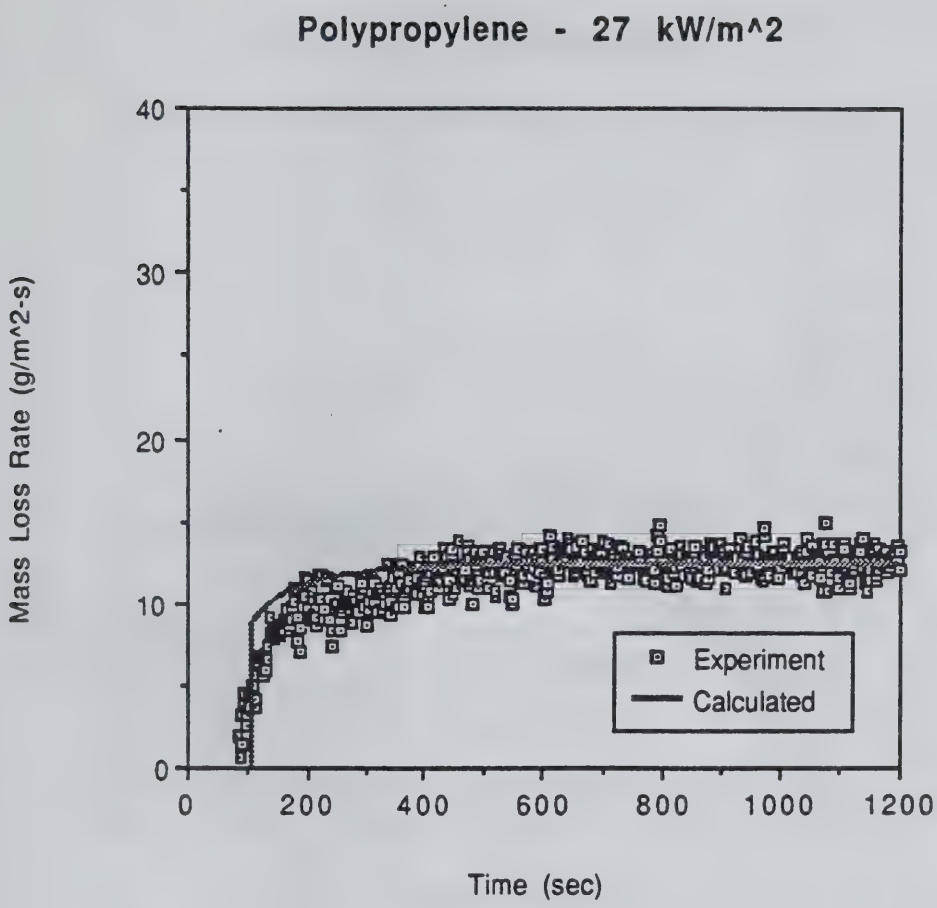

Figure 5.25 Calculated and experimental transient mass loss rate of Polypropylene with a 27 kW/m^2 external irradiance.

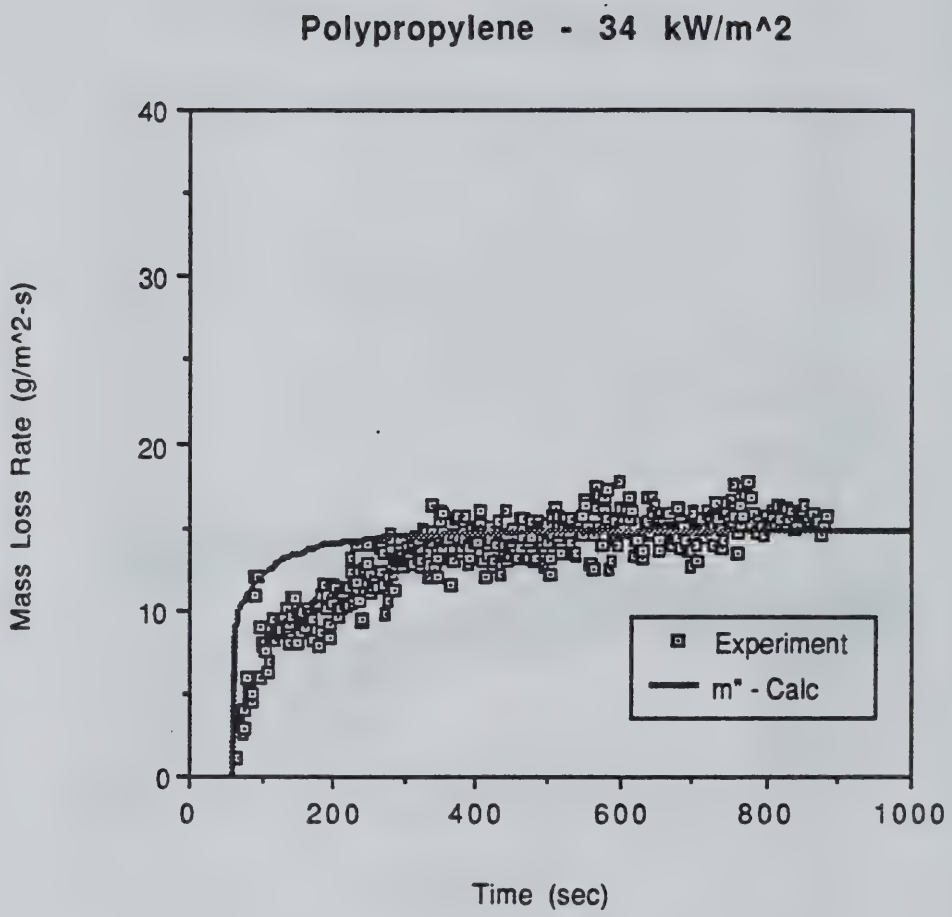

Figure 5.26 Calculated and experimental transient mass loss rate of Polypropylene with a 34 kW/m^2 external irradiance.

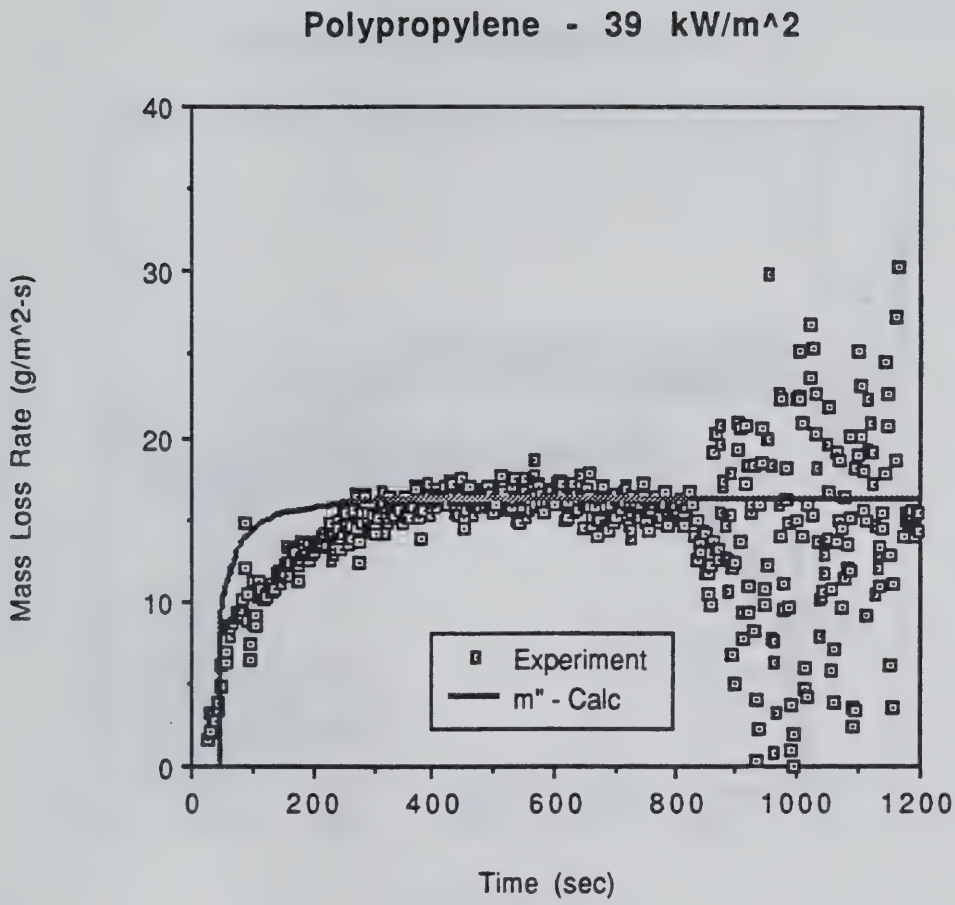

Figure 5.27 Calculated and experimental transient mass loss rate of Polypropylene with a 39 kW/m^2 external irradiance.

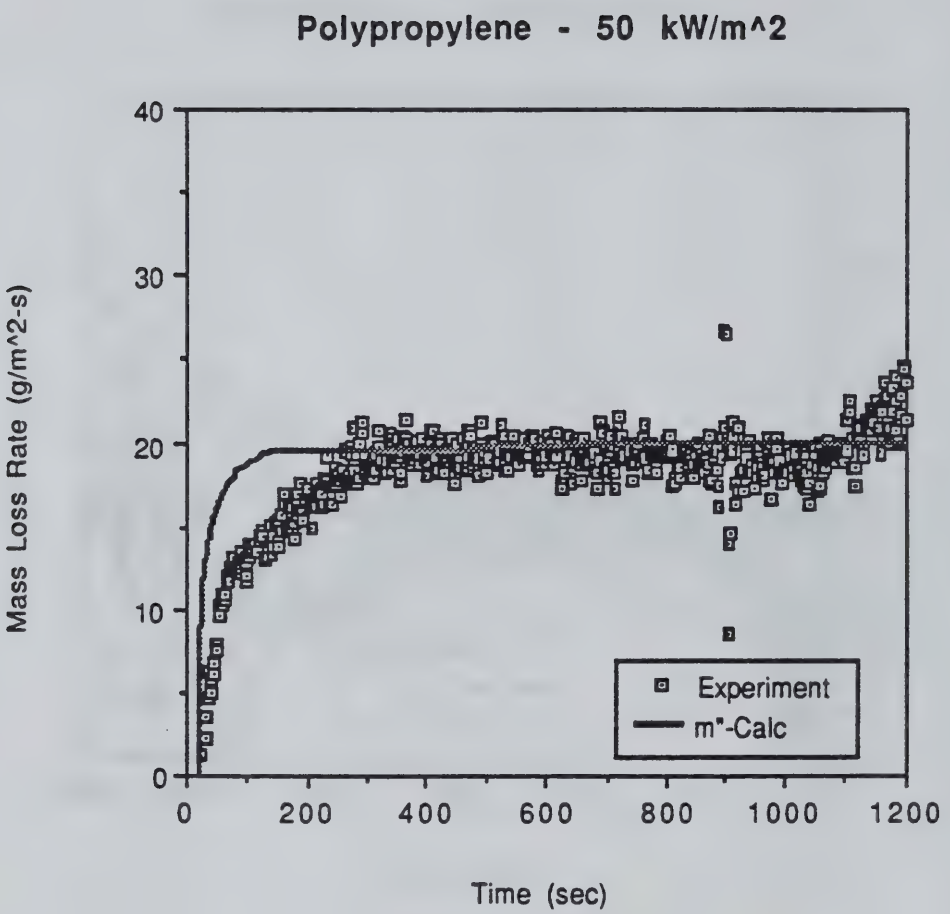

Figure 5.28 Calculated and experimental transient mass loss rate of Polypropylene with a 50 kW/m^2 external irradiance.

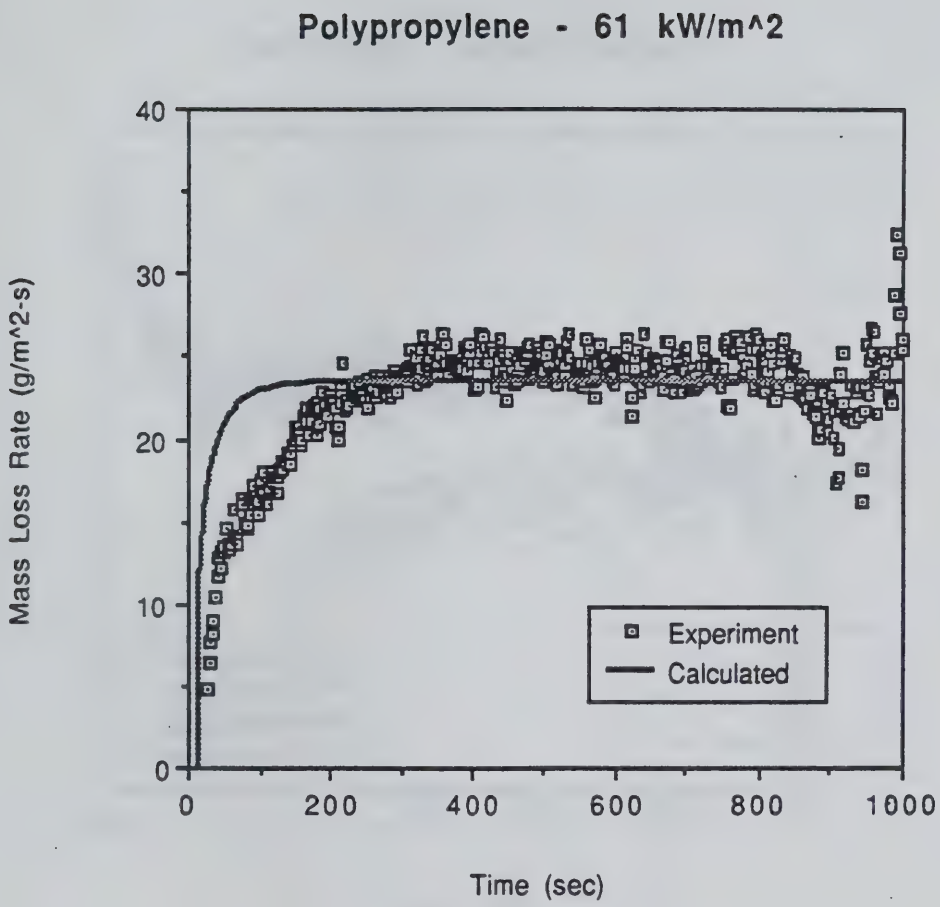

Figure 5.29 Calculated and experimental transient mass loss rate of Polypropylene with a 61 kW/m^2 external irradiance.

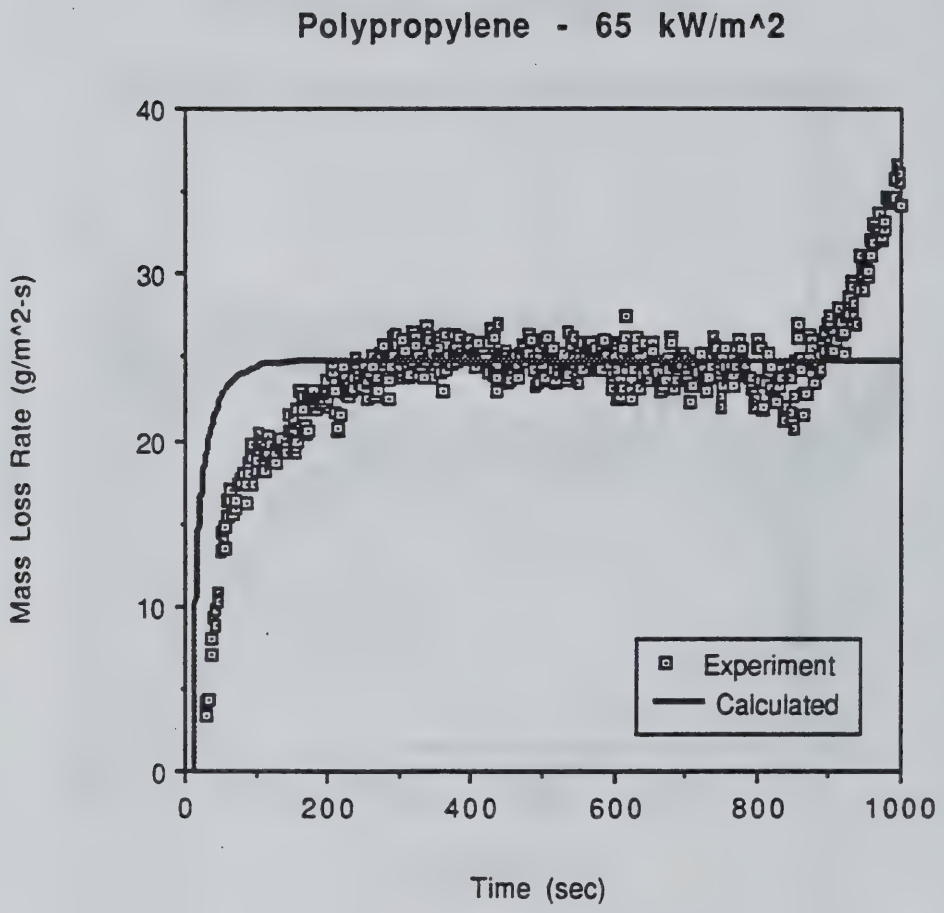

Figure 5.30 Calculated and experimental transient mass loss rate of Polypropylene with a 65 kW/m^2 external irradiance.

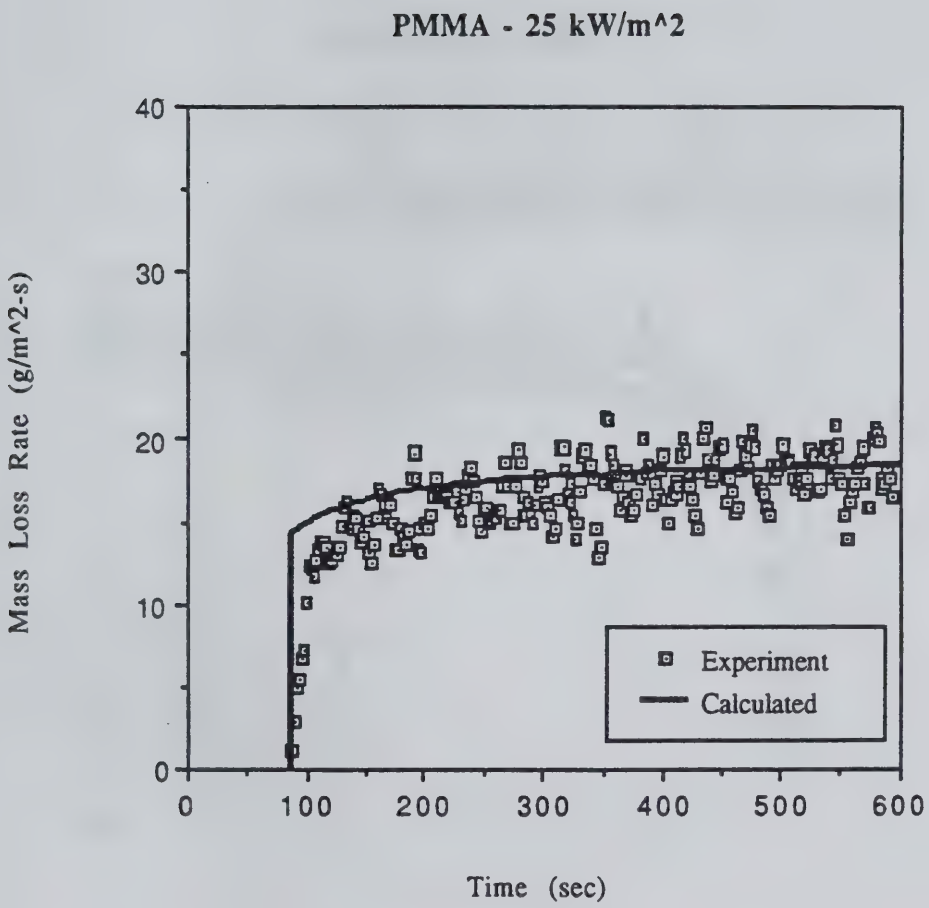

Figure 5.31 Calculated and experimental transient mass loss rate of PMMA with a 25 kW/m^2 external irradiance.

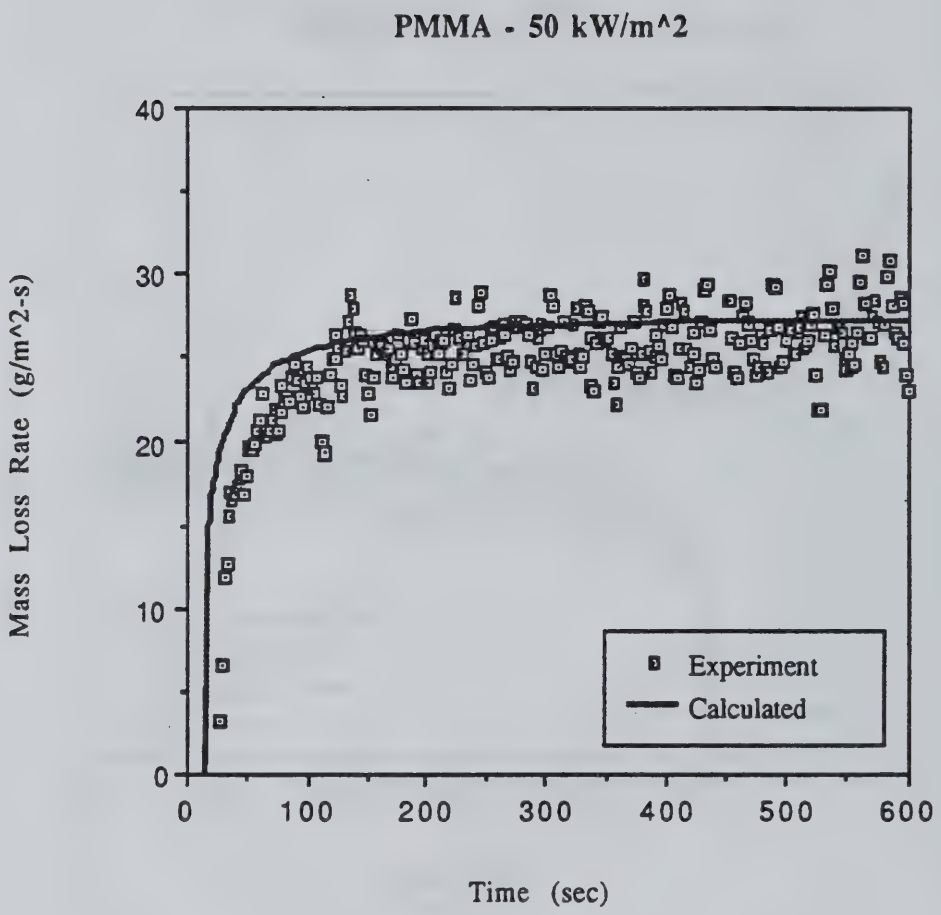

Figure 5.32 Calculated and experimental transient mass loss rate of PMMA with a 50 kW/m^2 external irradiance.

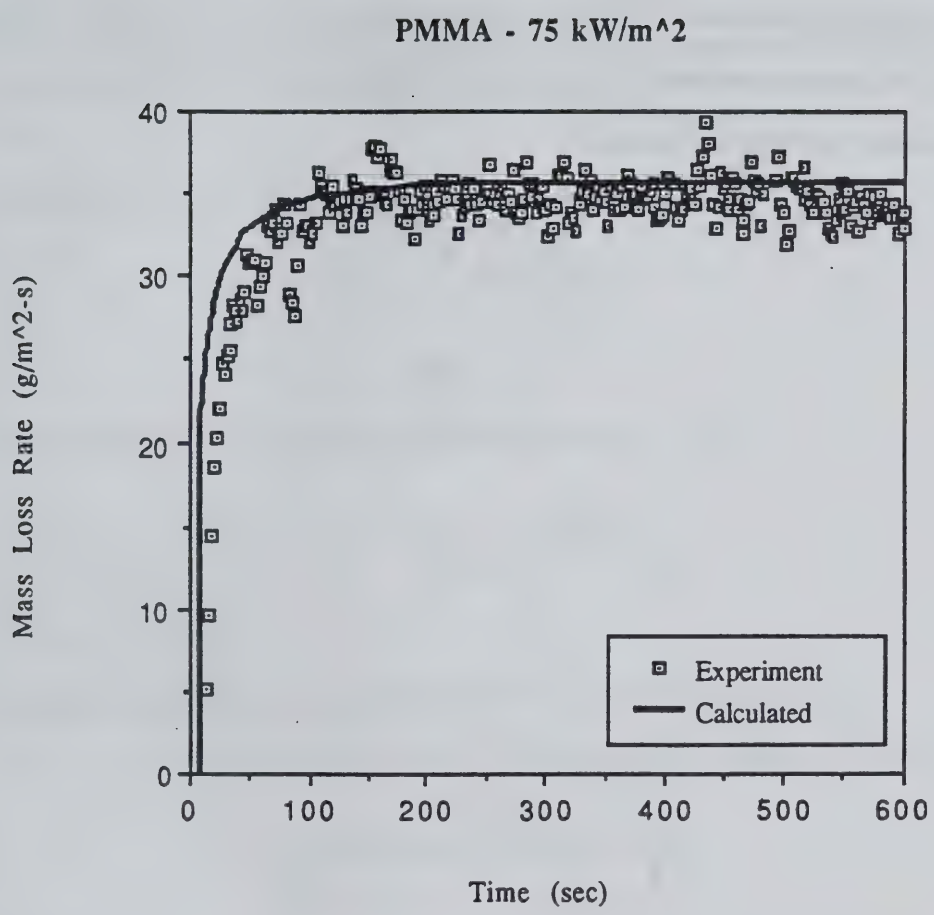

Figure 5.33 Calculated and experimental transient mass loss rate of PMMA with a 75 kW/m^2 external irradiance.

CHAPTER 6 DIMENSIONLESS FORM OF SOLUTION FOR THERMOPLASTICS

An alternate way of examining the thermoplastic solution is to look at it in terms of dimensionless parameters. The governing equation for the calculation of the ignition time and the burning rate can be represented in dimensionless form. The following dimensionless variables are defined:

$$y = \frac{\dot{m}''L}{\dot{q}''} \tag{6.1}$$

$$\phi = \frac{\Delta H_v}{L} \tag{6.2}$$

$$x = \frac{\delta}{\delta_s} \tag{6.3}$$

Using Equations (4.20a), (4.22), and (6.2) it can be shown that

$$\frac{\delta_{ig}}{\delta_s} = \sqrt{1.5\tau_{ig}} = (1-\phi)\left(\frac{\dot{q}_+''}{\dot{q}_-''}\right) \tag{6.4}$$

Using these dimensionless parameters, from equations (6.1) - (6.3), the mass loss rate per unit area, given by equation (4.19), is represented as,

$$y = 1 - \left(\frac{1}{\phi} - 1\right)\left(\frac{1}{x} - 1\right) \tag{6.5}$$

The dimensionless time is given as,

$$\tau = \frac{4\alpha t}{\delta_s^2}. \qquad (6.10)$$

δ is a parameter that physically represents the thermal penetration into a semi-infinite solid.

The steady state value, from equation (4.22), is given as,

$$\delta_s = \frac{2kL}{c\dot{q}_+''}. \qquad (6.7)$$

The δ at ignition, from equation (4.20a) is given as,

$$\delta_{ig} = \sqrt{6\alpha t_{ig}}. \qquad (6.8)$$

The time for ignition, from equation (4.10) is approximately given by

$$t_{ig} = \frac{2}{3} k\rho c \frac{(T_{ig} - T_0)^2}{\dot{q}_-''^2}. \qquad (6.9)$$

Subsequently, the dimensionless time after ignition , from equation (4.21) is,

$$\tau - \tau_{ig} = \frac{2\phi}{3}\left[\left(\sqrt{1.5\tau_{ig}} - x\right) - \ln\left(\frac{1-x}{1-\sqrt{1.5\tau_{ig}}}\right)\right]. \qquad (6.6)$$

The net surface heat flux, $\dot{q}''$, changes at ignition to account for the flame heat flux,

$\dot{q}''_{fl}$, which includes both radiative and convective fluxes to the surface. For our application, it has been shown that this net flame flux is constant for each thermoplastic

regardless of time and external irradiance [8]. The net surface heat flux before ignition is represented as,

$$\dot{q}^{"}_{-} = \dot{q}^{"}_{ext} - h_c(T_{ig} - T_0) - \sigma T_s^4, \text{ for } t \le t_{ig} \tag{6.11}$$

and after ignition as,

$$\dot{q}^{"}_{+} = \dot{q}^{"}_{ext} + \dot{q}^{"}_{fl} - \sigma T_{ig}^4, \text{ for } t > t_{ig}. \tag{6.12}$$

Figure 6.1 shows a plot of dimensionless mass loss rate versus dimensionless time after ignition for a constant value of external heat flux over the flame heat flux ($\dot{q}^{"}_{ext}/\dot{q}^{"}_{fl}$ = 1) for the three thermoplastics tested. Similarly , Figures 6.2 and 6.3 show the plots for values of $\dot{q}^{"}_{ext}/\dot{q}^{"}_{fl}$ equal to 2 and 3, respectively. It can be seen from these plots that there are only small variations in the solutions for the different materials for a given value of the ratio of external irradiance to flame heat flux. Figure 6.4 shows a plot of dimensionless mass loss rate versus dimensionless time after ignition for Nylon 6/6 at a number of ratios of external irradiance to flame heat flux. Figure 6.4 shows that the variation in the dimensionless mass loss rate for a given material is dependent on the values of the surface heat flux before and after ignition. However, it can be seen from Figures 6.1 - 6.4 that about 95% of the steady state mass loss rate is reached when the dimensionless time is approximately 0.3 - 0.5. The dimensionless time to ignition is represented by Equations (6.9) and (6.10), such that,

$$\tau_{ig} = \frac{2}{3}(1-\phi)^2\left(\frac{\dot{q}^{"}_{+}}{\dot{q}^{"}_{-}}\right)^2 \tag{6.12}$$

The dimensionless mass loss rate at ignition, which is the y-intercept in Figures 6.1- 6.4, can be represented as,

$$y_{ig} = 1 - \left(\frac{1}{\phi} - 1\right)\left(\frac{1}{(1-\phi)(\dot{q}_+^{-}/\dot{q}_-^{-})} - 1\right) \tag{6.13}$$

Examination of the dimensionless equations shows that,

$$\frac{\dot{m}''L}{\dot{q}_+^{-}} = f\left(\frac{\Delta H_v}{L}, \tau - \tau_{ig}, \frac{\dot{q}_{ext}^{-}}{\dot{q}_f^{-}}, \frac{\sigma T_{ig}^4}{\dot{q}_f^{-}}, \frac{h(T_{ig} - T_0)}{\dot{q}_f^{-}}\right)$$

where,

$$\frac{\Delta H_v}{L}, \frac{\sigma T_{ig}^4}{\dot{q}_f^{-}}, \text{ and } \frac{h(T_{ig} - T_0)}{\dot{q}_f^{-}}$$

are constant for a given material burning in the Cone Calorimeter.

Figures 6.5 - 6.6 show plots of the calculated dimensionless mass loss rate as a function of dimensionless time along with the experimental data for Nylon. Similarly, plots for Polyethylene are shown in Figures 6.7 - 6.8, plots for Polypropylene are shown in Figures 6.9 - 6.10, and plots for PMMA are shown in Figures 6.11 - 6.12. These plots represent an alternative way of viewing the results. The scatter in the data in Figure 6.7 is attributed to bad data from the experiment.

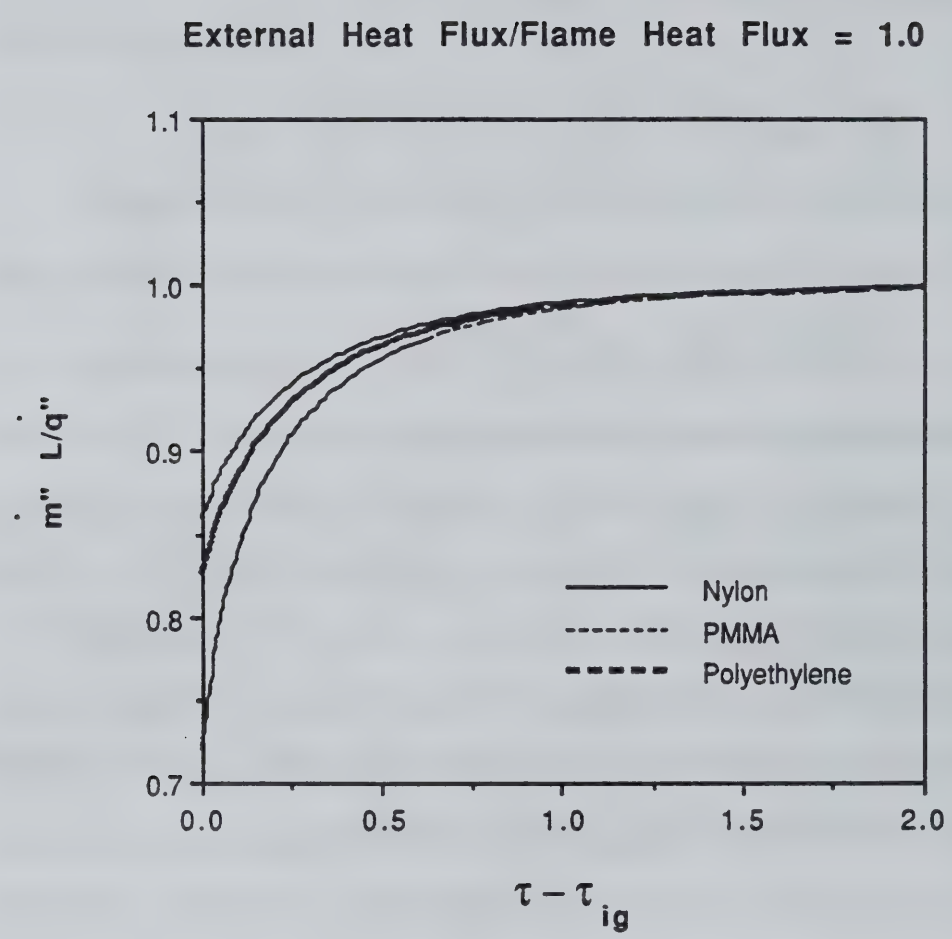

Figure 6.1 Dimensionless mass loss rate as a function of dimensionless time for $\dot{q}''_{ext}/\dot{q}''_{fl} = 1$.

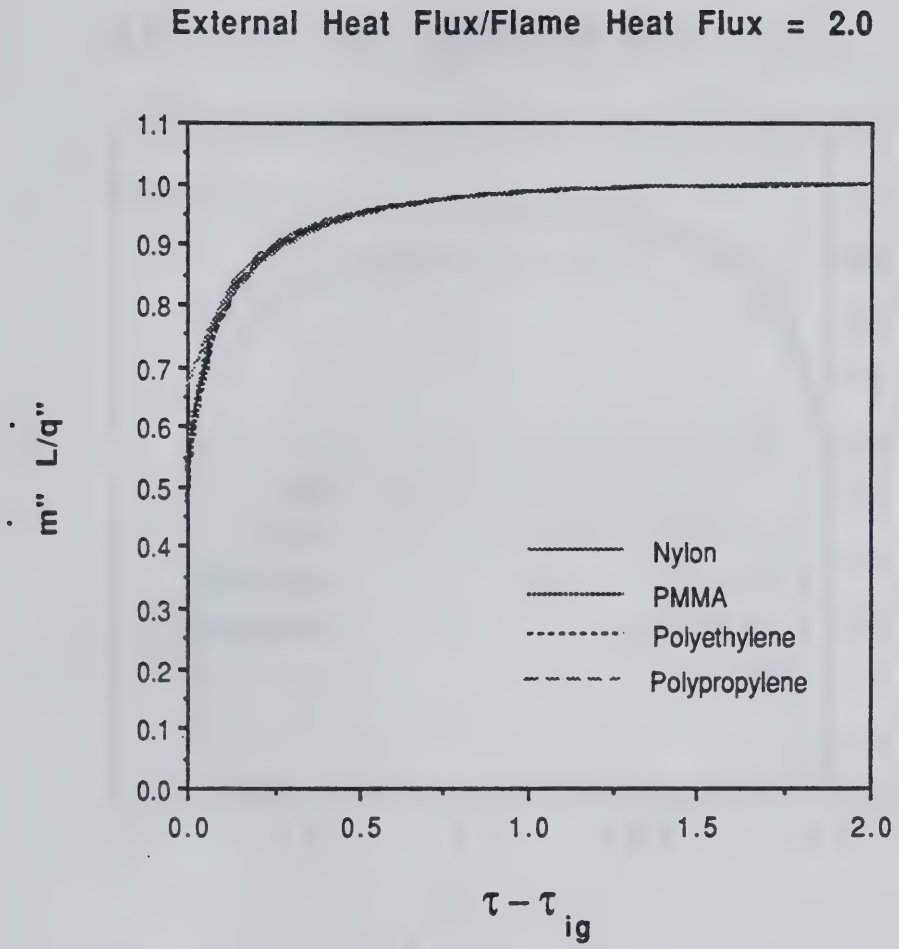

Figure 6.2 Dimensionless mass loss rate as a function of dimensionless time for $\dot{q}''_{ext}/\dot{q}''_{fl} = 2$.

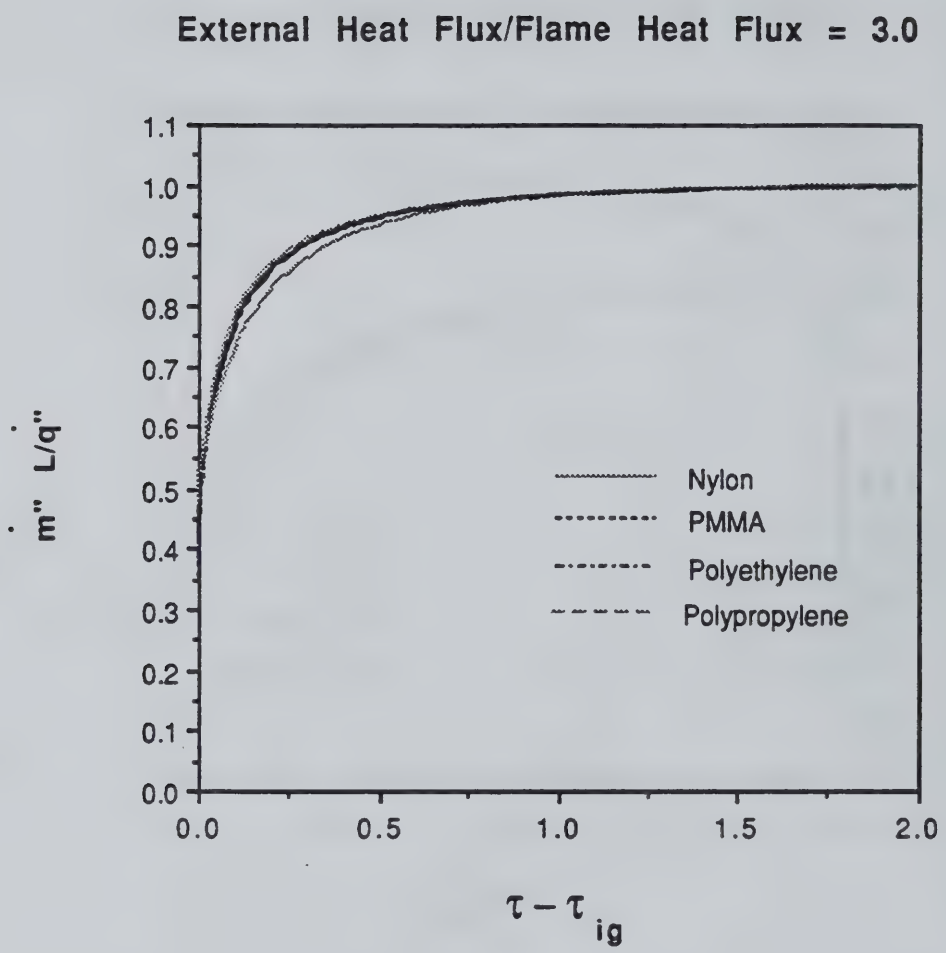

Figure 6.3 Dimensionless mass loss rate as a function of dimensionless time for $\dot{q}''_{ext}/\dot{q}''_{fl} = 3$.

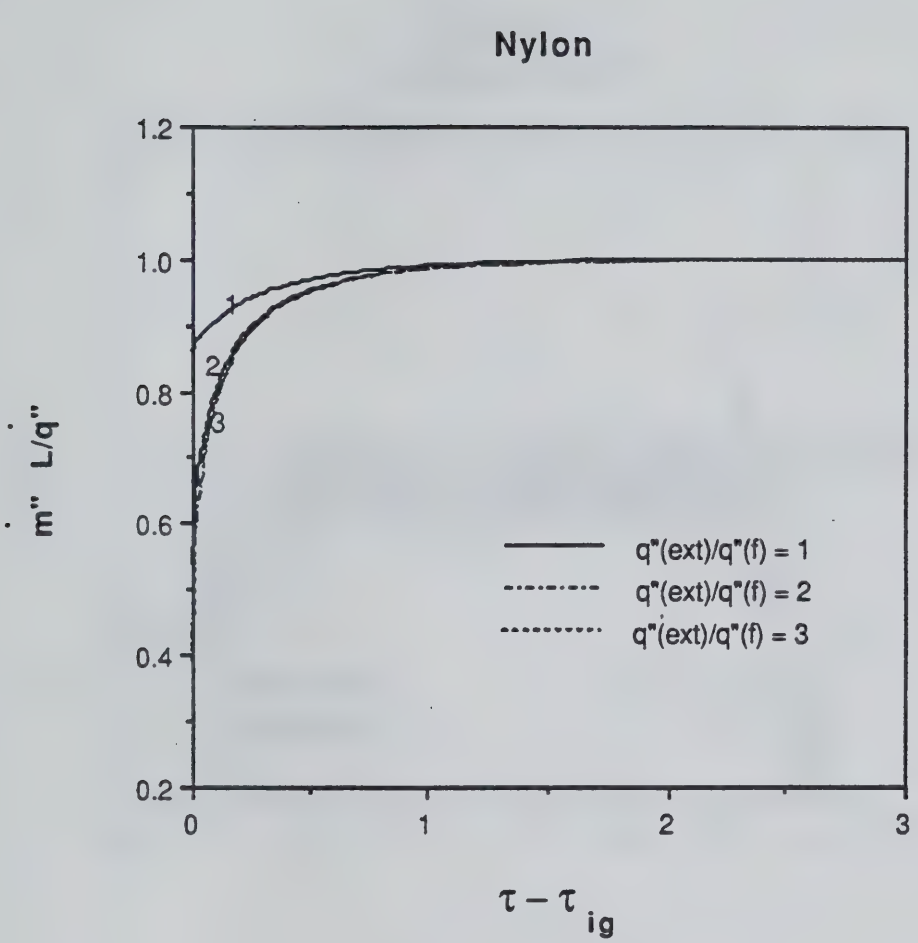

Figure 6.4 Dimensionless mass loss rate as a function of dimensionless time for Nylon.

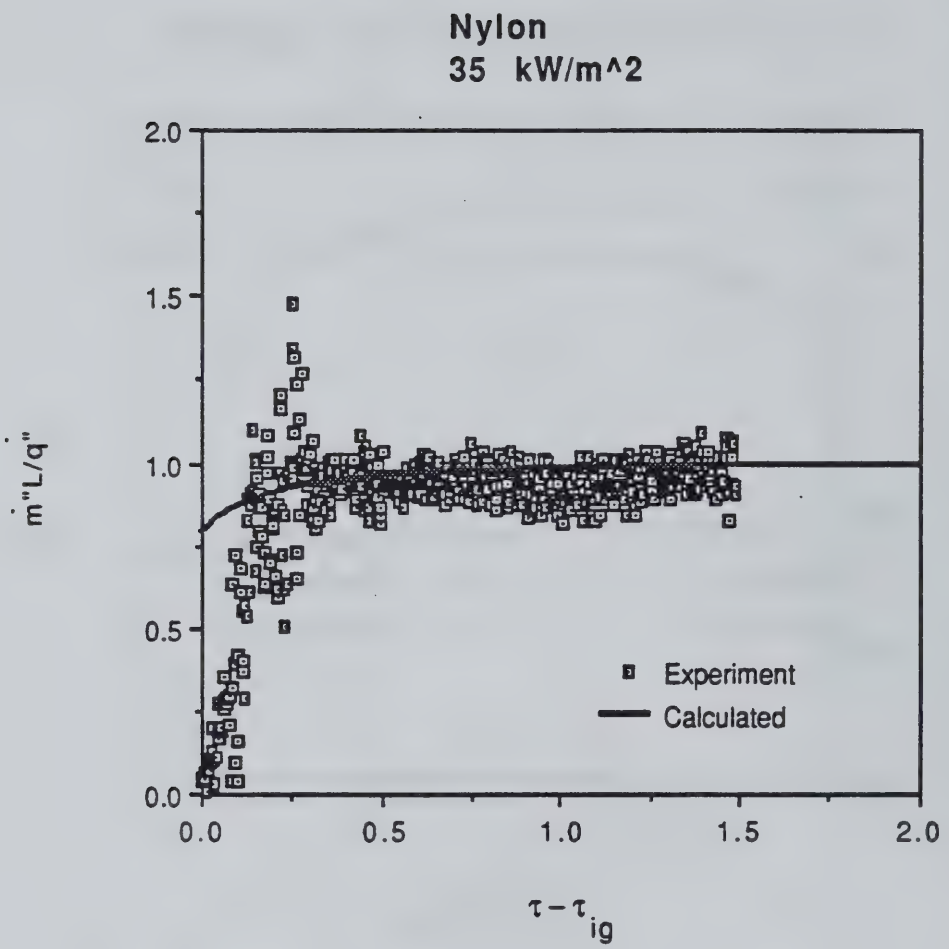

Figure 6.5 Theoretical and experimental dimensionless mass loss rate as a function of dimensionless time for Nylon with a 35 kW/m^2 external irradiance.

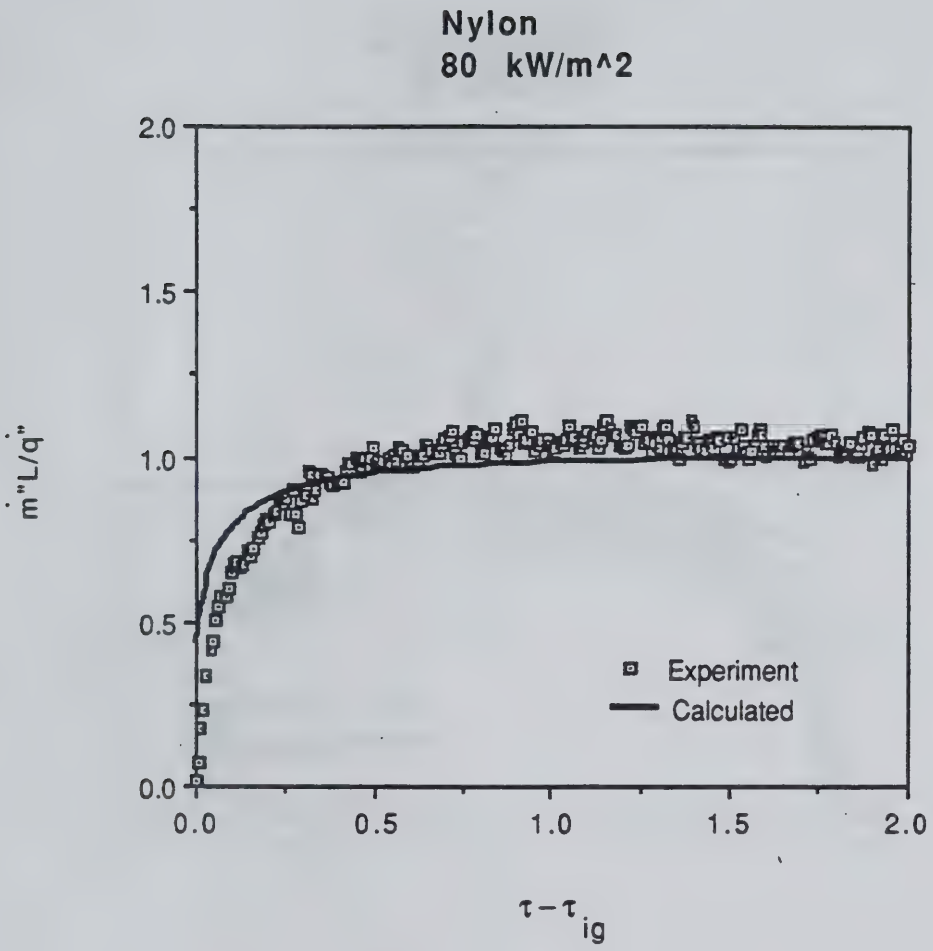

Figure 6.6 Theoretical and experimental dimensionless mass loss rate as a function of dimensionless time for Nylon with an 80 kW/m^2 external irradiance.

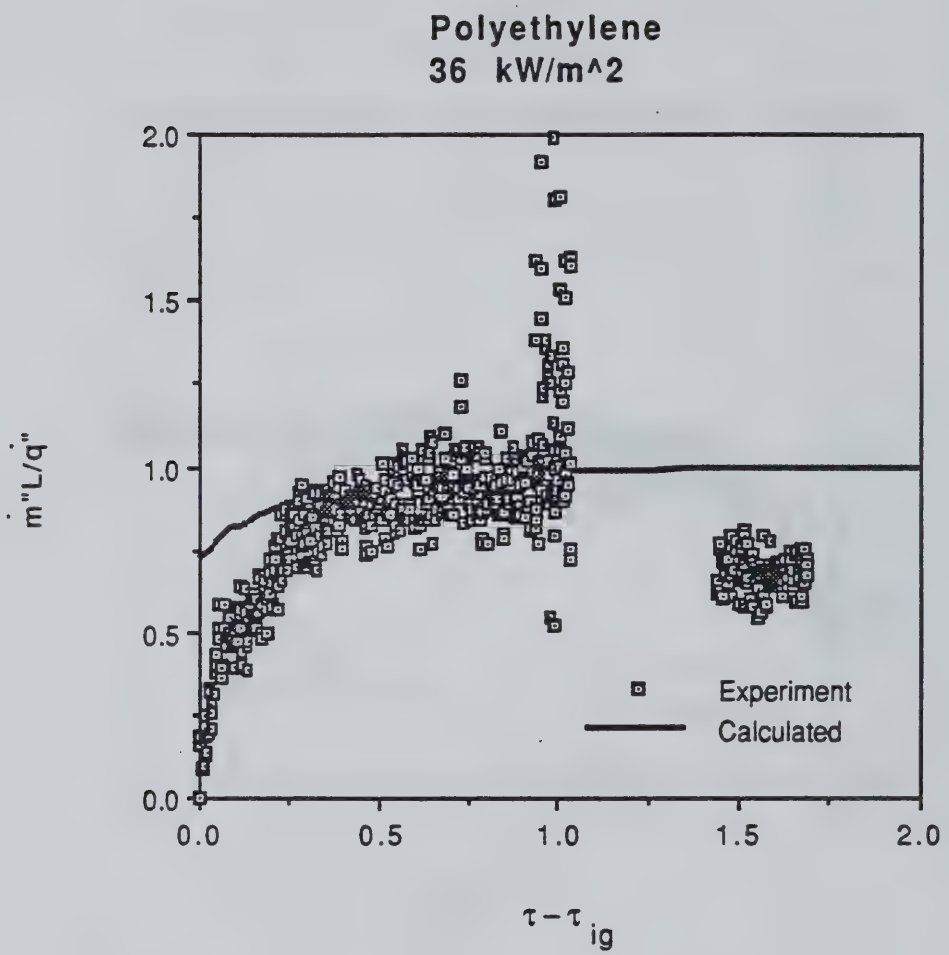

Figure 6.7 Theoretical and experimental dimensionless mass loss rate as a function of dimensionless time for Polyethylene with a 36 kW/m^2 external irradiance.

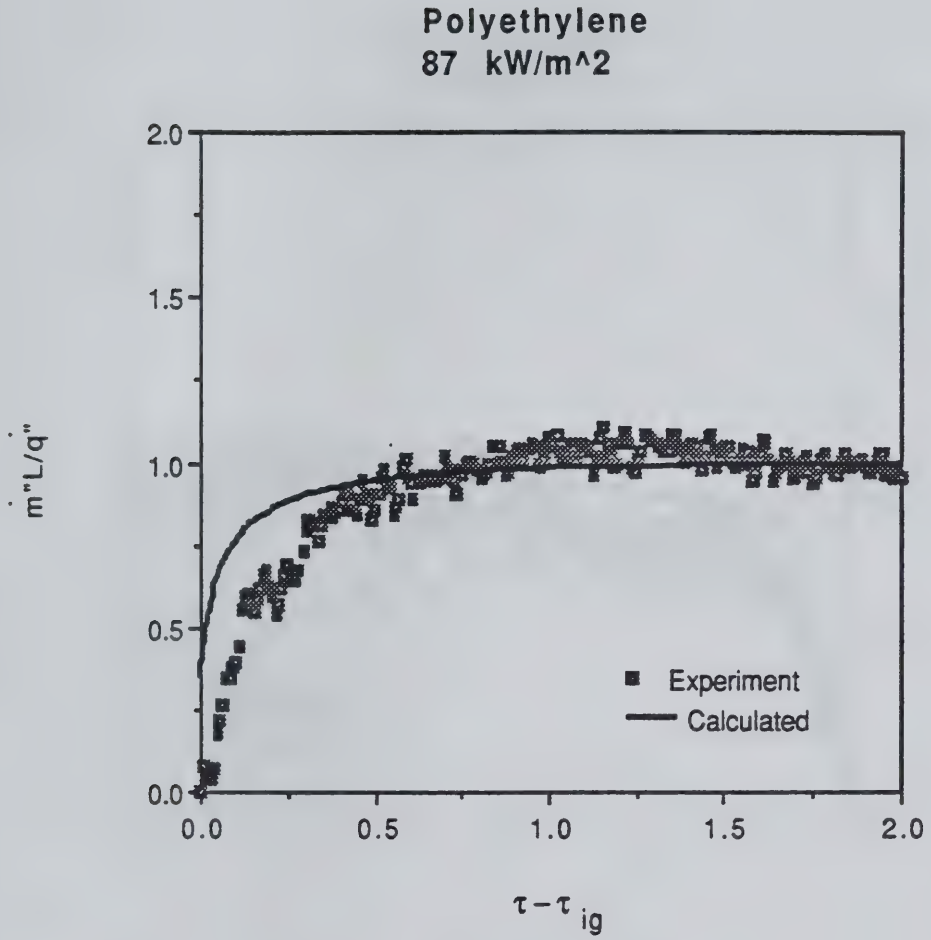

Figure 6.8 Theoretical and experimental dimensionless mass loss rate as a function of dimensionless time for Polyethylene with an 87 kW/m^2 external irradiance.

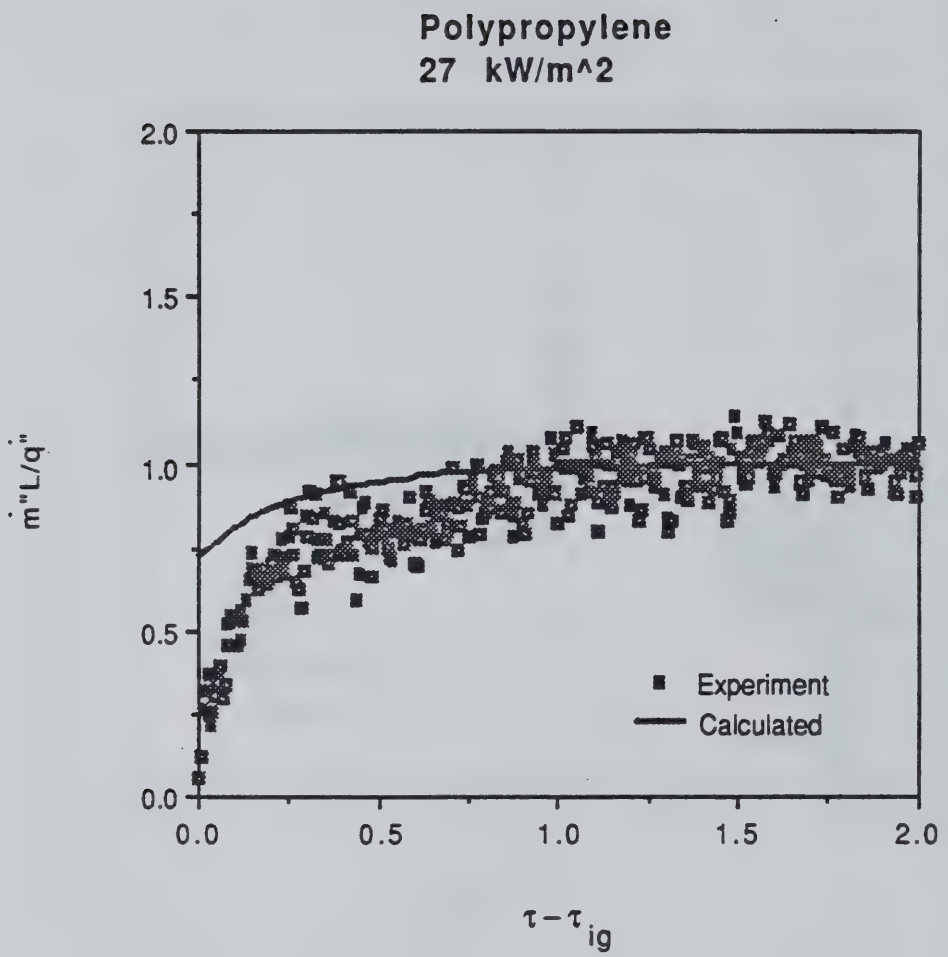

Figure 6.9 Theoretical and experimental dimensionless mass loss rate as a function of dimensionless time for Polypropylene with a 27 kW/m^2 external irradiance.

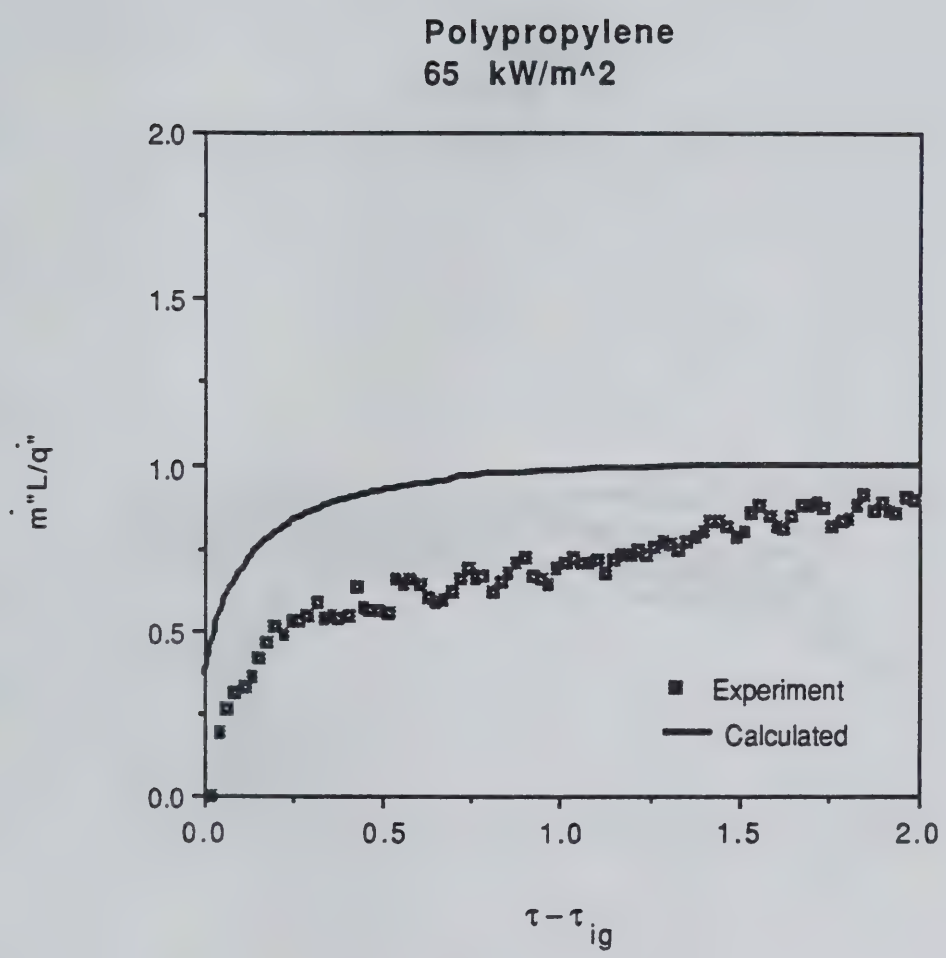

Figure 6.10 Theoretical and experimental dimensionless mass loss rate as a function of dimensionless time for Polypropylene with a 65 kW/m^2 external irradiance.

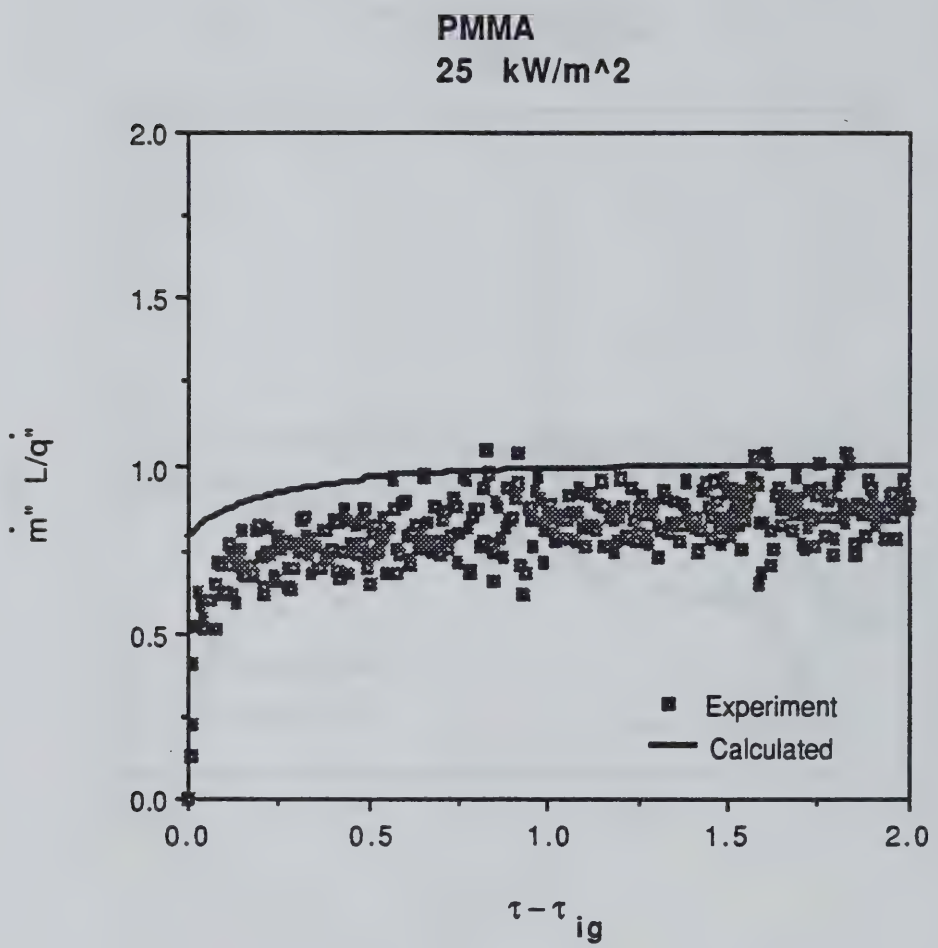

Figure 6.11 Theoretical and experimental dimensionless mass loss rate as a function of dimensionless time for black PMMA with a 25 kW/m^2 external irradiance.

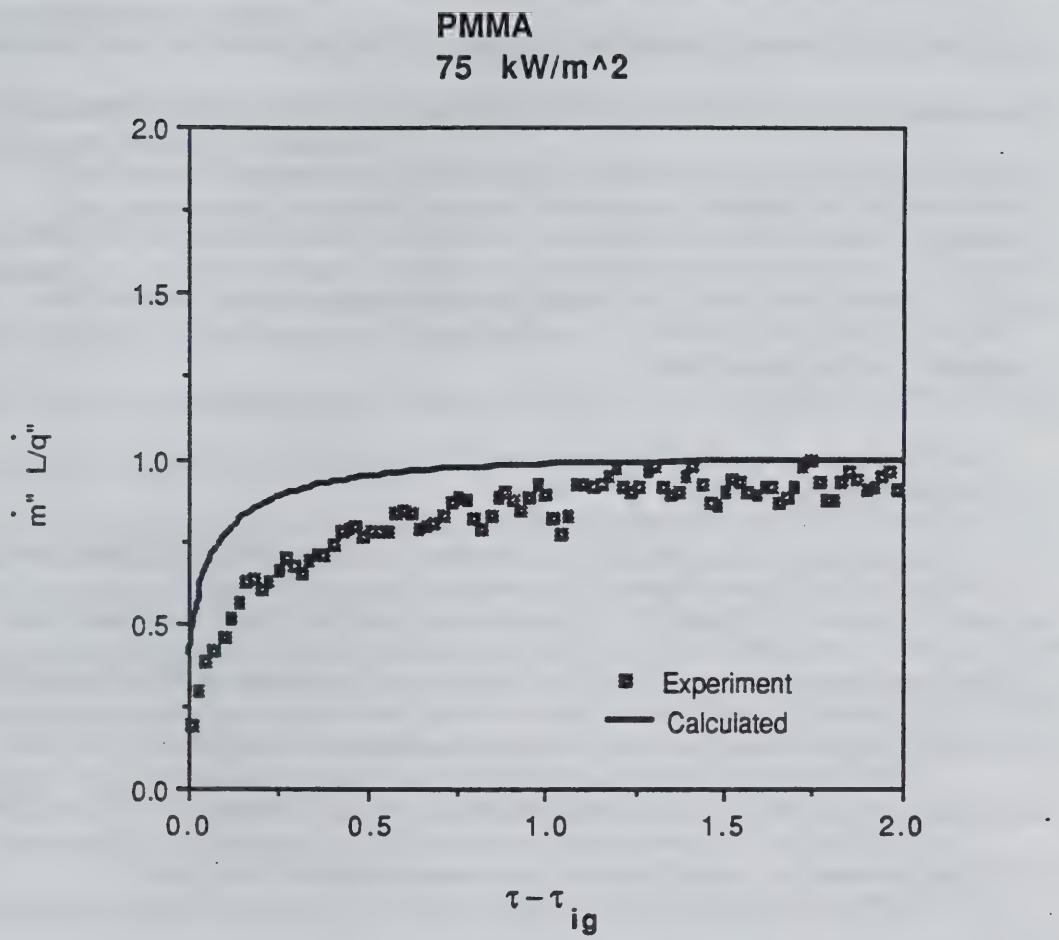

Figure 6.12 Theoretical and experimental dimensionless mass loss rate as a function of dimensionless time for black PMMA with a 75 kW/m^2 external irradiance.

CHAPTER 7 WOOD EXPERIMENTAL SETUP, PROCEDURE, AND MEASUREMENTS

The wood experiments were performed in manner consistent with the testing of the thermoplastic materials described in chapter 3. The analysis of the wood results and the development of a model for charring materials is the focus of future work on this project. For now, only a description of the testing procedure and the results is presented. Further analysis of the results for both the mass loss rate and the heat flux is needed. Observations were taken during the experiments and were recorded in a notebook to aid in the analysis.

7.1 Experimental System

Ignition and burning rate experiments were performed using a radiant cone heater assembly as shown in Figure 3.1. Thermocouple, heat flux meter, and mass loss readings were recorded using a LabView data acquisition system and a Macintosh IIFX computer. Data was recorded every second throughout the experiments. The data acquisition system was compiled using the simple virtual instruments (VI's) built into LabView, however, a copy of the program is not included in this report.

7.2 Wood Samples

Two materials were selected for analysis in this study, namely; Red Oak and Redwood. The Redwood samples measured 10 cm (4 in.) x 10 cm (4 in.) x 1.91 cm (0.75 in.) thick. The Red Oak samples measured 10 cm (4 in.) x 10 cm (4 in.) x 3.175 cm (1.25 in.) thick. The samples were conditioned in an atmosphere of approximately 20 °C and 50% relative humidity for at least two weeks prior to testing. Aluminum foil was wrapped around the sides of the samples in an attempt to inhibit edge burning. This did not completely eliminate edge burning effects, but it did significantly reduce the

effects of edge burning to maintain one dimensional burning behavior.

Samples were placed on a standard metal cone holder in the horizontal orientation on a bed of Kaowool so that heat loss effects through the back of the samples remained as insignificant as possible.

7.3 Experimental Procedure

The experimental procedure consisted of exposing a sample, in the horizontal orientation, to a constant external irradiance from the cone heater assembly. The time to piloted ignition was measured and mass loss data recorded for each test. Prior to the onset of each experiment the cone heater needed to be set to the desired constant external irradiance. The initial incident heat flux was determined using a Medtherm 2.5 cm (1 inch) diameter thermopile type heat flux transducer (Model # 64-5SB-20) situated such that it was in the same location that the center of the sample would be, and so that the face of the gauge was 2.5 cm (1 inch) below the base of the cone heater. The experiment was not started until a constant heat flux recording was obtained for at least a one minute period. The heat flux gauge could not be left in place during the experiment. Subsequently, the constancy of the cone heater was ensured by monitoring the temperature of the cone coil. Two thermocouples were located in the cone coil. The thermocouple readings were averaged and displayed every second so that the cone heat flux, which corresponds to a given coil temperature, could be monitored. The cone coil temperature was kept constant ($\pm$ 5° C) by manually adjusting the current to the coil using a 220 Volt transformer. This approach allowed for adjustment of the current to compensate for temperature fluctuations induced by flame impingement on the cone coil.

7.3.1 Ignition

The arrangement of the assembly was such that the top of the sample was initially located 2.5 cm (1 inch) below the base of the cone heater as is done for standard Cone Calorimeter tests [3]. The load cell was oriented between two guide bars to ensure proper placement of the sample underneath the center of the cone heater assembly. A one inch methane flame, located on one edge approximately 1.25 cm (1/2 inch) above the surface of the sample, was used as a pilot ignition source. Figure 3.3 shows the arrangement of the pilot and the assembly.

Once the cone was set to the desired constant external irradiance and the sample was prepared and situated on the load cell, the load cell was shifted into position underneath the cone. Simultaneously, the data acquisition system was initiated. It should be noted that sliding the sample into place caused some bouncing of the load cell. This effects the mass loss recordings for the first few seconds of the experiment. This is not however expected to have adverse effects on the results since ignition nominally took longer than ten seconds.

The ignition time is defined as the time at which a continuous flame is supported on the material surface. In some instances flashing occurred on the surface of the sample prior sustained flaming. However, in all cases the ignition time was taken as the time at which flaming was sustained over the entire surface of the specimen. Ignition times for all of the wood tests for irradiances ranging from 20 kW/m^2 to about 80 kW/m^2 are shown in Appendix G.

In some experiments a fine wire Type K thermocouple (0.003 in. diameter) was mounted on the thermoplastic material surface to attempt to measure the surface temperature at ignition. The placement of the thermocouples on the wood samples was done in a manner consistent with a method recommended by Atreya [18]. The wires and the bead were flattened to obtain a film thermocouple approximately 0.001 inches thick.

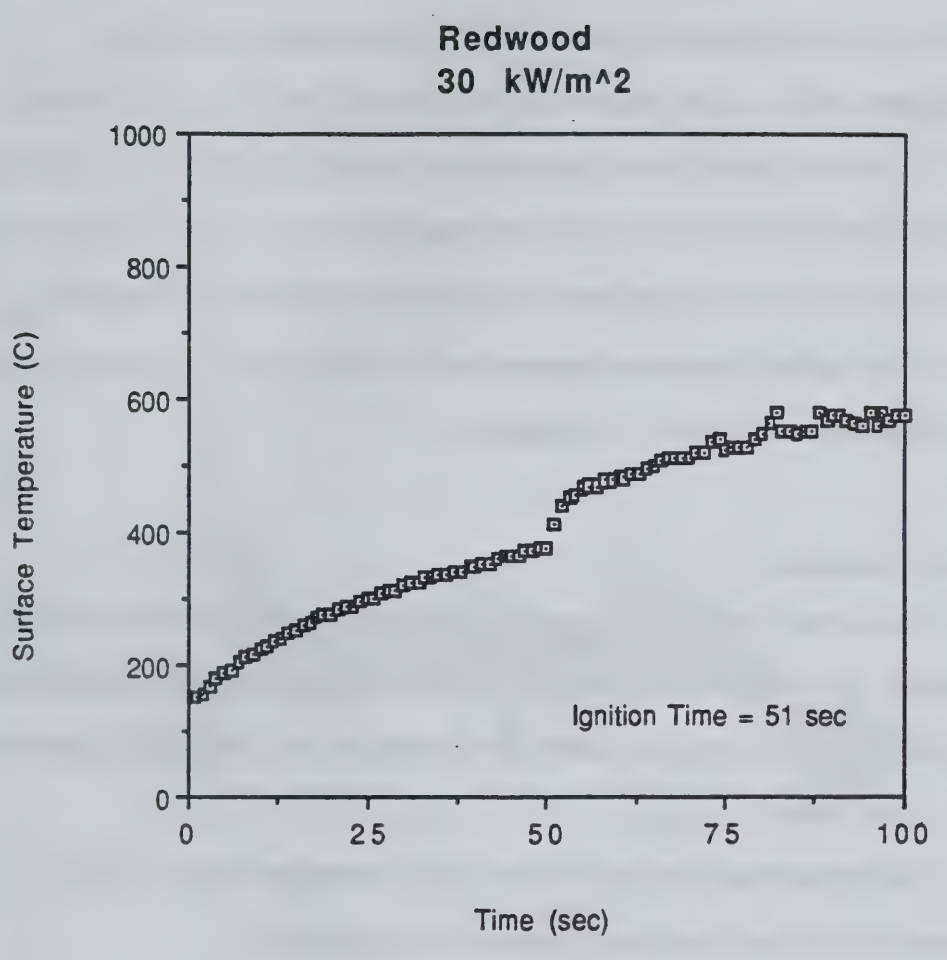

Figure 7.1 Surface temperature of Redwood as a function of time with a 30 kW/m^2 external irradiance.

A very fine incision was made in the surface of the sample and the thermocouple was slid underneath the skin of the incision which was approximately 0.001 inches thick. A small amount of wood glue was used to secure the rest of the thermocouple. The entire assembly was then pressed and allowed to set for approximately one hour. Measurements of the surface temperature were recorded until the onset of burning. Figure 7.1 shows a typical result of the measured surface temperature for the preheating period for Redwood exposed to a 30 kW/m^2 external irradiance. The temperature at the onset of the sudden rise in temperature is defined as the ignition temperature (T_{ig}). Results for the surface temperature measurements for the wood experiments at various external irradiances are shown in Appendix H.

7.3.2 Mass Loss Rate

Experiments to determine the mass loss rate of the materials were performed concurrently with the ignition experiments. The mass loss of the samples was recorded using a load cell. The mass loss readings were recorded every second for approximately a 1200 second period.

The transient mass loss rate is found using a seven point least squares fit of the mass loss data. The mass loss rate at some time t_i is given as,

$$\dot{m}'' = \frac{7 \sum_{n=i-2}^{i+2} (m_n t_n) - \sum_{n=i-2}^{i+2} (m_n) \sum_{n=i-2}^{i+2} (t_n)}{7 \sum_{n=i-2}^{i+2} (t_n)^2 - \left[\sum_{n=i-2}^{i+2} (t_n) \right]^2} \qquad (7.1)$$

where, i is a given measured data point,

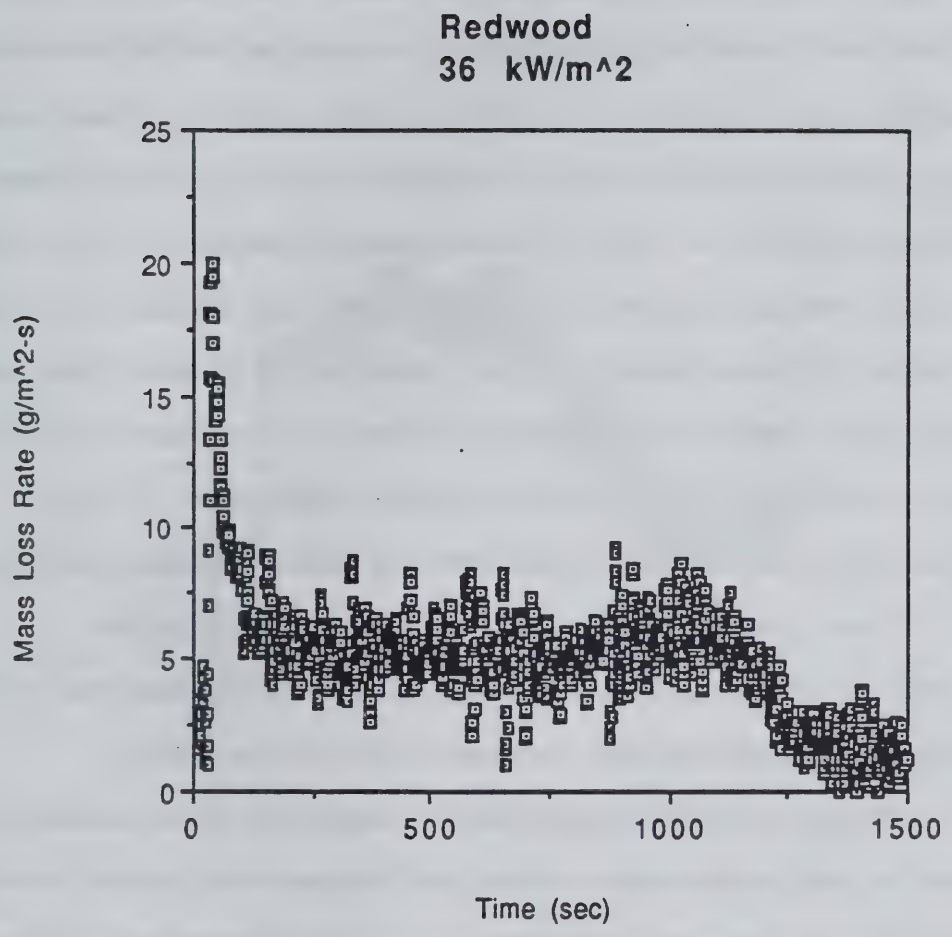

Figure 7.2 Transient mass loss rate of Redwood with a 36 kW/m^2 external irradiance.

m is the mass at i,

and, t is the time at i.

Figure 7.2 shows a typical mass loss rate result for Redwood exposed to an 36 kW/m^2 irradiance. Results for Redwood at other exposures and for Red Oak are shown in Appendixes I and J respectively. It should be noted that a seven point least squares fit was used for the calculation of the mass loss rates for the wood experiments whereas a five point least squares fit was used for the thermoplastic experiments. The reason for the increased fit was due to scatter in the data. A low pass filter consisting of a 10 kΩ resistor and an 8 μF capacitor was used to help reduce some of the noise. Data points were taken every second for the experiments, however, the recommended approach for future experiments using LabView is to take a number of data points, say 100, per second and to have LabView average these points and return a single data point at each second. This would yield much better results and is recommended for future experiments. In addition, use of the intermediate and advanced VI's built into LabView would allow for filtering of the data to be done with the LabView system.

In addition to the use of the seven point least squares fit, it was necessary to perform a five point smooth on the mass loss data. Because of this, the peak mass loss rates for the wood experiments were determined manually by plotting the mass loss versus time for each experiment and taking the slope at the time the maximum occurred. This enabled for a more accurate determination of the peak mass loss rate. The plots in Appendices I and J contain the corrected peak mass loss rates.

7.3.3 Flame Heat Flux

The flame plus external heat flux was measured during some of the experiments using a 3.175 mm (1/8 inch) Medtherm thermopile type heat flux gage (Model # 8-1-10-4-0-36-20680K). Due to contraction of the wood against the gage causing erroneous

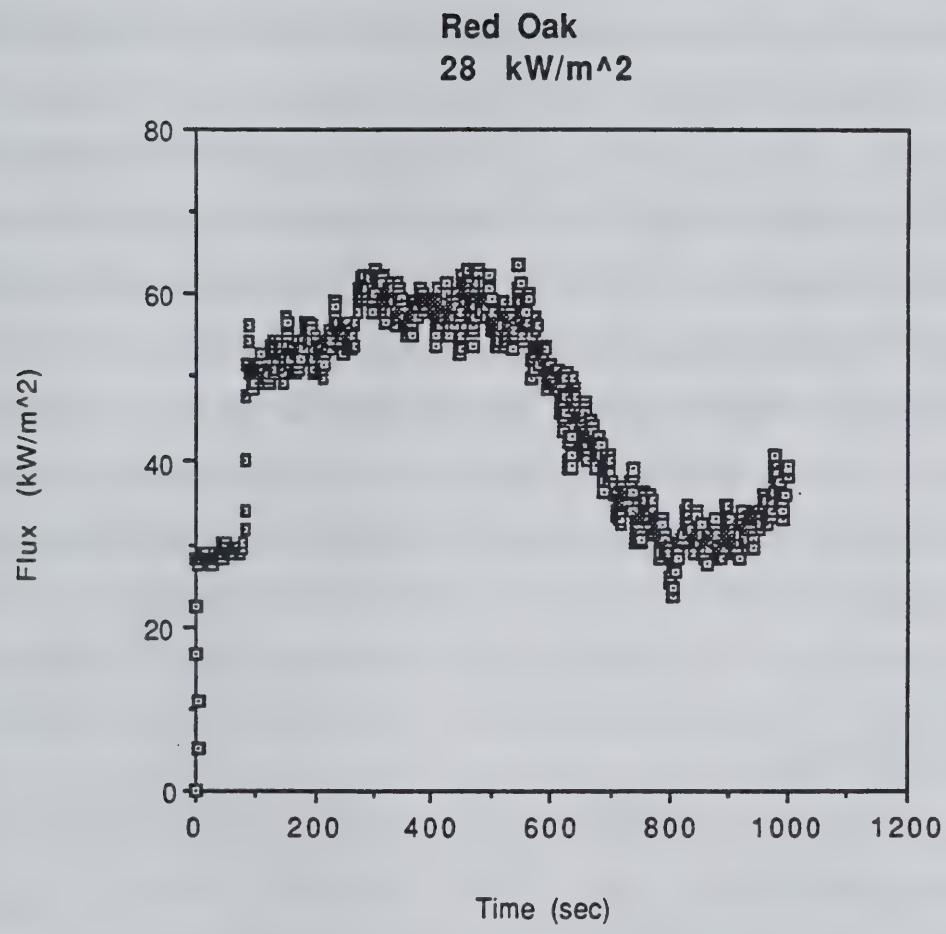

Figure 7.3 Total incident heat flux, measured by sensor, of Red Oak with a 28 kW/m^2 external irradiance.

mass loss measurements, it was not possible to measure the mass loss and the heat flux to the surface in the same experiments. Subsequently, separate tests at approximately the same external irradiance were performed to measure the mass loss and the heat flux respectively. To avoid excessive condensation and re-evaporation of pyrolisates on the surface of the heat flux gauge the water temperature was raised to approximately 65 °C. This was accomplished by circulating water through a copper coil which was heated by a methane flame. While raising the temperature of the water to 65 °C may have reduced the amount of condensation on the sensor, some slight condensation and re-evaporation did occur. The gauge was insulated on the sides with Kaowool to help minimize extraneous results. Figure 7.3 shows a typical result for the heat flux measurement for Red Oak exposed to a 28 kW/m^2 external irradiance. Results for the other experiments where the heat flux was measured are shown in Appendix K for Redwood and Appendix L for Red Oak.

7.4 Calibration

Calibration of the load cell, thermocouples, and heat flux gages was necessary before any experiments were conducted and only occasionally once testing began. The methods used to calibrate each of the instruments are discussed below.

7.4.1 Load Cell

The load cell was calibrated by first adjusting the weight of the sample holder and insulation to approximately zero. At this point, standard weights between 1 and 100 gram were added to the load cell and the voltage readings were recorded. The relationship between weight and voltage was found to be linear, with a calibration constant of 582.0 g/V. Since only mass loss rate is desired, only the difference in mass is necessary. Therefore, small fluctuations in the zero weight did not affect the results.

At the start of each day, the load cell was rechecked for accuracy using 1 and 2 gram weights. Furthermore, in some instances the mass of the sample was measured using a scale and the results compared to that indicated by the load cell. No significant errors were found for the mass loss measurements.

7.4.2 Heat Flux Gages

The 2.5 cm (1 inch) and 3.175 mm (1/8 inch) heat flux gages were initially calibrated using the standard NIST heat lamp calibration box. They were tested with water at room temperature and again with water at 46 °C. No notable differences in the calibration constant were observed. Although the water temperature did not affect the calibration constants, it did affect the zero reading. Unlike the mass loss, the heat flux measurement must be zero when there is no incident heat flux. The hot water resulted in an initial negative heat flux measurement due to convection between the sensor and the atmosphere. The heat flux measurement was calibrated to be zero, under no external irradiance, before each experiment in order to obtain consistent results. Besides the zero flux measurement, the 2.5 cm (1 inch) gage did not require calibration before each of the experiments because it was positioned such that it did not get disturbed or touched. However, the 3.175 mm (1/8 inch) heat flux meter often became dirty after an experiment. Subsequently, it was calibrated before each experiment using the 2.5 cm (1 inch) gage as a standard. Differences between the 3.175 mm (1/8 inch) heat flux gage's measurement before and after each experiment were found to be within 5 percent. The calibration constant for the 2.5 cm (1 inch) heat flux meter was determined to be 5235 kW/m^2 V and the calibration constant for the 3.175 mm (1/8 inch) heat flux gage was determined to be 1184 kW/m^2 V.

7.4.3 Thermocouples

The thermocouples used to measure the coil temperature and surface temperature were calibrated before any testing began. This was done by placing them in an ice bath and also in boiling water for a prolonged period of time. Temperature readings were found to be accurate within ± 2 °C. The thermocouples in the coil did not require additional calibration as the absolute temperature was not necessary. The thermocouples for the surface were calibrated against each other before each experiment.

Although the experiments yielded extraneous results for some tests, no major calibration errors were found. Inconsistencies in the results are likely to be due to factors other than calibration errors.

CHAPTER 8 CONCLUSIONS

The modeling prescription developed by Quintiere and Rhodes [8], which can utilize Cone Calorimeter data to derive useful properties needed to predict ignition and transient burning rates for thermoplastic-like materials, has been shown to yield good results. The level of accuracy has been demonstrated for Nylon 6/6, Polyethylene, Polypropylene, and PMMA. The simplicity of the ignition model is advantageous and can be used to infer the critical flux for ignition without direct measurement.

Heat flux to the material surface was not measured for the present experiments, rather the flame heat flux to the surface was inferred using the method described in section 5.2. The inference of a constant flame heat flux to the surface for thermoplastic-like materials burning in the Cone Calorimeter has been shown to yield good results. Values for the flame heat flux were found to be 30 kW/m^2 for Nylon, 25 kW/m^2 for Polyethylene, 14 kW/m^2 for Polypropylene, and 37 kW/m^2 for PMMA. The constancy of the flame heat flux appears to be an attribute of all thermoplastics burning in the Cone Calorimeter due to the long column like shape of the flame.

For all of the thermoplastic materials examined thus far, the calculated ignition temperature has been found to be less than the measured ignition temperature. This is expected to be an attribute of the modeling prescription and the results are not expected to be void of physical significance. Use of the calculated ignition temperatures in the model has been shown to yield good results.

Ignition, burning rate, and heat flux measurements have been taken for Redwood and Red Oak burning in the Cone Calorimeter. An assessment of the results and an attempt to formulate a modeling prescription for charring materials, similar to the prescription for thermoplastics, should be attempted. The intent is to maintain simplicity while maintaining completeness of the important processes. The framework for the

charring model can be found in the formulation by Quintiere [1].

APPENDIX A THERMOPLASTIC DATA ACQUISITION PROGRAM

```
10      OPTION BASE 1
20      DIM In$[100], Out(6)
21      P0=-5.115307103E-2
22      P1=2.485028007E+4
23      P2=-3.826622822E+5
24      P3=9.966105673E+7
25      P4=-1.082062357E+10
26      P5=6.039285524E+11
27      P6=-1.910899962E+13
28      P7=3.478234730E+14
29      P8=-3.399102821E+15
30      P9=1.382851398E+16
32      CALL Set_datacom
33      CLEAR 722
34      CLEAR 709
35      FOR I=1 TO 8
36        ON KEY I LABEL "            " GOSUB Beeper
37      NEXT I
38      OUTPUT 709;"F00 L05 I1"
39      OUTPUT 709;"00"
40      OUTPUT 722;"L1 RS1 D0 Z0 F1 R1 0.01STD SO1 10.0STI 6STN T4 SM004 -
        7STR RER Q"
41      OUTPUT 722;"X1"
42      Oncom=0
43      ON KEY 1 LABEL " COM   OFF " GOSUB Comonoff
44      ON KEY 4 LABEL " END   TEST " GOTO Endit
45      ON KEY 5 LABEL " START   TEST " GOTO Onward
46      !
47      !
48  Spin: !
49      GOTO Spin
50      !
51      !
52  Onward:  Ti0=TIMEDATE MOD 86400
53  Restart: !
54      TRIGGER 722
55      TI1=(TIMEDATE MOD 86400)-TI0
58      ENTER 722;In$
59      OUTPUT 722;"X1"
60      ENTER In$;Out(*)
61      IF Oncom=1 THEN
62      FOR I=2 TO 6 STEP 2
63        C(I)=Out(I)*(P6+Out(I)*(P7+Out(I)*(P8+Out(I)*P9)))
64        T(I)=P0+Out(I)*(P1+Out(I)*(P2+Out(I)*(P3+Out(I)*(P4+Out(I)*(P5+C(I))))))
65      NEXT I
66        OUTPUT 9 USING "DDDD.D,#";Ti1
69        OUTPUT 9;"     ";
70        OUTPUT 9 USING "DD.D,#";Out(1)*5465
71        OUTPUT 9;"     ";
72        ON ERROR GOTO Error
74        OUTPUT 9 USING "DDDD.D,#";T(2)-2.3
```

```
75        OUTPUT 9;"     ";
76        OUTPUT 9 USING "DDD.D,#";Out(3)*11360
77        OUTPUT 9;"     ";
78        OUTPUT 9 USING "DDD.D,#";T(4)
79        OUTPUT 9;"     ";
80        OUTPUT 9 USING "DDDD.DD,#";Out(5)*1000*(-0.58597)
81        OUTPUT 9;"     ";
82        OUTPUT 9 USING "DDDD.D";T(6) +0.4
83      ENDIF
84      PRINT USING "DDDD.D,#";Ti1
85      PRINT "  ";Out(*)
86      LOOP
87        EXIT IF (TIMEDATE MOD 86400)-Ti0>=Ti1+2
88      END LOOP
89      GOTO Restart
90  Comonoff: !
91      IF Oncom=0 THEN
92        Oncom=1
93        ON KEY 1 LABEL " COM   ON " GOSUB Comonoff
94      ELSE
95        Oncom=0
96        ON KEY 1 LABEL " COM   OFF " GOSUB Comonoff
97      ENDIF
98      RETURN
99  Beeper: !
100     BEEP
101     RETURN
102 Error: !
103     OUTPUT 9:"     ";
104     GOTO 75
106 Endit: !
107     ABORT 7
108     CLEAR 722
109     CLEAR 709
110     END
111     !
112 SUB Set_datacom
113     Sc=9
114     CONTROL Sc,0;1
115     CONTROL Sc,3;9600
124     CONTROL Sc,4;3
134     CONTROL Sc,5;0
144 SUBEND
```

APPENDIX B IGNITION TIME FOR THERMOPLASTICS

Test Number	External Irradiance (kW/m^2)	Time to Ignite (sec)
n1	35	132
n2	50	47
n3	75	21
n4	31	372
n5	42	80
n6	80	19
n7	60	30
n8	31	505

Table B1 Experimental ignition time for Nylon 6/6

Test Number	External Irradiance (kW/m^2)	Time to Ignite (sec)
pe1	46	76
pe2	38	94
pe3	27	230
pe4	87	27
pe5	70	30
pe6	61	54
pe7	25	388
pe8	59	35
pe9	36	126

Table B2 Experimental ignition time for polyethylene.

Test Number	External Irradiance (kW/m^2)	Time to Ignite (sec)
pp1	39	27
pp2	20	167
pp3	70	-------
pp4	65	25
pp5	27	88
pp6	50	28
pp7	61	19
pp8	61	22
pp9	34	66

Table B3 Experimental ignition time for polypropylene.

APPENDIX C

MEASURED SURFACE TEMPERATURE FOR THERMOPLASTICS

Material/Test Number	External Irradiance (kW/m^2)	Measured Ignition Temperature (°C)
Nylon/n7	60	------
Nylon/n8	31	500
Polyethylene/pe8	59	320
Polyethylene/pe9	36	390
Polypropylene/pp8	61	330
Polypropylene/pp9	34	315

TABLE C1 Measured ignition temperature for thermoplastics.

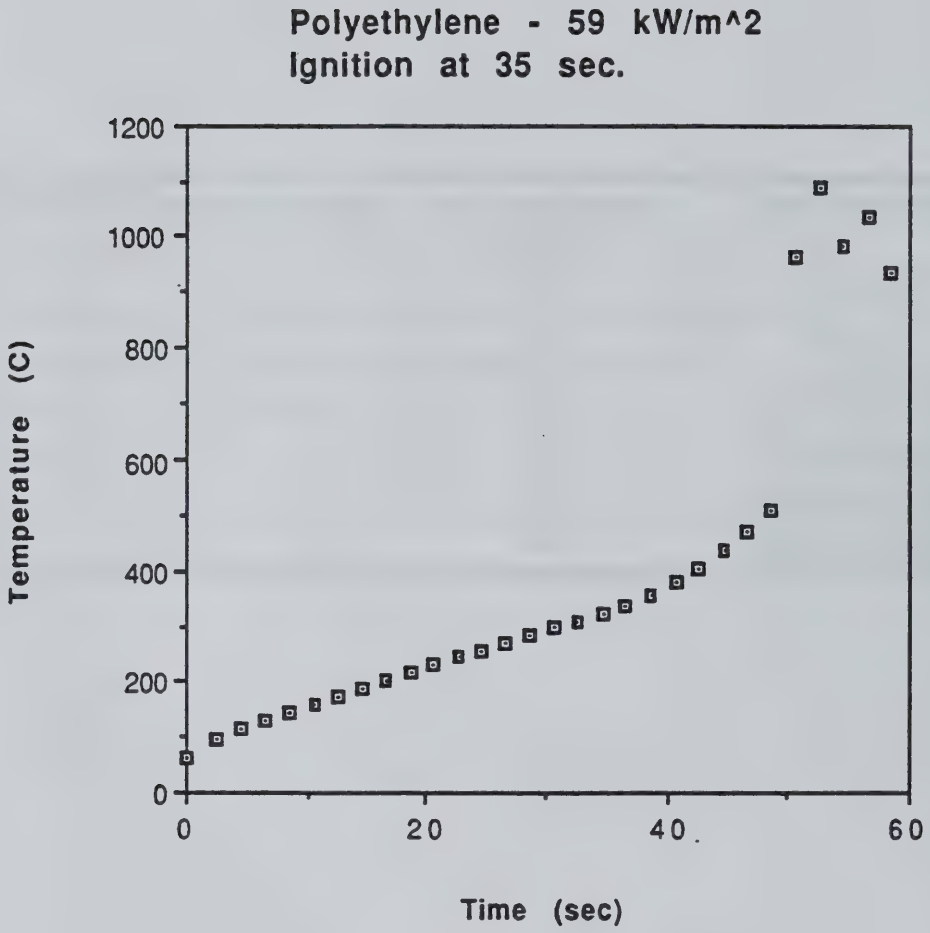

Figure C1 Surface temperature results for Polyethylene with a 59 kW/m^2 external irradiance.

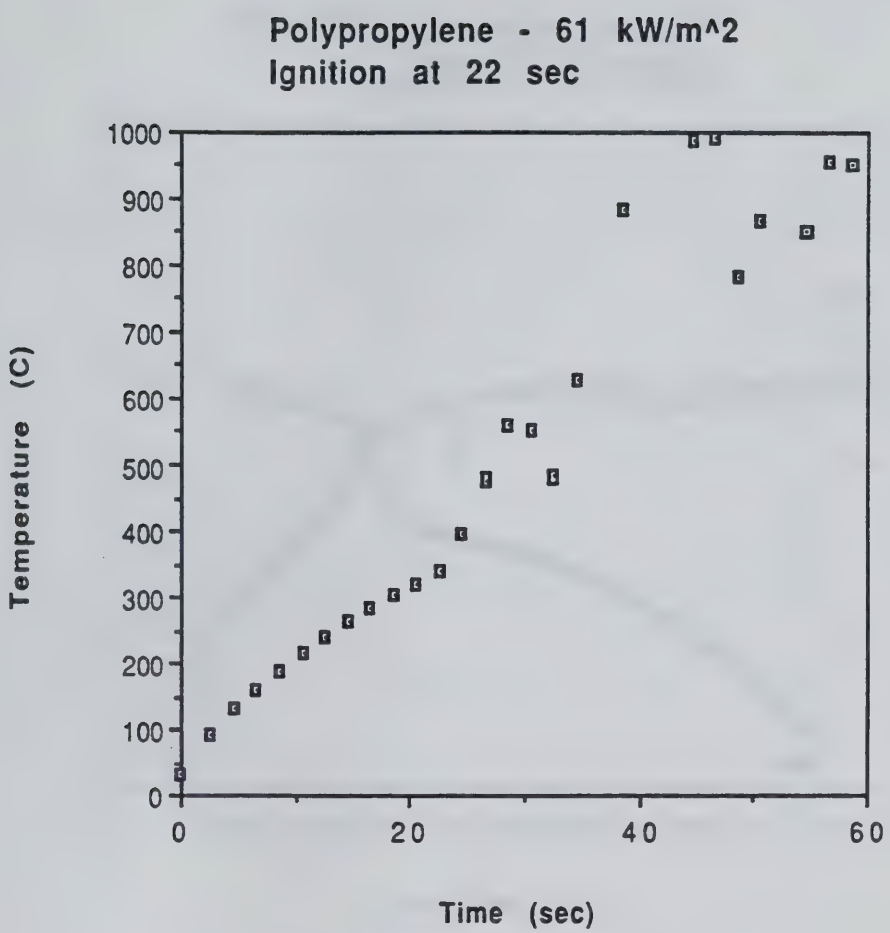

Figure C2 Surface temperature results for Polypropylene with a 61 kW/m^2 external irradiance.

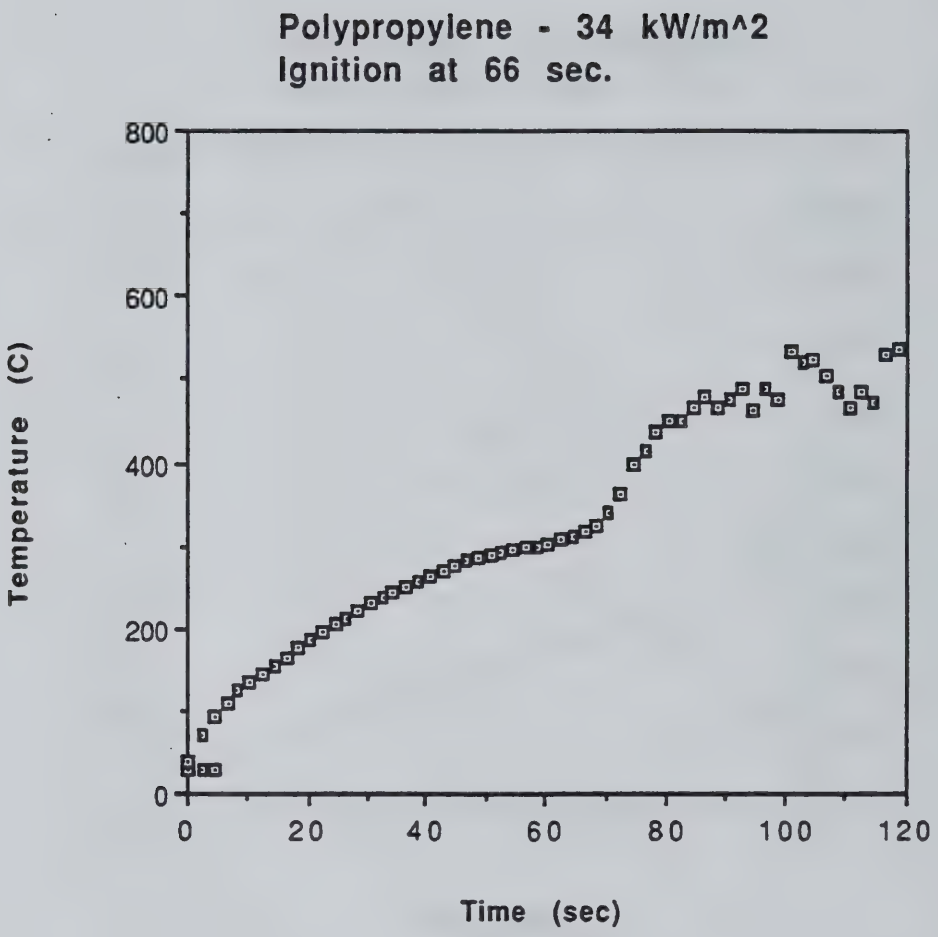

Figure C3 Surface temperature results for Polypropylene with a 34 kW/m^2 external irradiance.

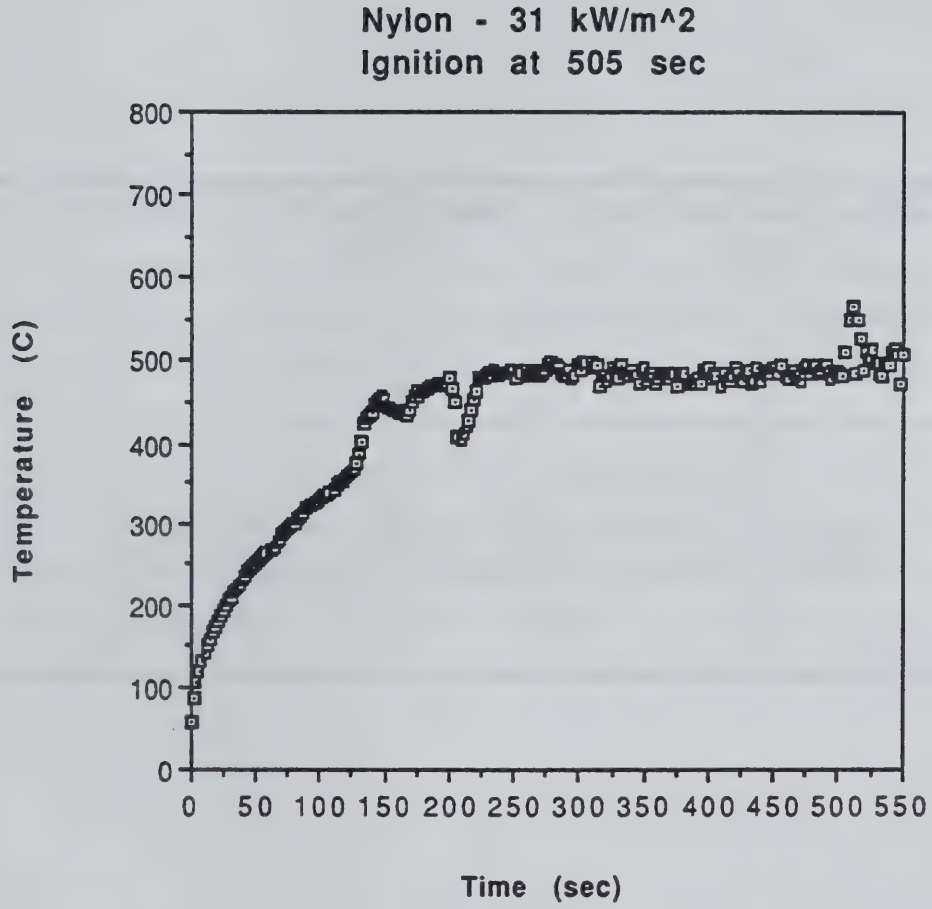

Figure C4 Surface temperature results for Nylon with a 31 kW/m^2 external irradiance.

APPENDIX D

NYLON MASS LOSS RATE

Test Number	External Irradiance (kW/m^2)	Steady State Mass Loss Rate (g/m^2 s)
n1	35	14
n2	50	18
n3	75	25
n4	31	14
n5	42	-----
n6	80	27
n7	60	21
n8	31	14

TABLE D1 Steady state mass loss rate for Nylon 6/6.

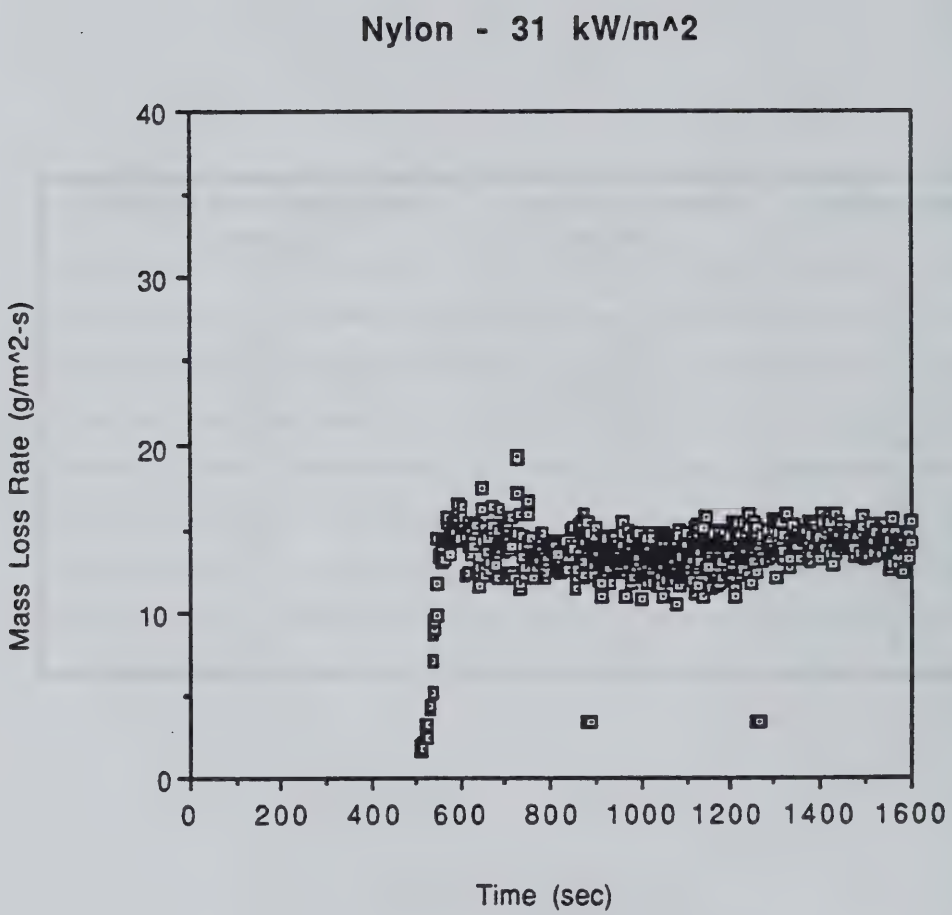

Figure D1 Transient mass loss rate results for Nylon with a 31 kW/m^2 external irradiance.

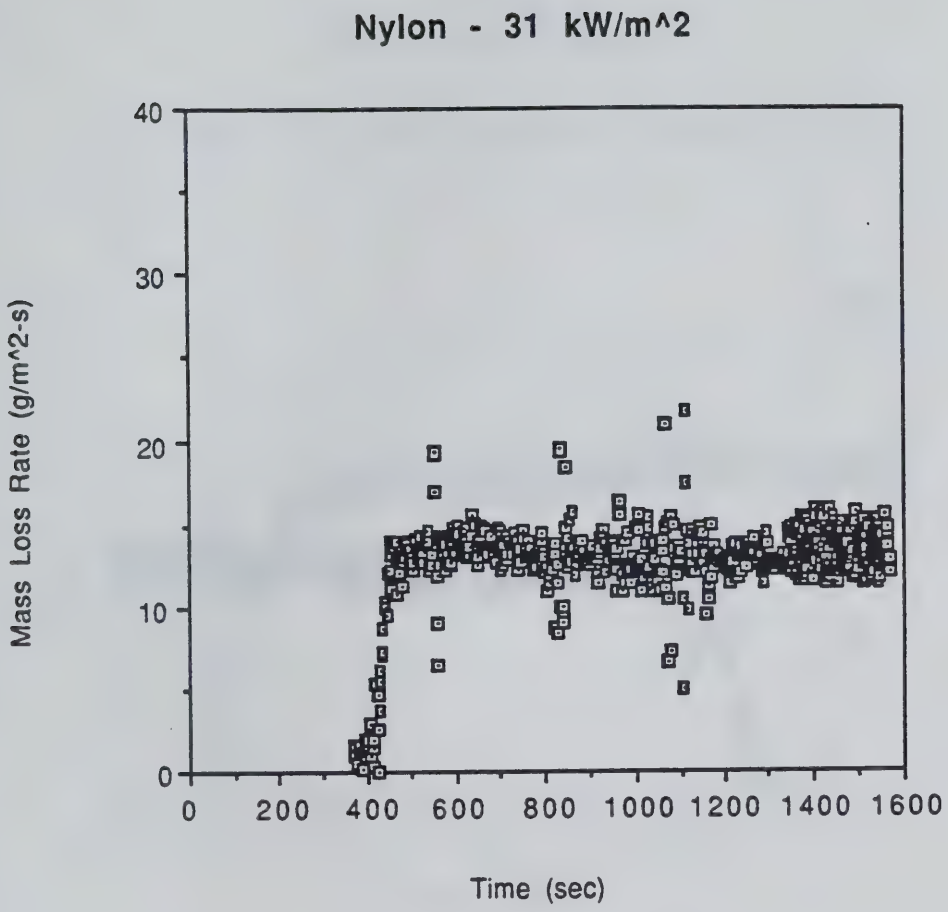

Figure D2 Transient mass loss rate results for Nylon with a 31 kW/m^2 external irradiance.

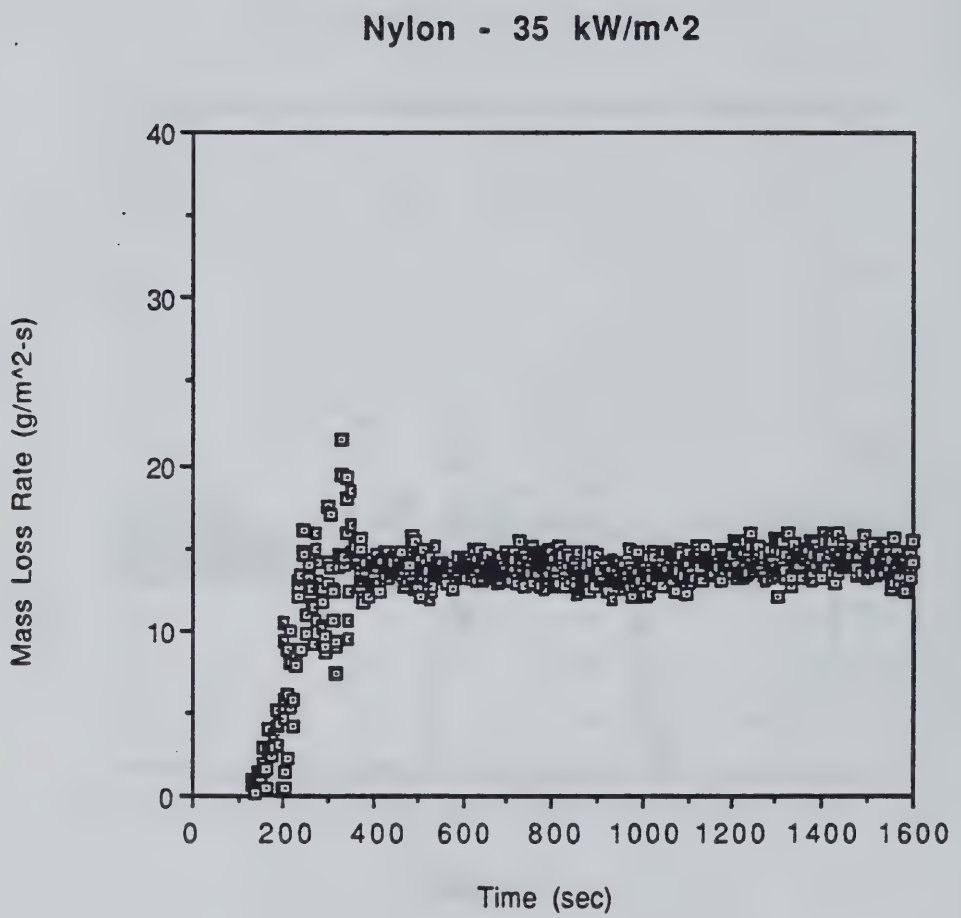

Figure D3 Transient mass loss rate results for Nylon with a 35 kW/m^2 external irradiance.

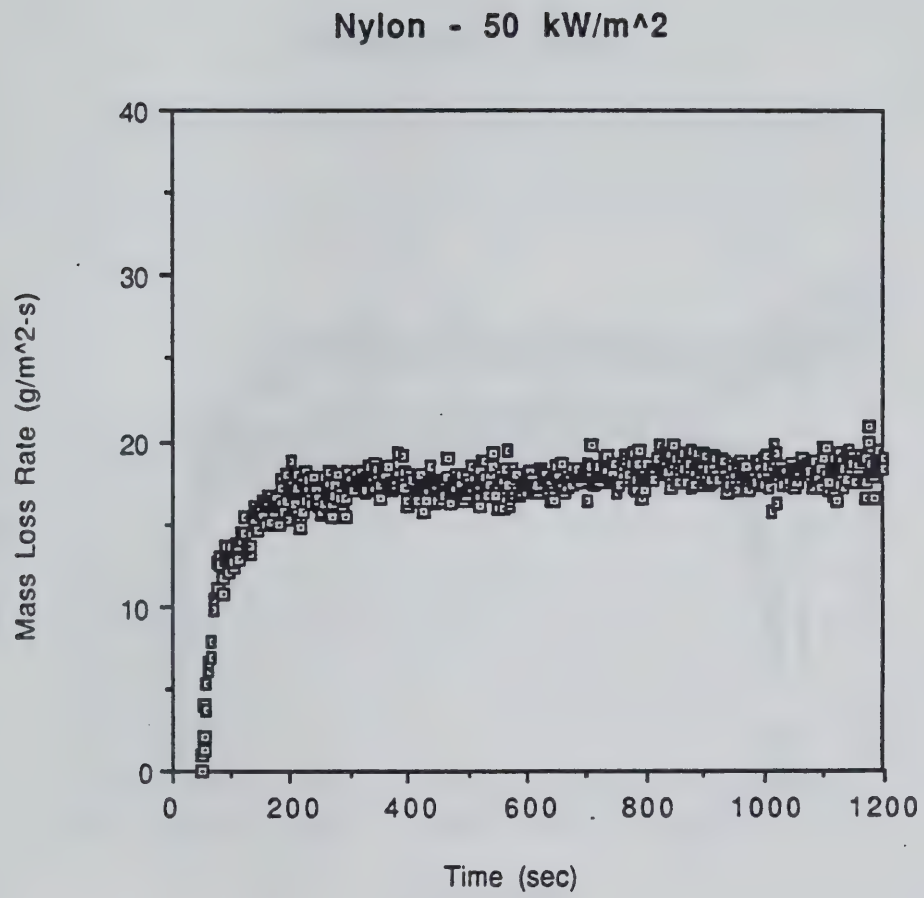

Figure D4 Transient mass loss rate results for Nylon with a 50 kW/m^2 external irradiance.

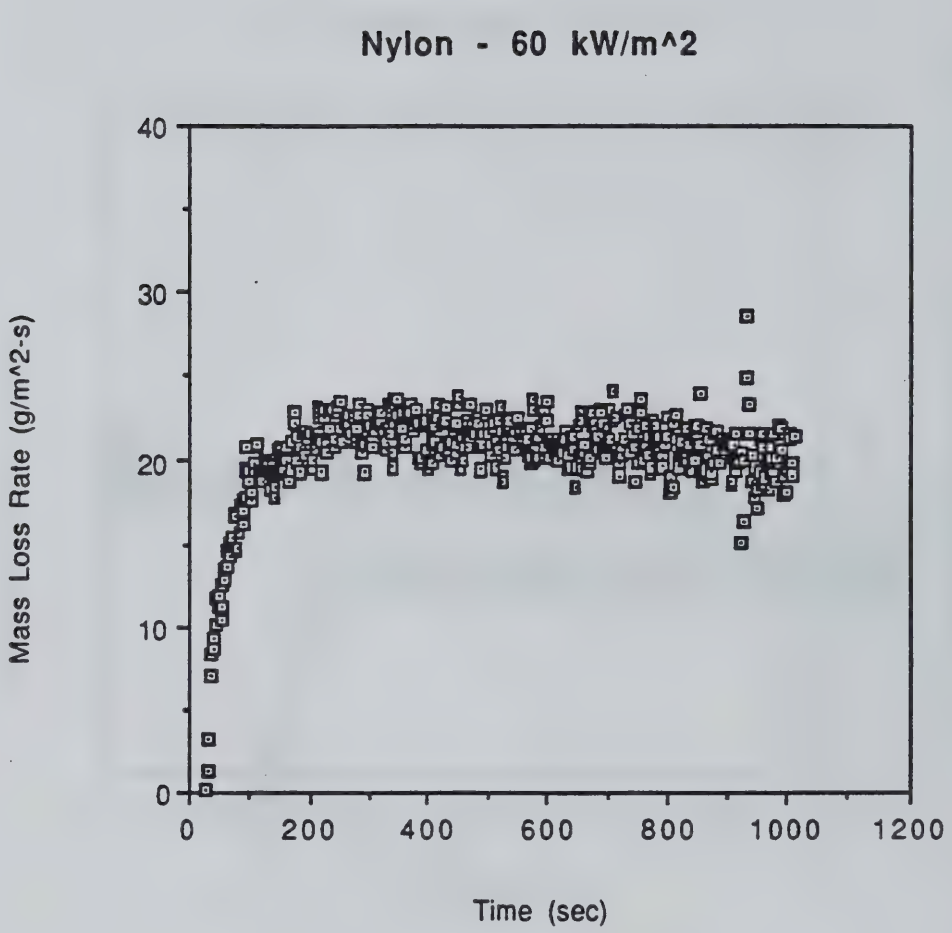

Figure D5 Transient mass loss rate results for Nylon with a 60 kW/m^2 external irradiance.

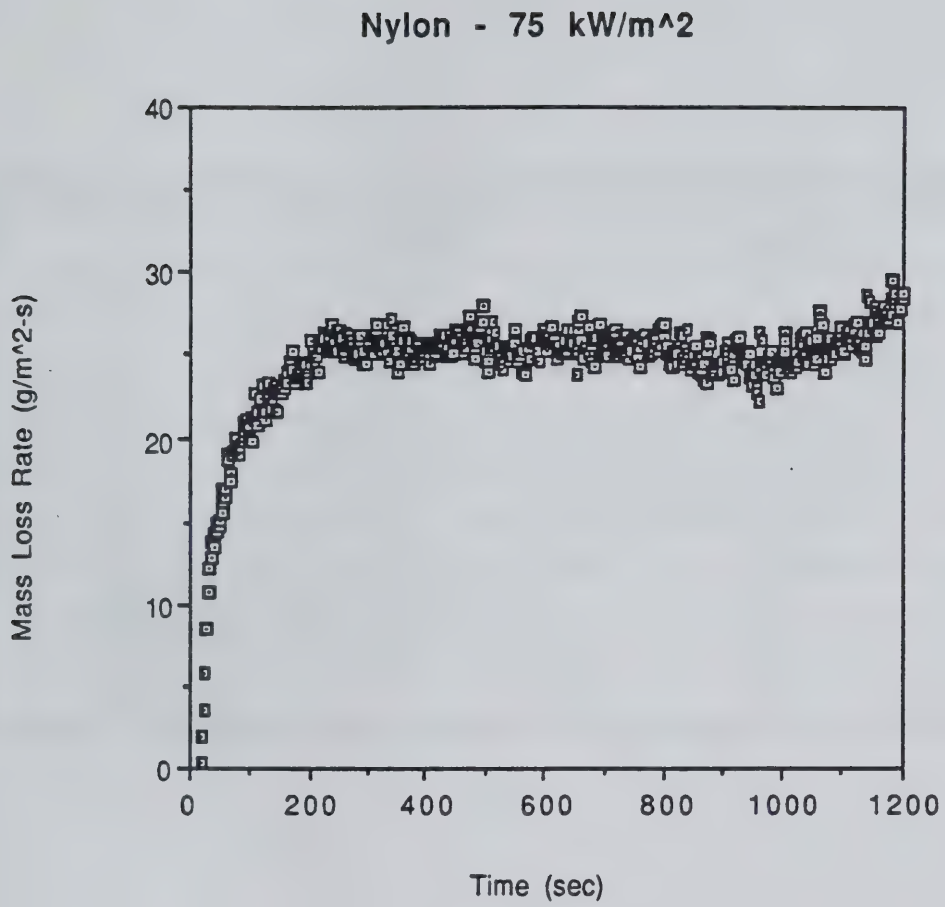

Figure D6 Transient mass loss rate results for Nylon with a 75 kW/m^2 external irradiance.

APPENDIX E POLYETHYLENE MASS LOSS RATE

Test Number	External Irradiance (kW/m^2)	Steady State Mass Loss Rate (g/m^2 s)
pe1	46	18
pe2	38	----
pe3	27	----
pe4	87	30
pe5	70	25
pe6	61	21
pe7	25	11
pe8	59	21
pe9	26	14

TABLE E1 Steady state mass loss rate for Polyethylene.

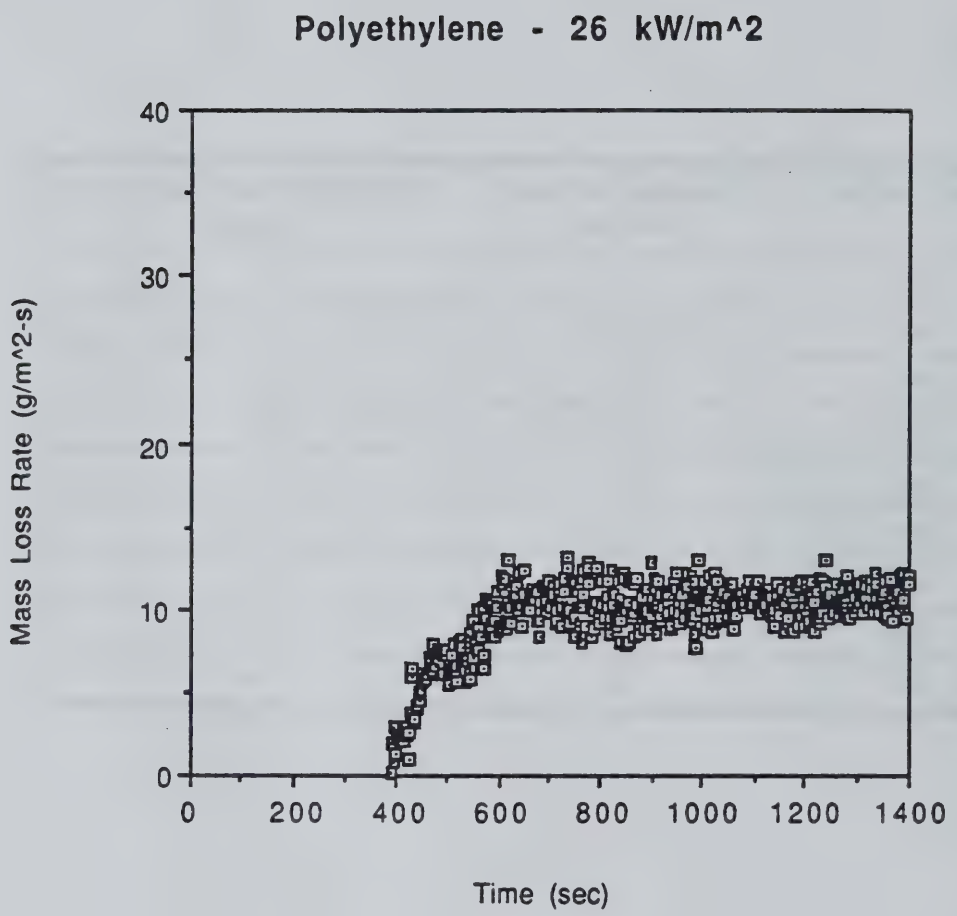

Figure E1 Transient mass loss rate results for Polyethylene with a 26 kW/m^2 external irradiance.

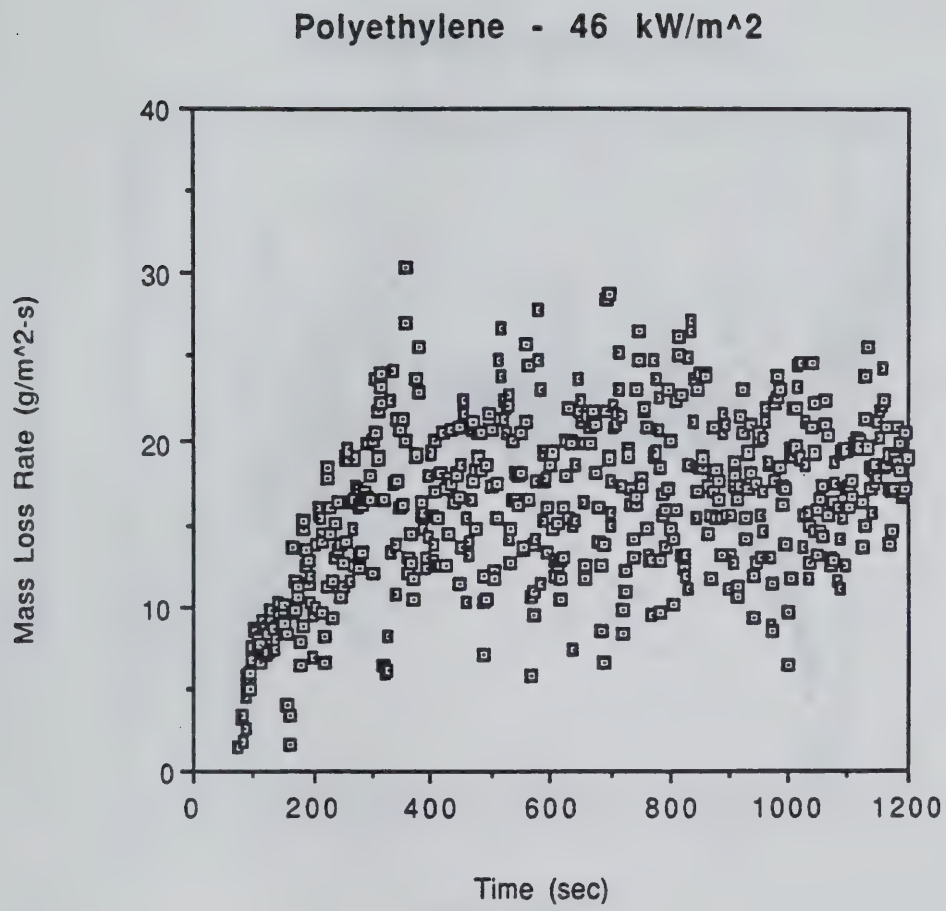

Figure E2 Transient mass loss rate results for Polyethylene with a 46 kW/m^2 external irradiance.

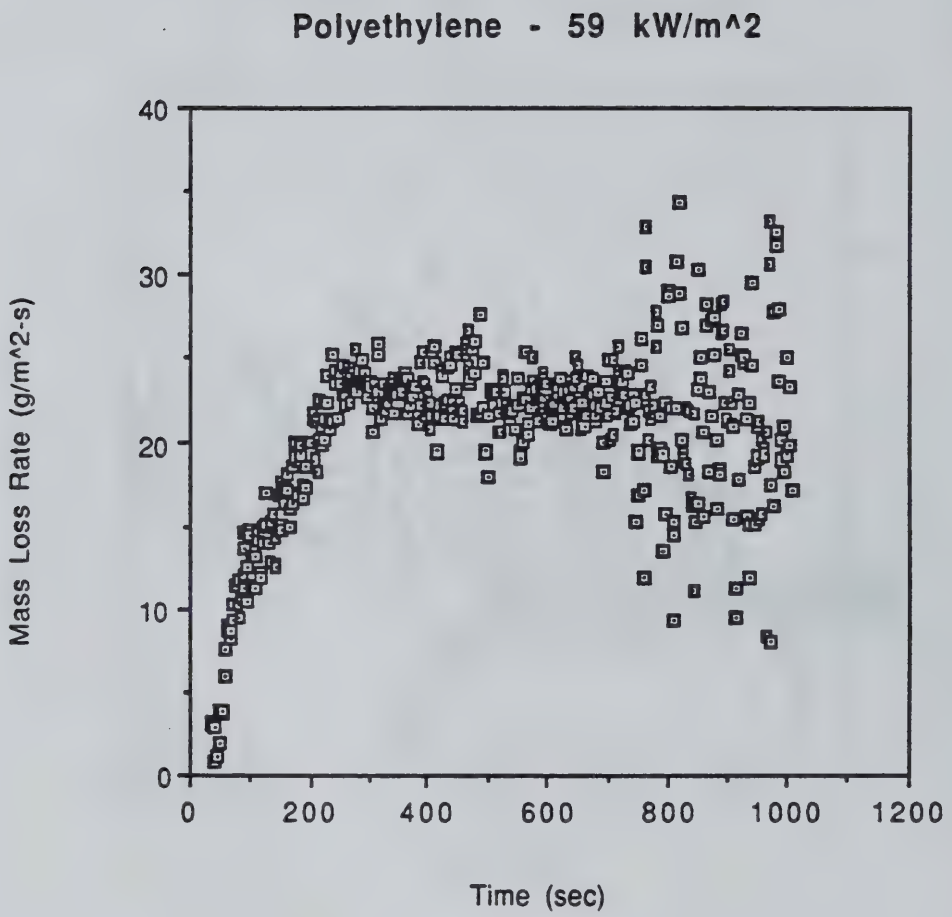

Figure E3 Transient mass loss rate results for Polyethylene with a 59 kW/m^2 external irradiance.

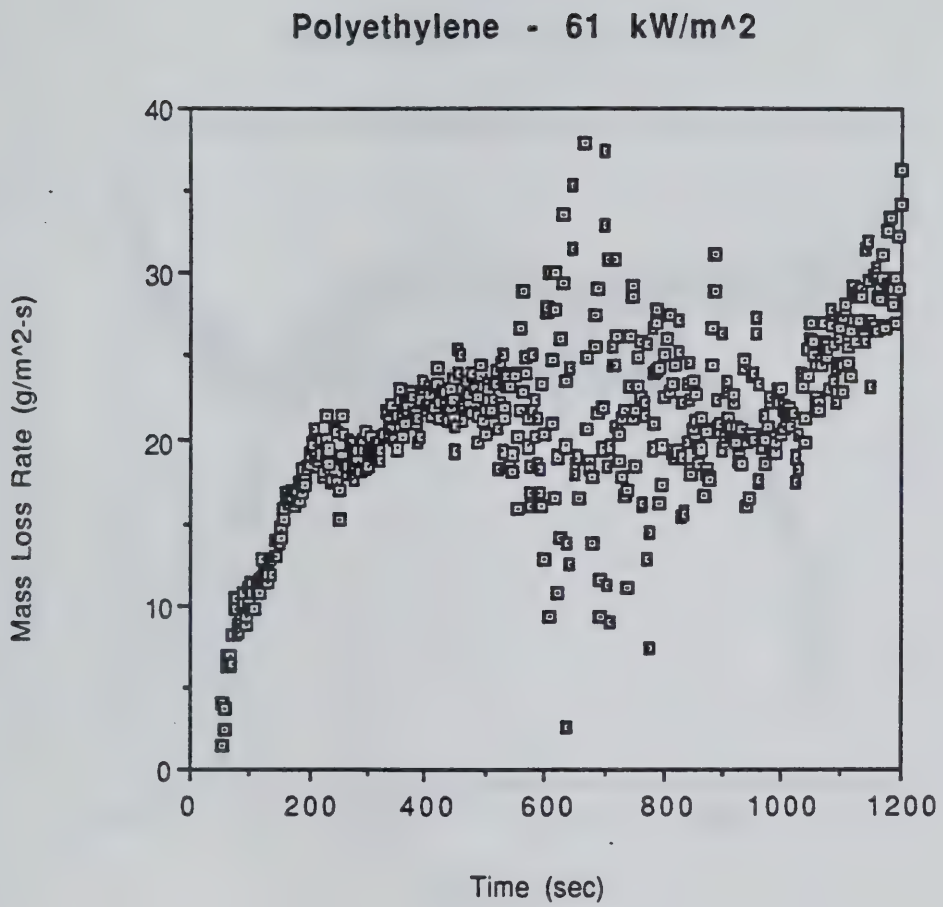

Figure E4 Transient mass loss rate results for Polyethylene with a 61 kW/m^2 external irradiance.

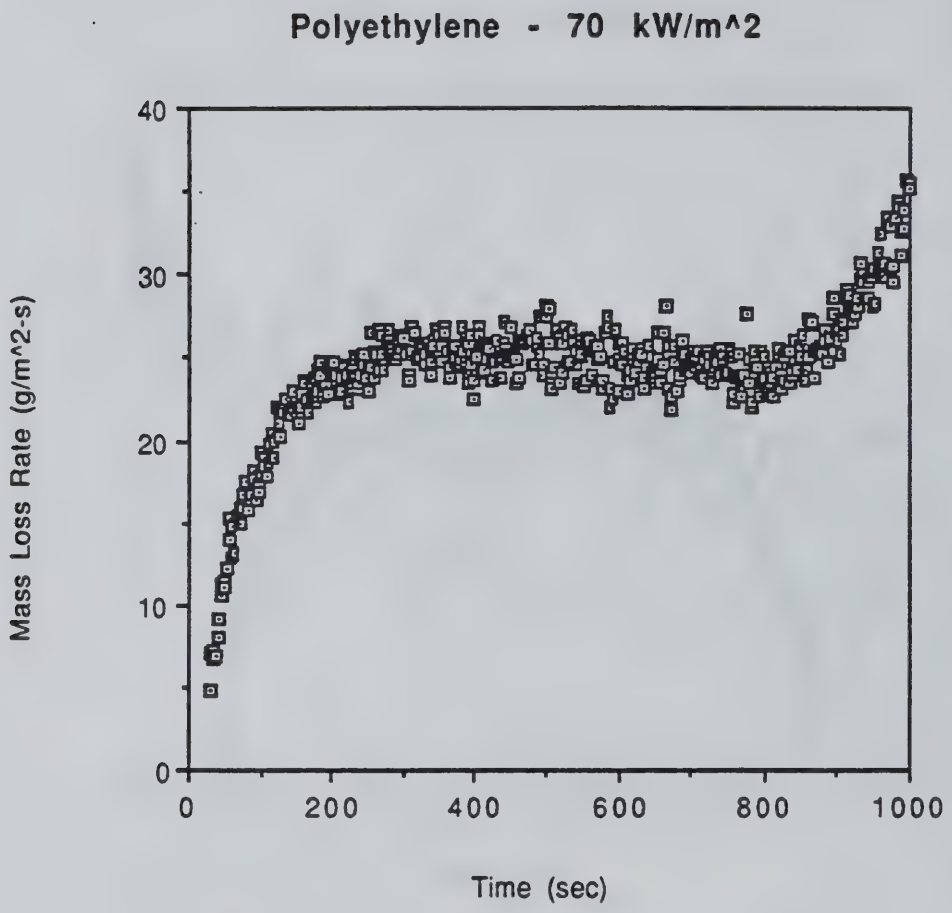

Figure E5 Transient mass loss rate results for Polyethylene with a 70 kW/m^2 external irradiance.

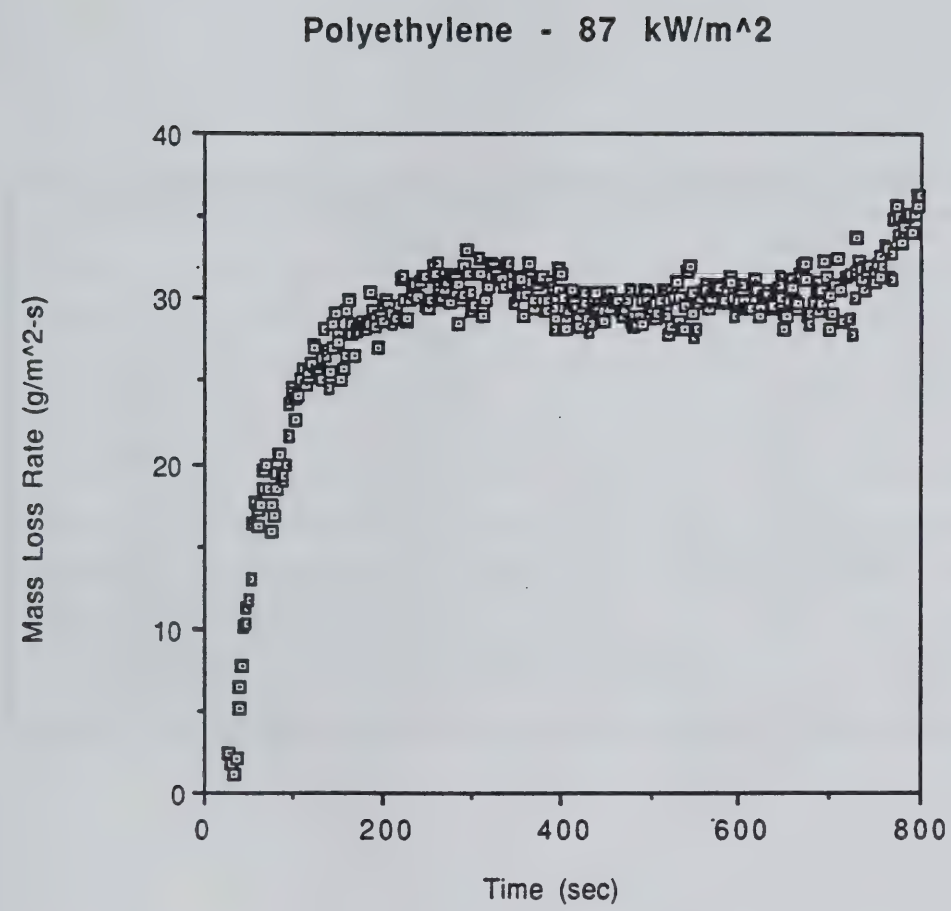

Figure E6 Transient mass loss rate results for Polyethylene with a 87 kW/m^2 external irradiance.

APPENDIX F POLYPROPYLENE MASS LOSS RATE

Test Number	External Irradiance (kW/m^2)	Steady State Mass Loss Rate ($g/m^2\ s$)
pp1	39	16
pp2	20	10
pp3	70	16
pp4	65	25
pp5	27	13
pp6	50	19
pp7	61	24
pp8	61	---
pp9	34	15

TABLE F1 Steady state mass loss rate for Polypropylene.

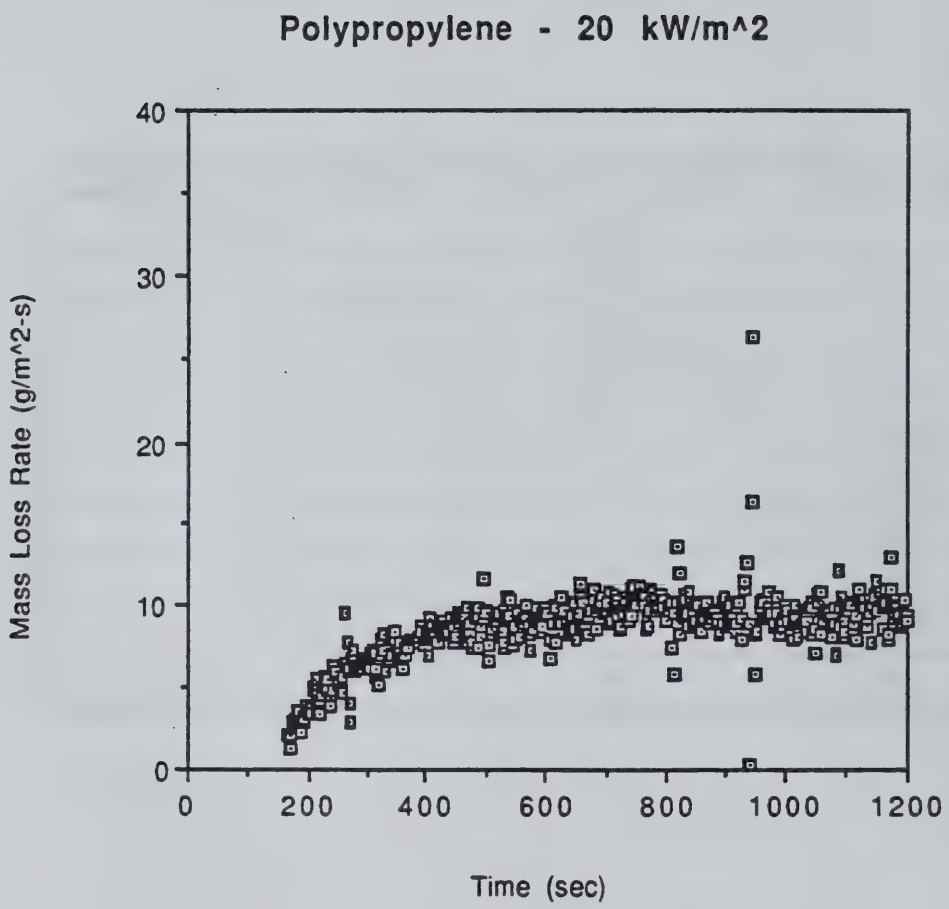

Figure F1 Transient mass loss rate results for Polypropylene with a 20 kW/m^2 external irradiance.

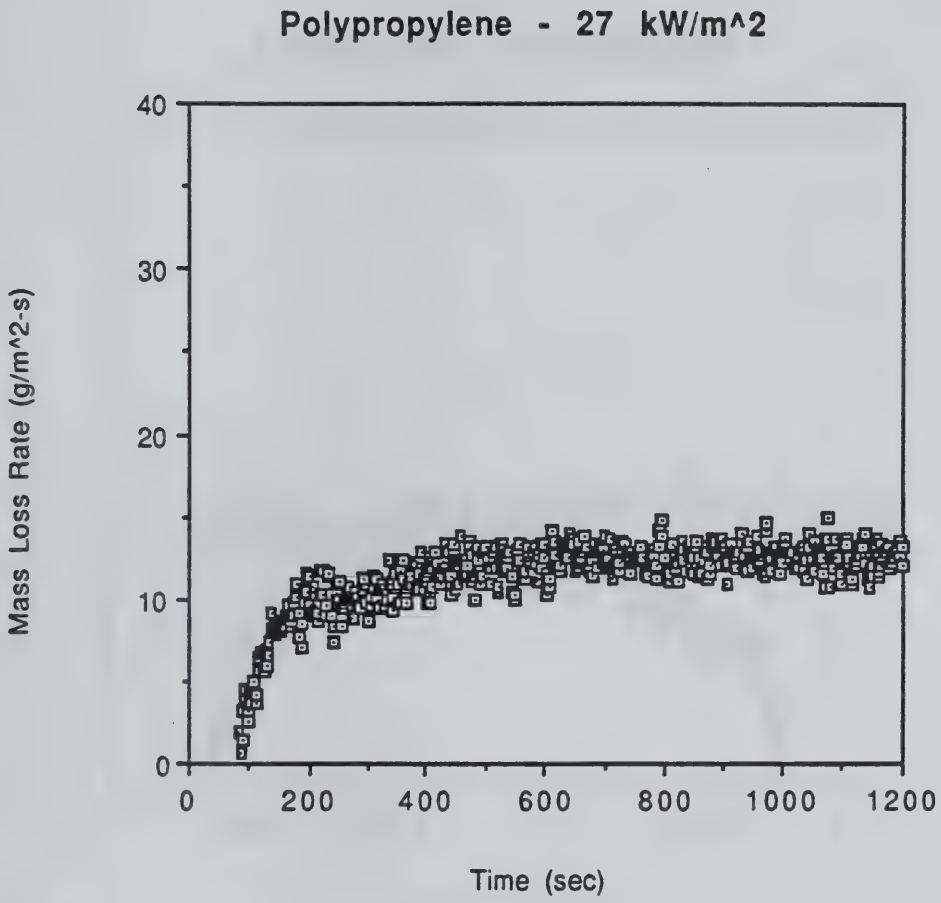

Figure F2 Transient mass loss rate results for Polypropylene with a 27 kW/m^2 external irradiance.

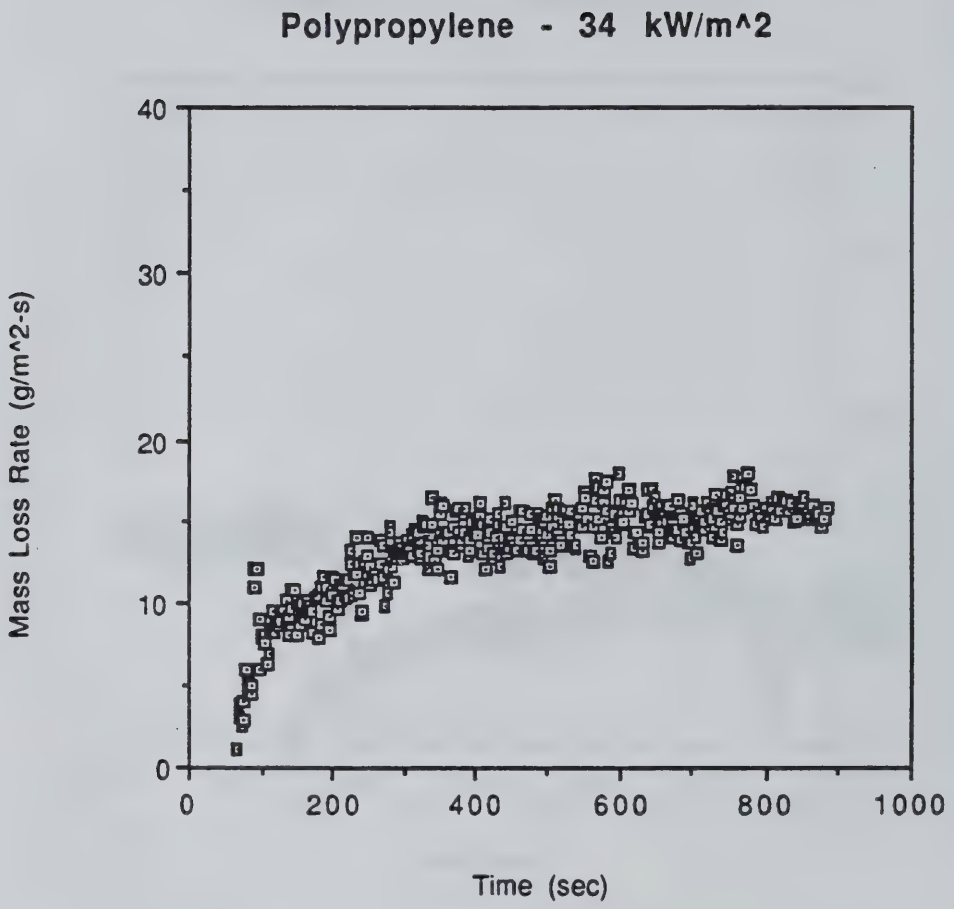

Figure F3 Transient mass loss rate results for Polypropylene with a 34 kW/m^2 external irradiance.

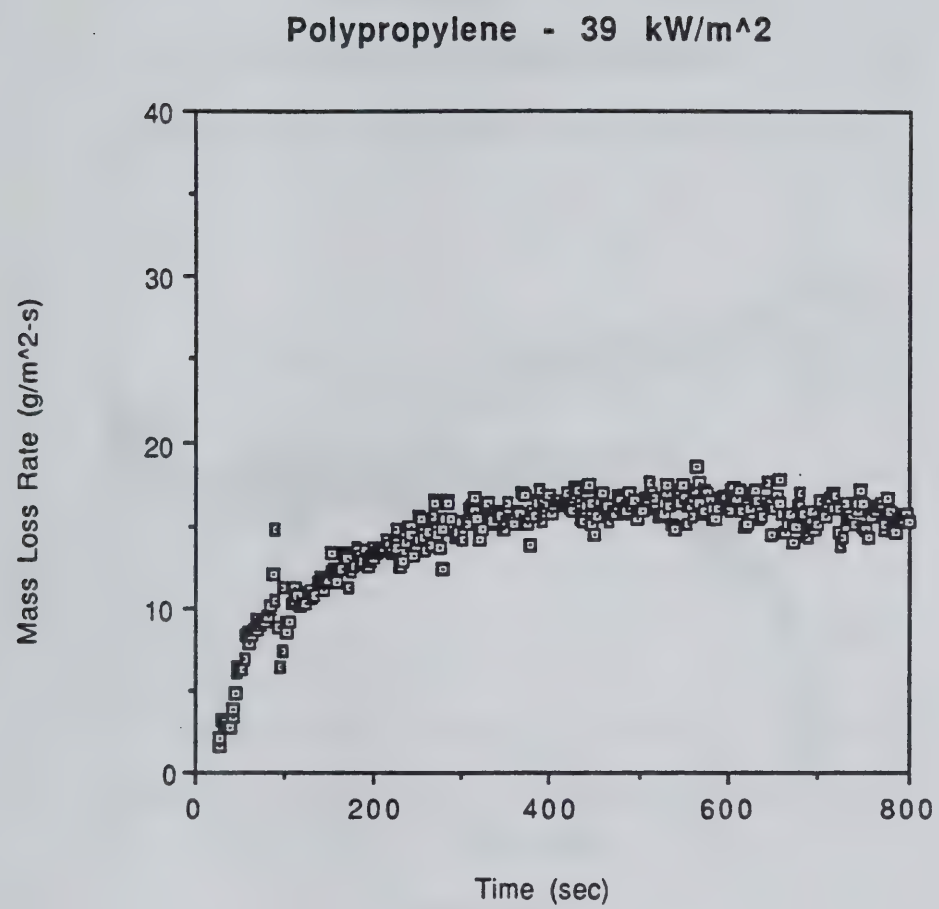

Figure F4 Transient mass loss rate results for Polypropylene with a 39 kW/m^2 external irradiance.

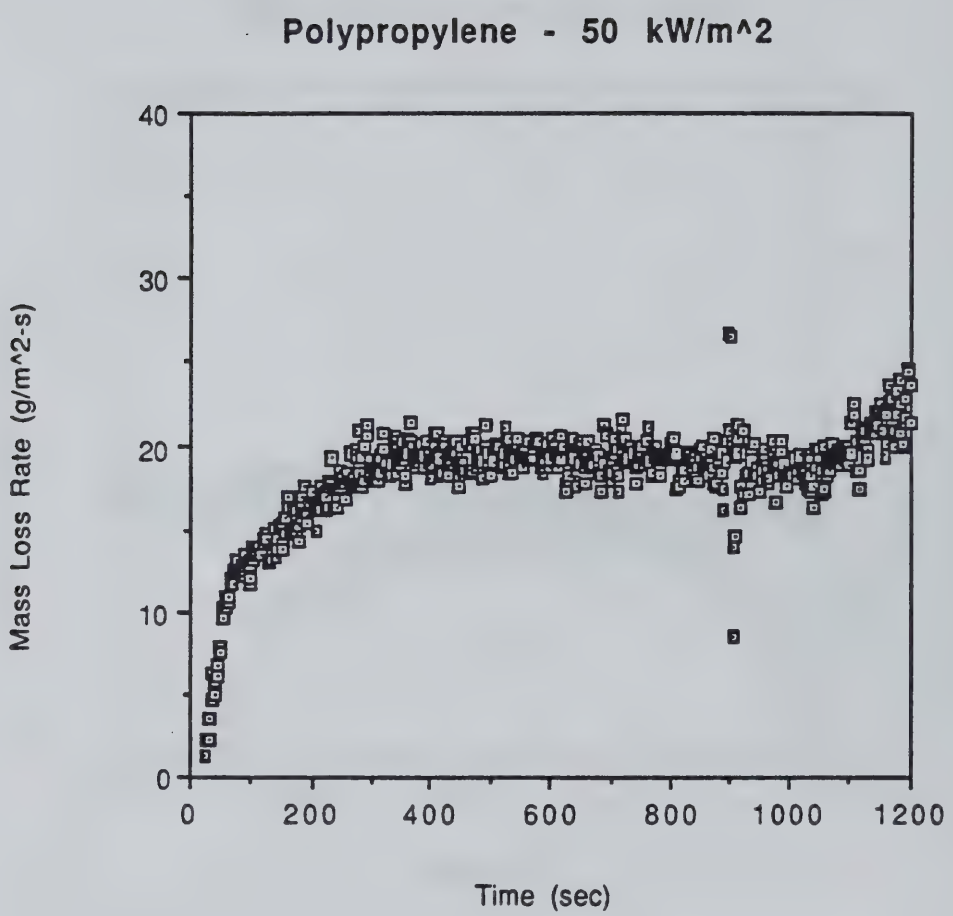

Figure F5 Transient mass loss rate results for Polypropylene with a 50 kW/m^2 external irradiance.

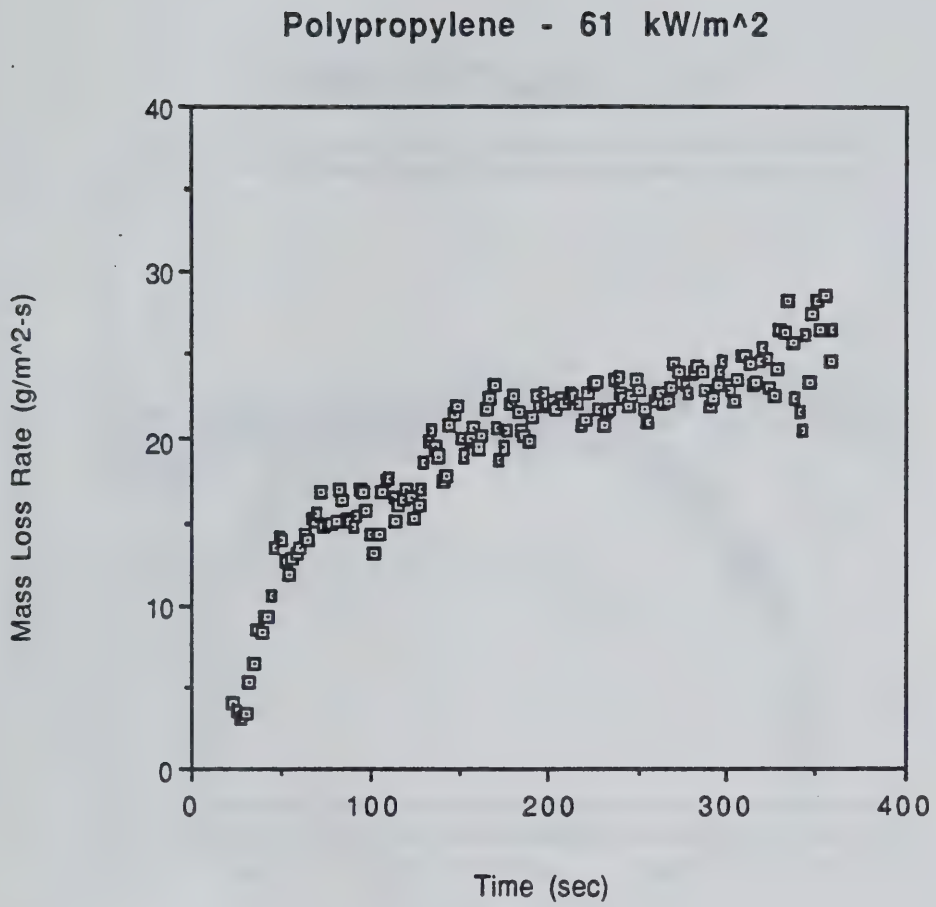

Figure F6 Transient mass loss rate results for Polypropylene with a 61 kW/m^2 external irradiance.

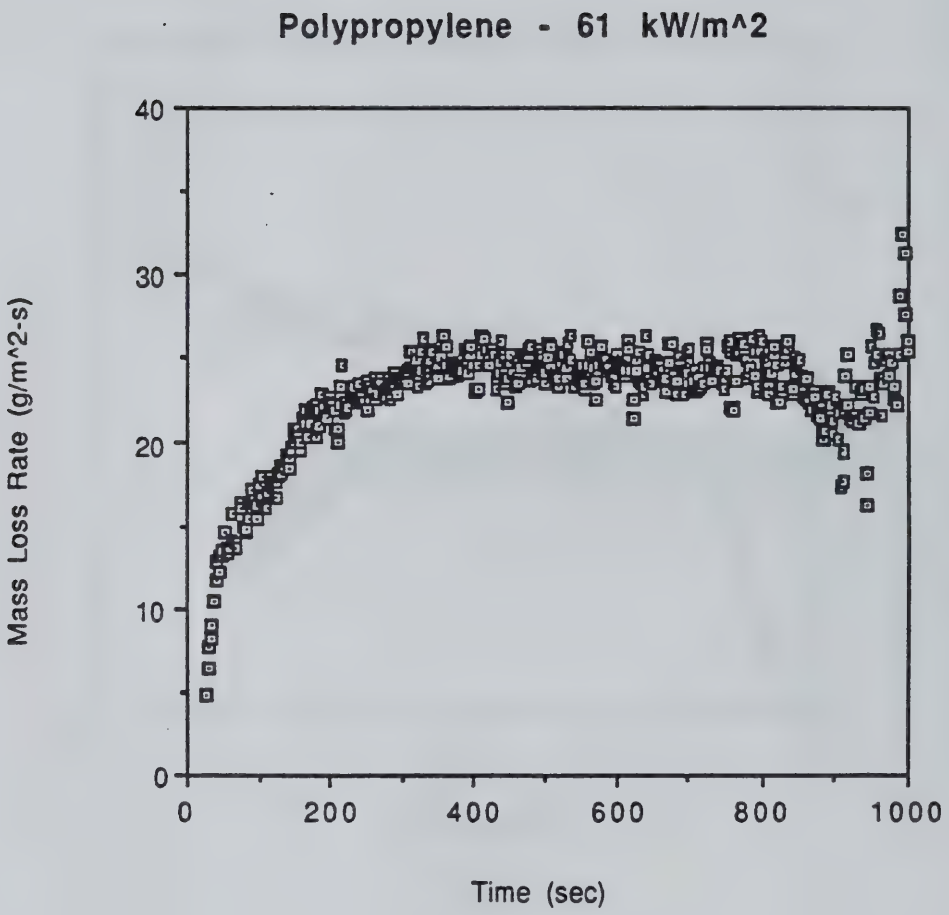

Figure F7 Transient mass loss rate results for Polypropylene with a 61 kW/m^2 external irradiance.

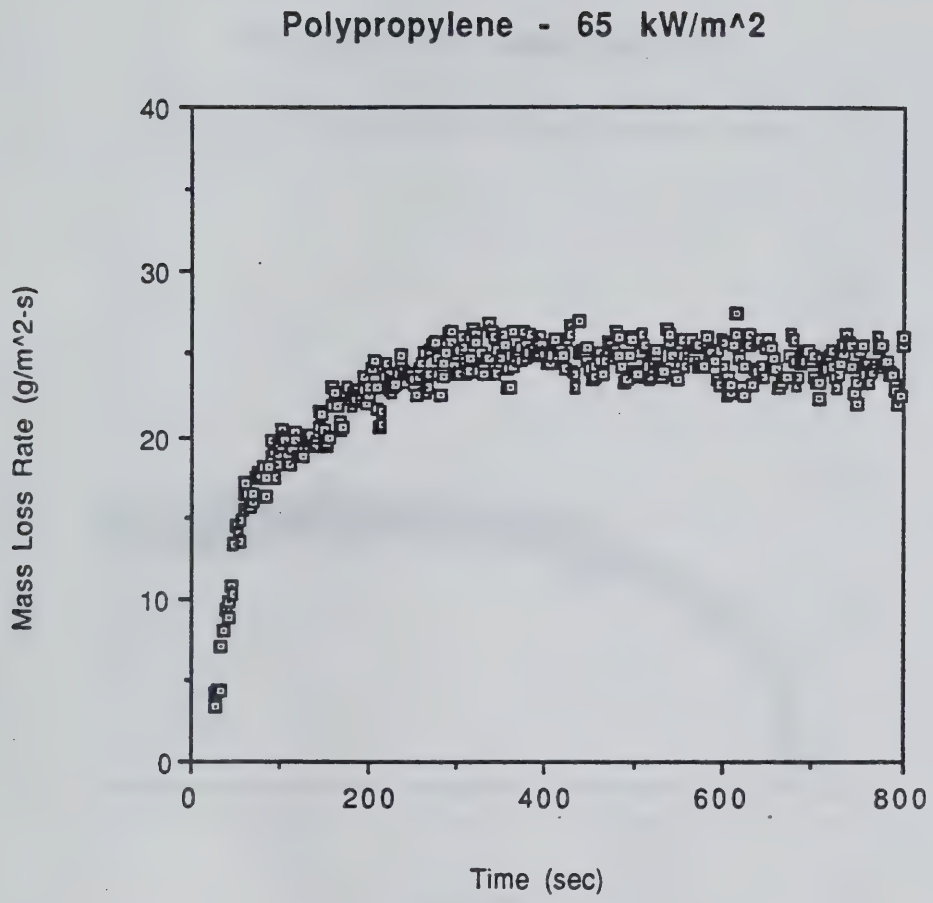

Figure F8 Transient mass loss rate results for Polypropylene with a 65 kW/m^2 external irradiance.

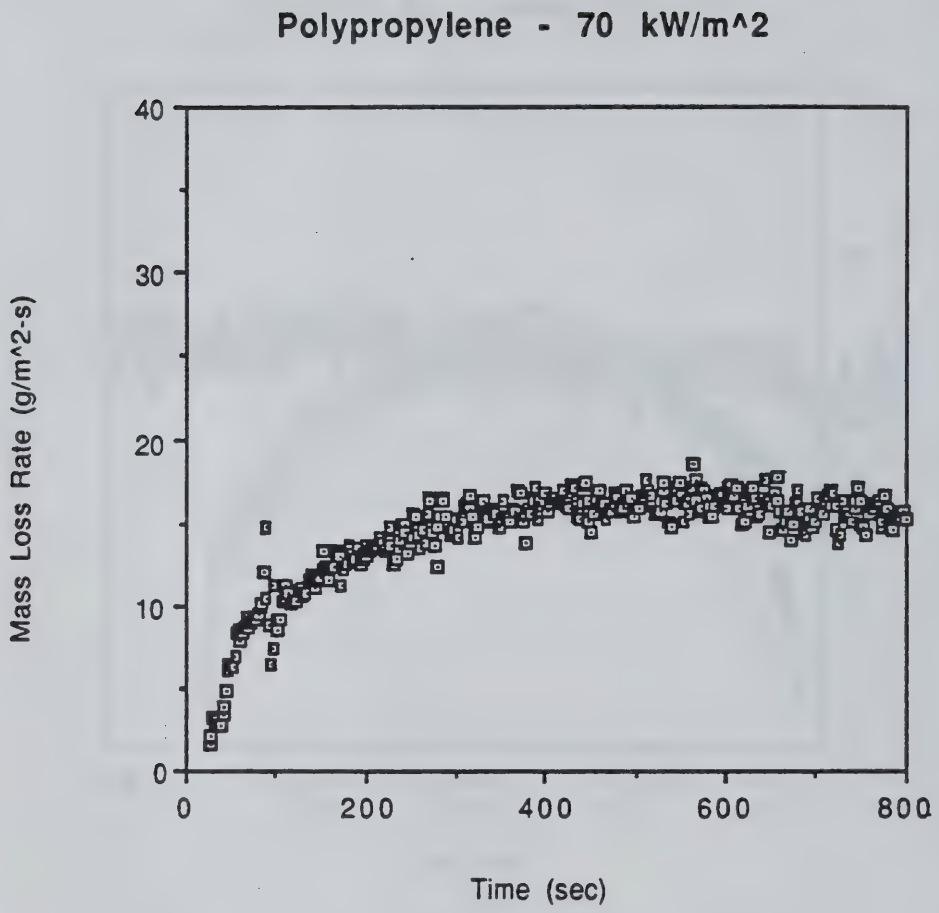

Figure F9 Transient mass loss rate results for Polypropylene with a 70 kW/m^2 external irradiance.

APPENDIX G IGNITION TIME FOR WOODS

Material/Test Number	External Irradiance (kW/m^2)	Ignition Time (sec)
Redwood/Rw1	36	36
Redwood/Rw2	55	10
Redwood/Rw3	42	20
Redwood/Rw4	23	110
Redwood/Rw5	44	27
Redwood/Rw6	20	645
Redwood/Rw7	55	10
Redwood/Rw8	14	----
Redwood/Rw9	76	3
Redwood/Rw10	30	42
Redwood/Rw11	60	8
Redwood/Rw12	20	408
Redwood/Rw13	30	51
Redwood/Rw14	21	412
Redwood/Rw15	42	18
Redwood/Rw16	54	14
Red Oak/RO1	46	23
Red Oak/RO2	52	16
Red Oak/RO3	76	6
Red Oak/RO4	27	73
Red Oak/RO5	49	20
Red Oak/RO6	80	9
Red Oak/RO7	28	74

TABLE G1 Experimental ignition times for Redwood and Redoak.

APPENDIX H MEASURED SURFACE TEMPERATURE FOR WOODS

Material/Test Number	External Irradiance (kW/m^2)	Measured Ignition Temperature (° C)
Redwood/RW13	30	390
Redwood/RW14	21	450
Redwood/RW15	42	380
Redwood/RW16	54	430
Red Oak/RO2	52	350
Red Oak/RO3	76	280
Red Oak/RO4	27	295

Table H1 Measured ignition temperature for Redwood and Red Oak.

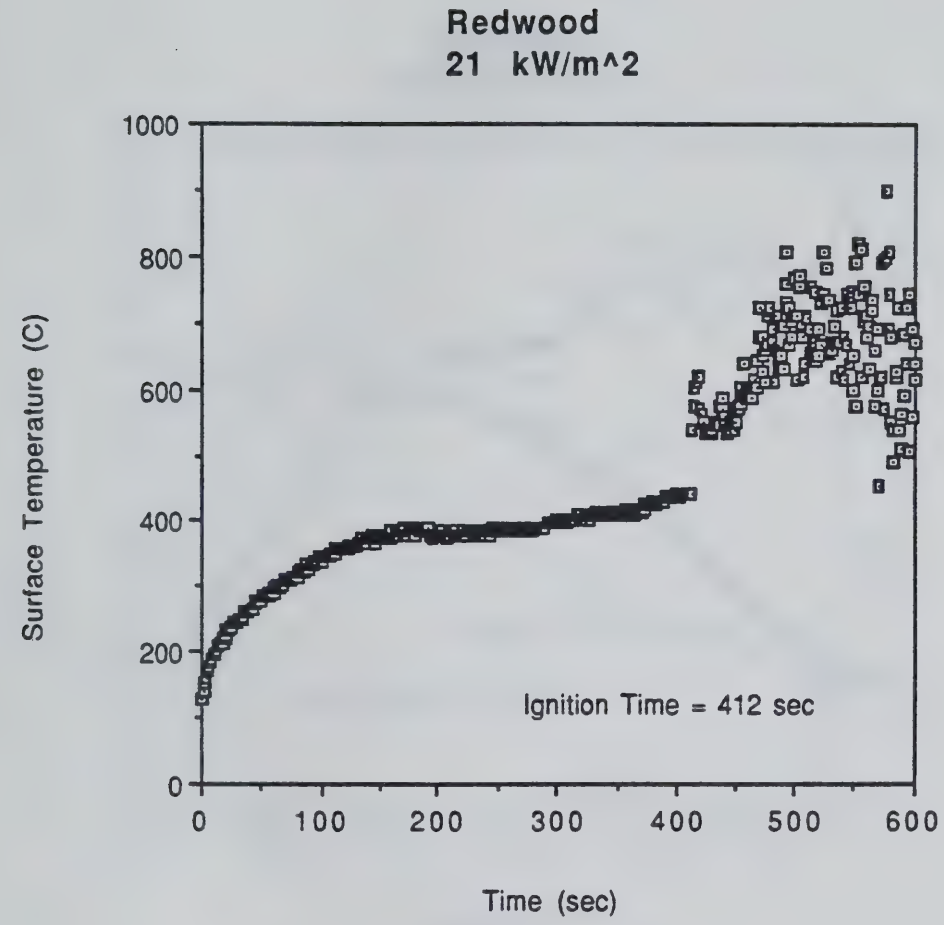

Figure H1 Surface temperature results for Redwood with a 21 kW/m^2 external irradiance.

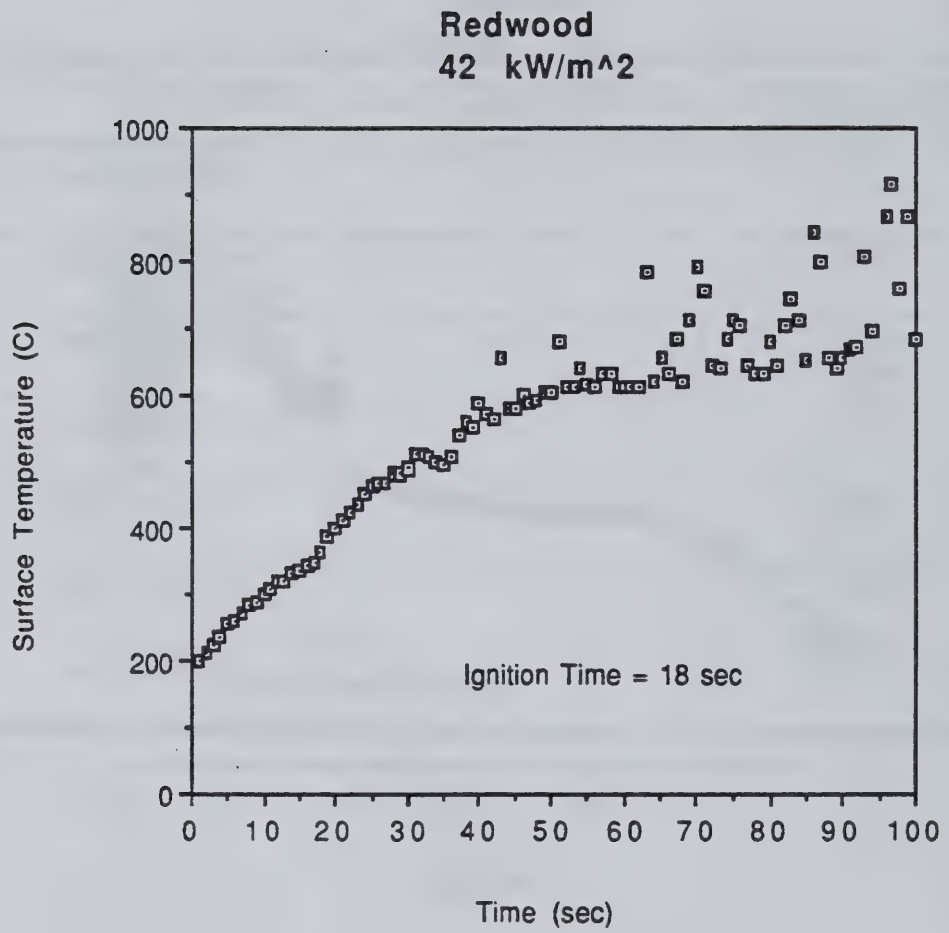

Figure H2 Surface temperature results for Redwood with a 42 kW/m^2 external irradiance.

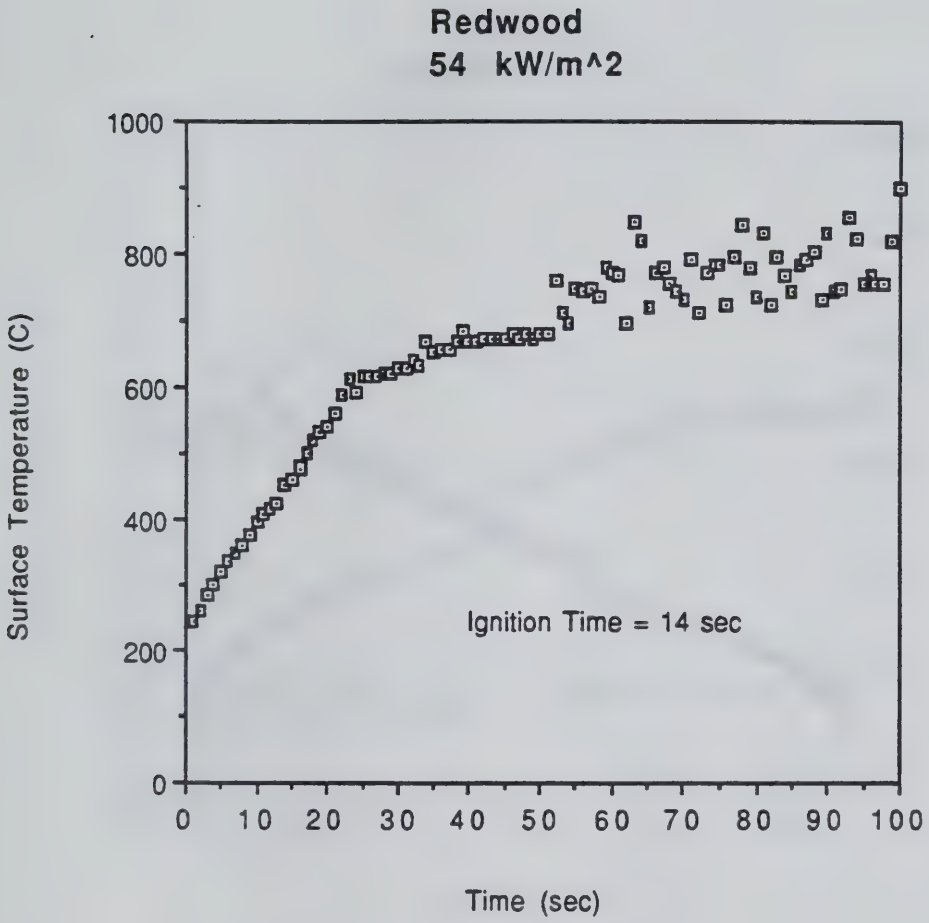

Figure H3 Surface temperature results for Redwood with a 54 kW/m^2 external irradiance.

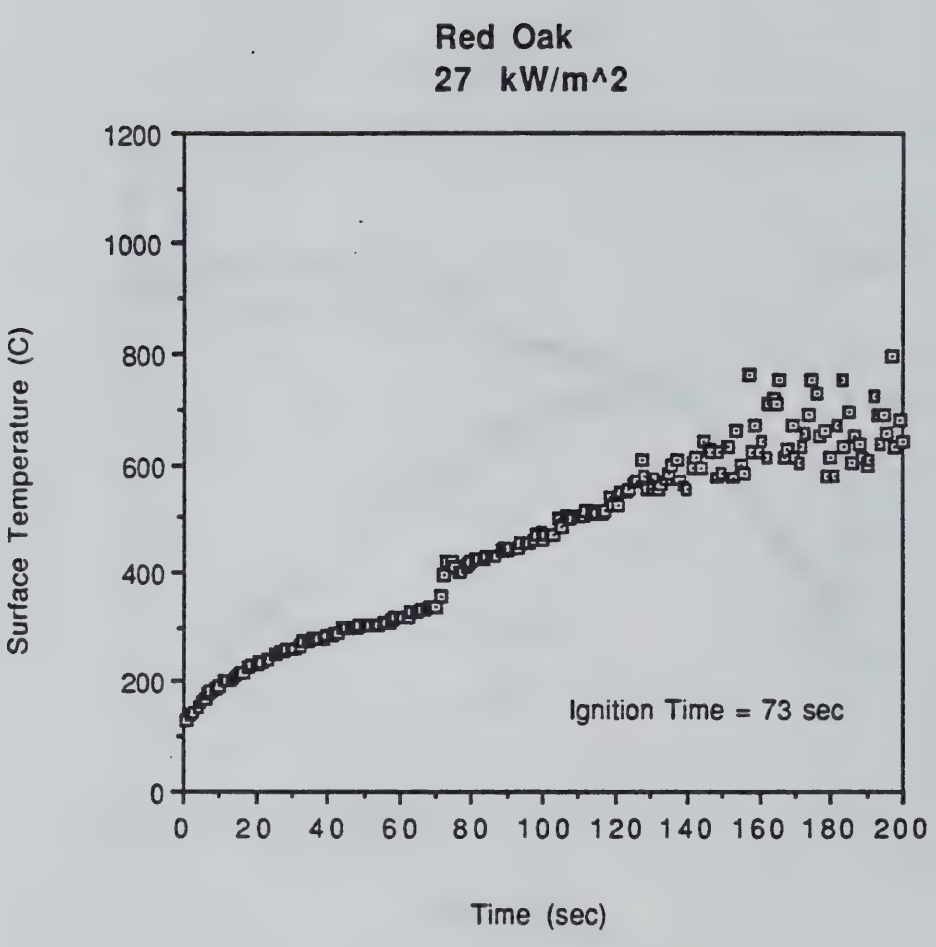

Figure H4 Surface temperature results for Red Oak with a 27 kW/m^2 external irradiance.

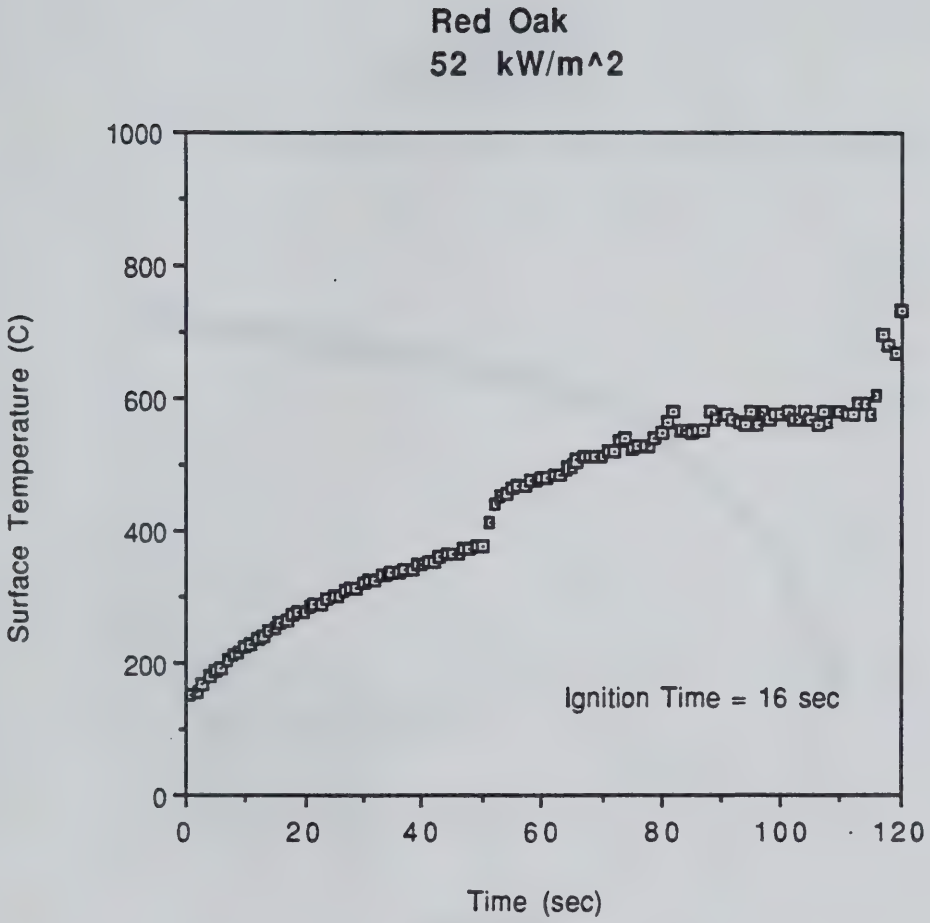

Figure H5 Surface temperature results for Red Oak with a 52 kW/m^2 external irradiance.

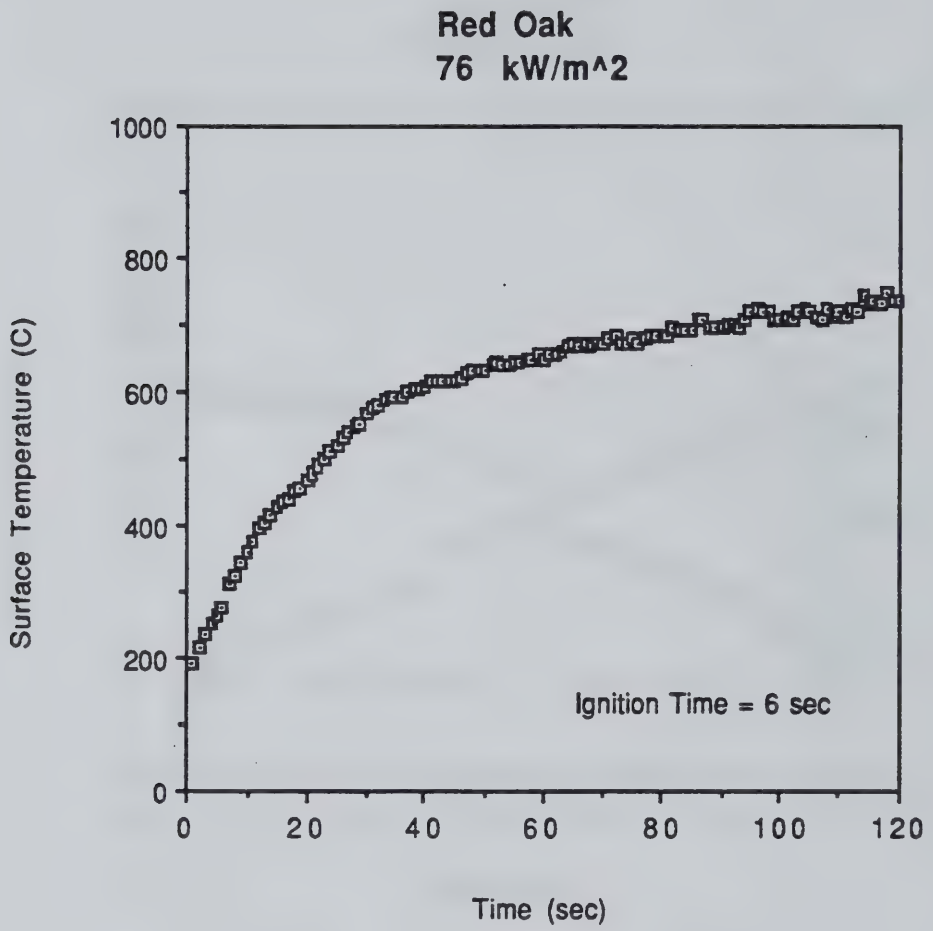

Figure H6 Surface temperature results for Red Oak with a 76 kW/m^2 external irradiance.

APPENDIX I REDWOOD MASS LOSS RATE

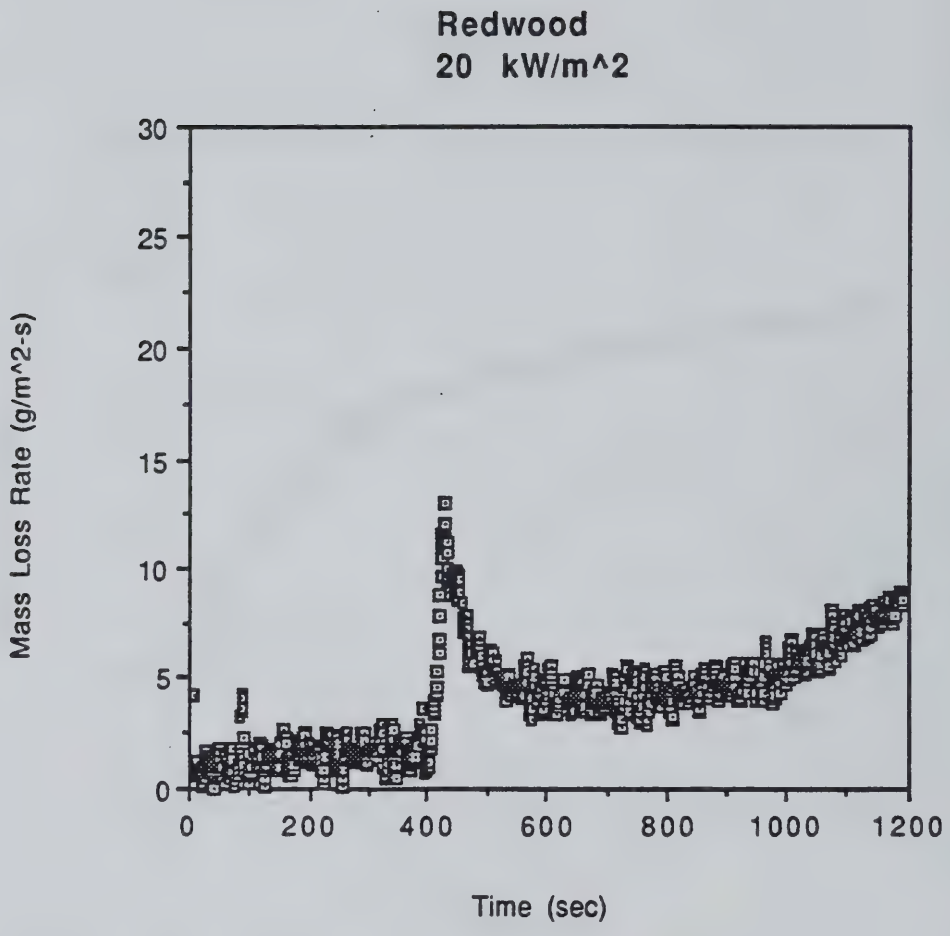

Figure I1 Mass loss rate results of Redwood with a 20 kW/m^2 external irradiance.

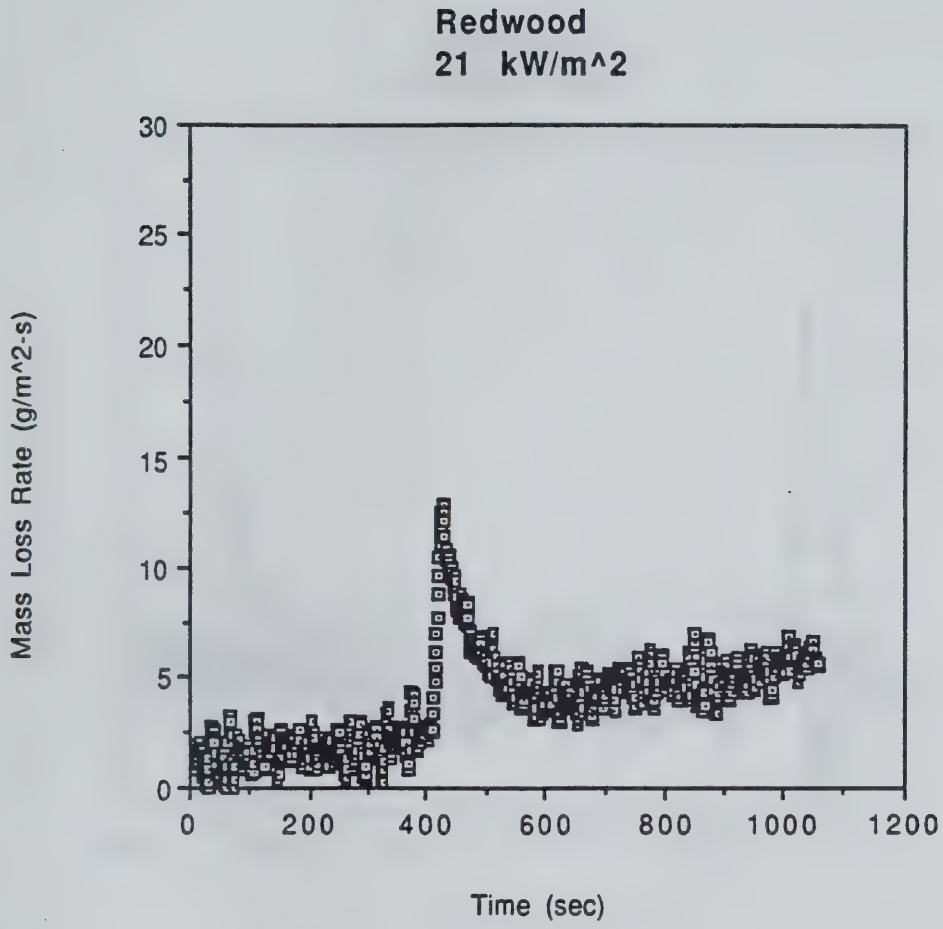

Figure I2 Mass loss rate results of Redwood with a 21 kW/m^2 external irradiance.

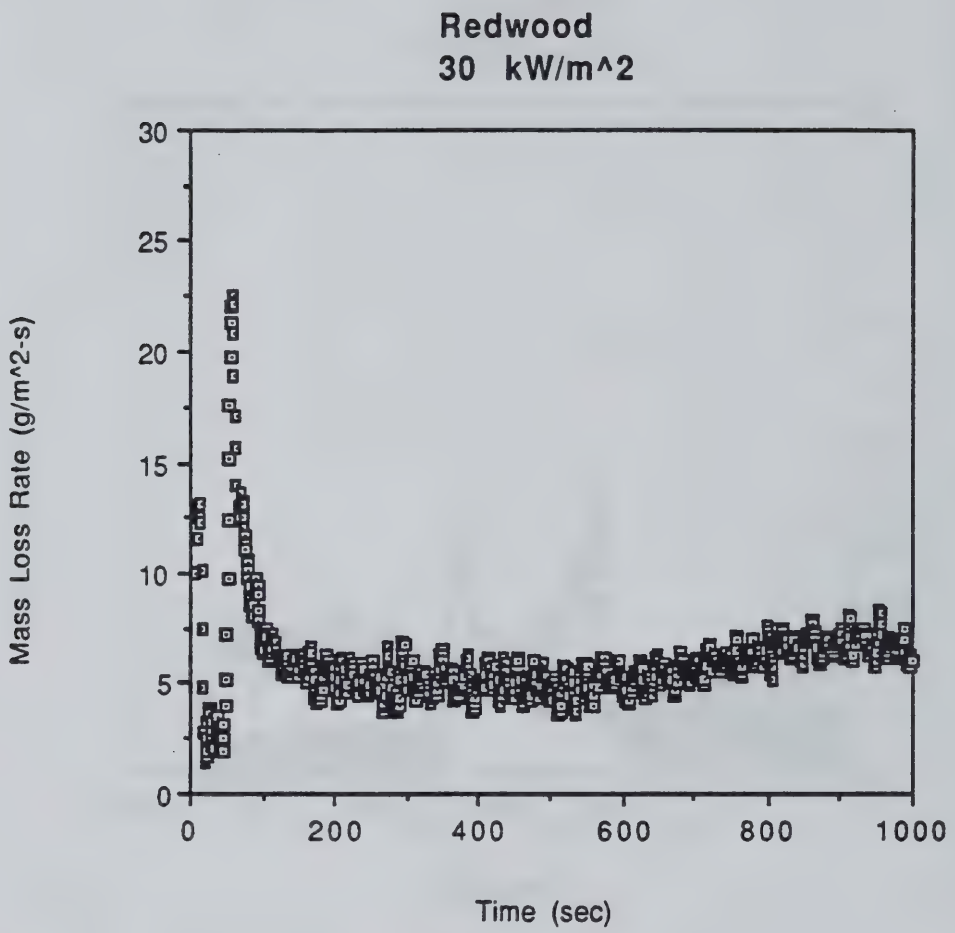

Figure I3 Mass loss rate results of Redwood with a 30 kW/m^2 external irradiance.

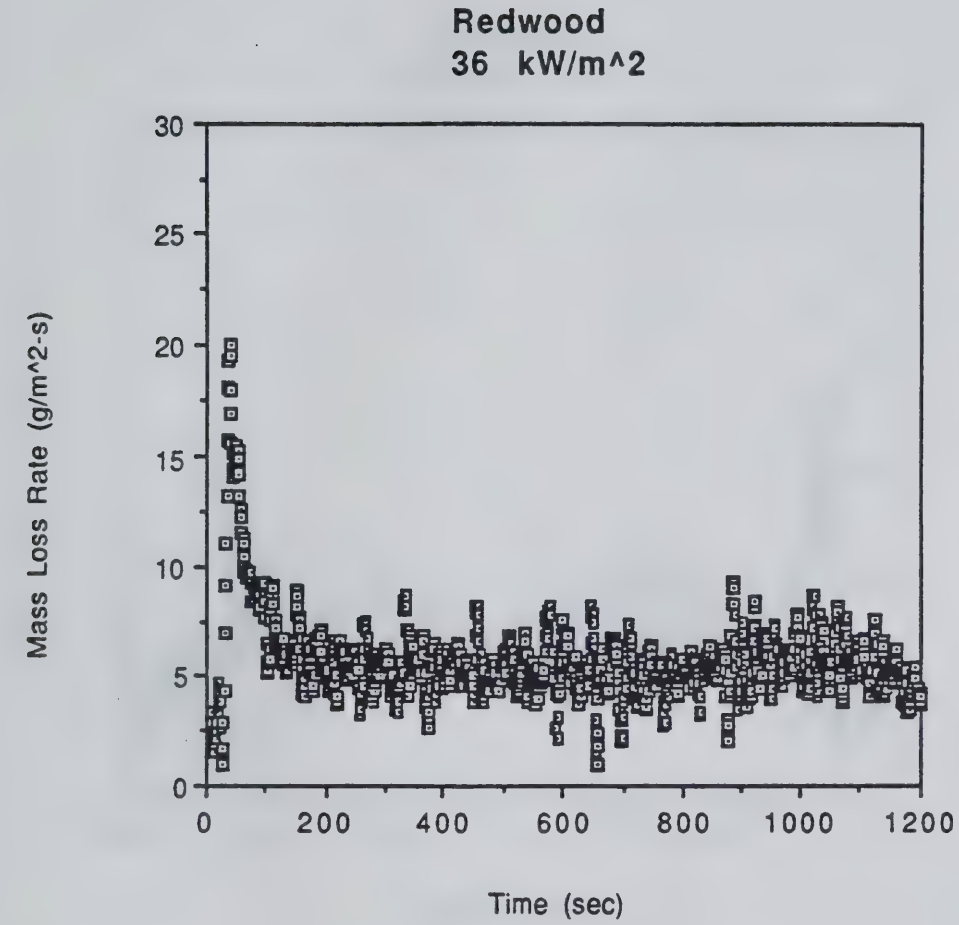

Figure I4 Mass loss rate results of Redwood with a 36 kW/m^2 external irradiance.

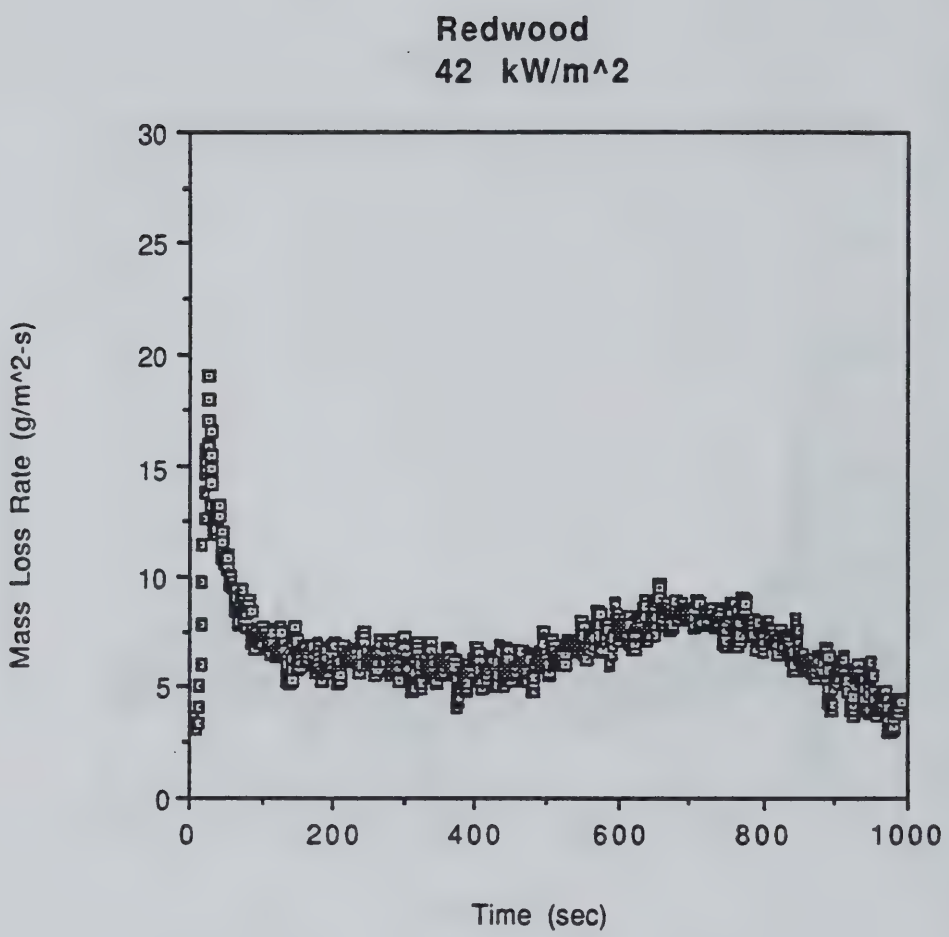

Figure I5 Mass loss rate results of Redwood with a 42 kW/m^2 external irradiance.

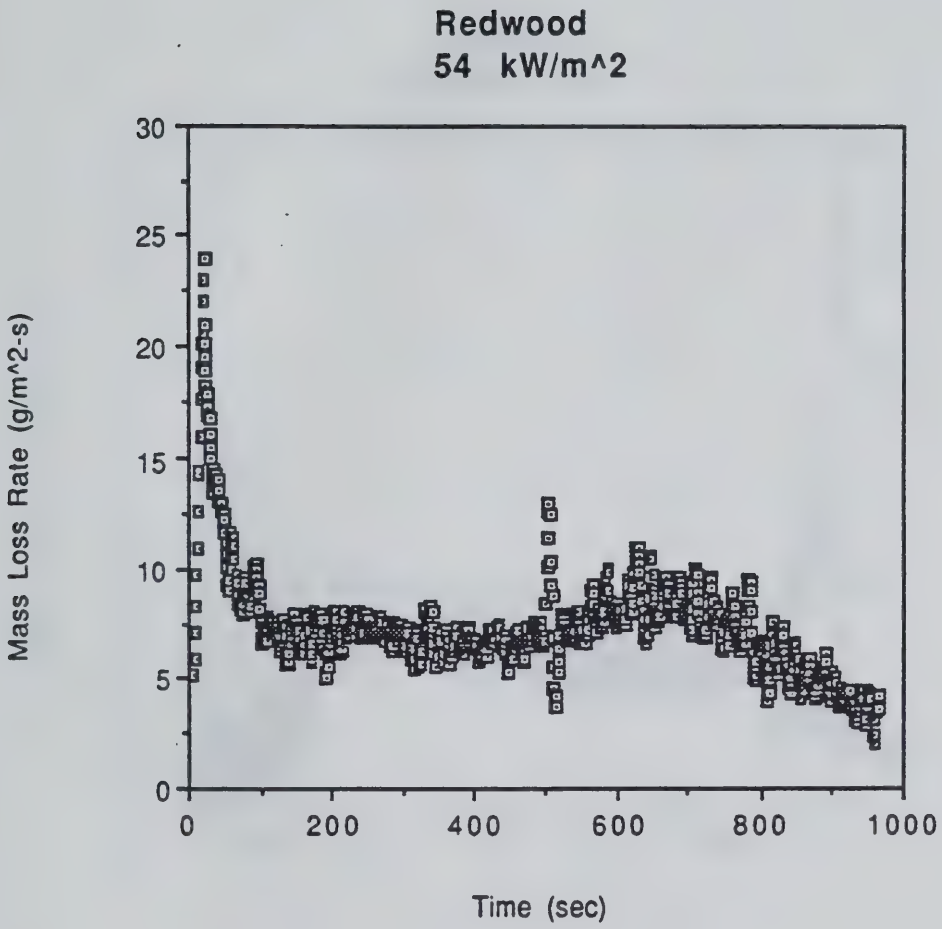

Figure I6 Mass loss rate results of Redwood with a 54 kW/m^2 external irradiance.

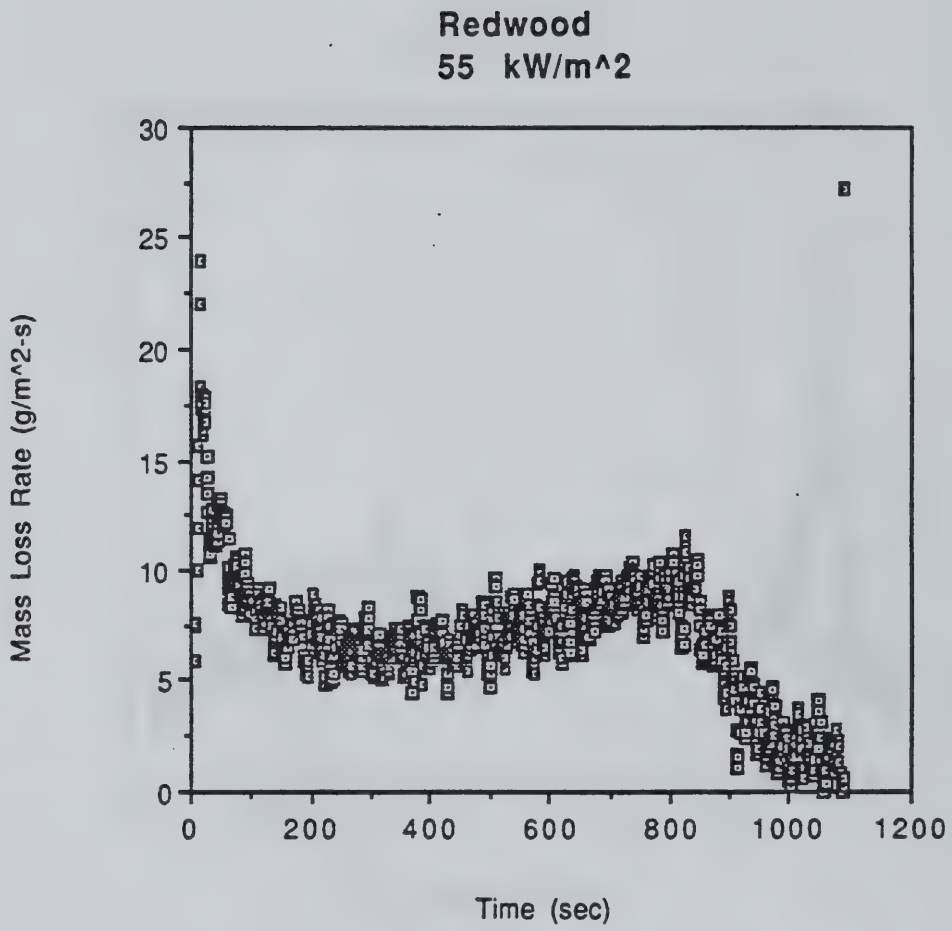

Figure I7 Mass loss rate results of Redwood with a 55 kW/m^2 external irradiance.

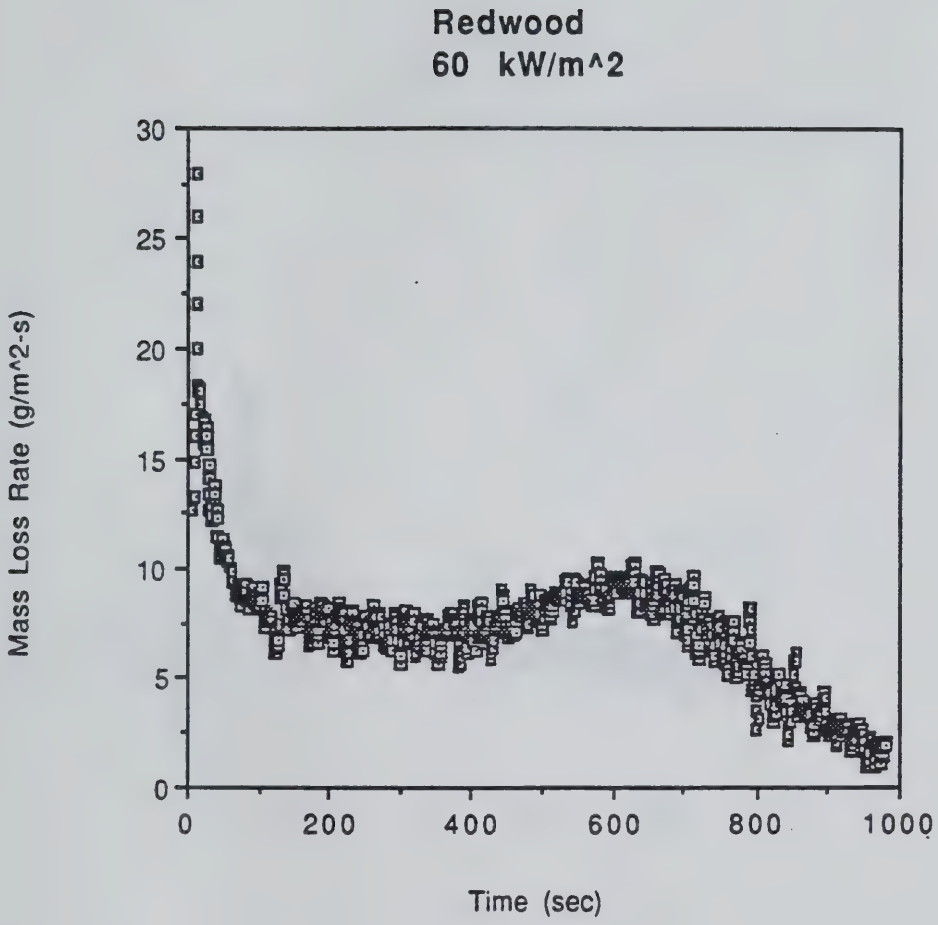

Figure I8 Mass loss rate results of Redwood with a 60 kW/m^2 external irradiance.

APPENDIX J

RED OAK MASS LOSS RATE

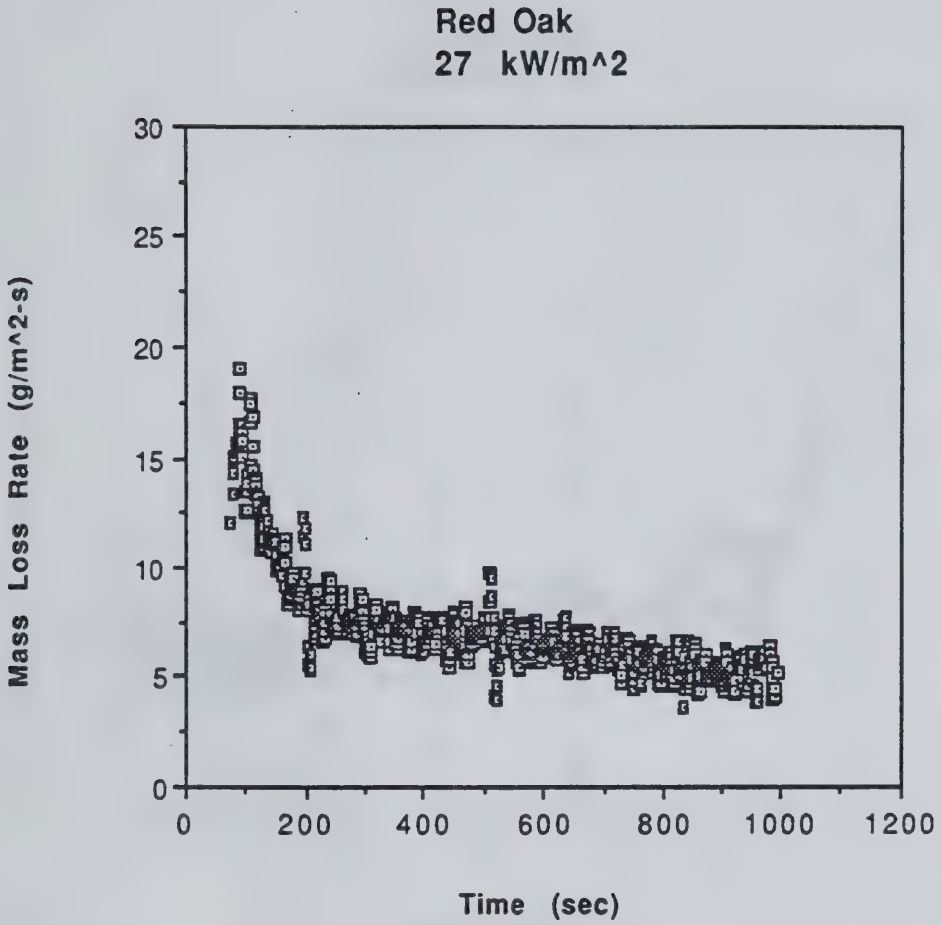

Figure J1 Mass loss rate results of Red Oak with a 27 kW/m^2 external irradiance.

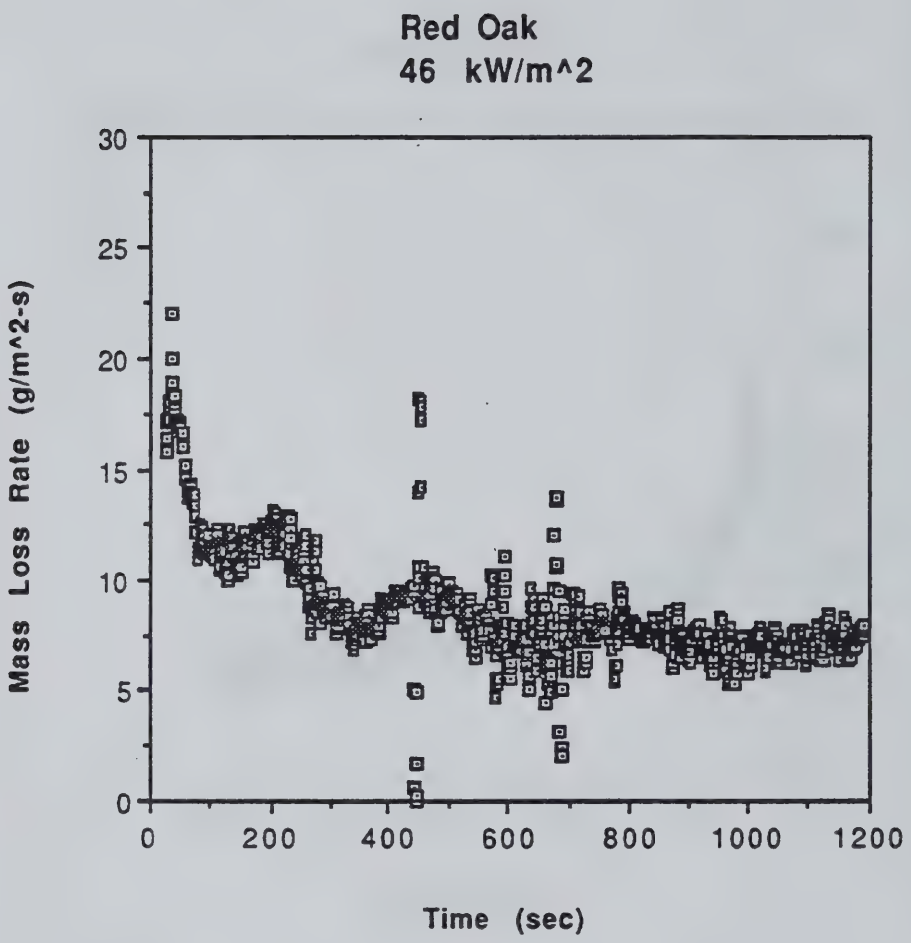

Figure J2 Mass loss rate results of Red Oak with a 46 kW/m^2 external irradiance.

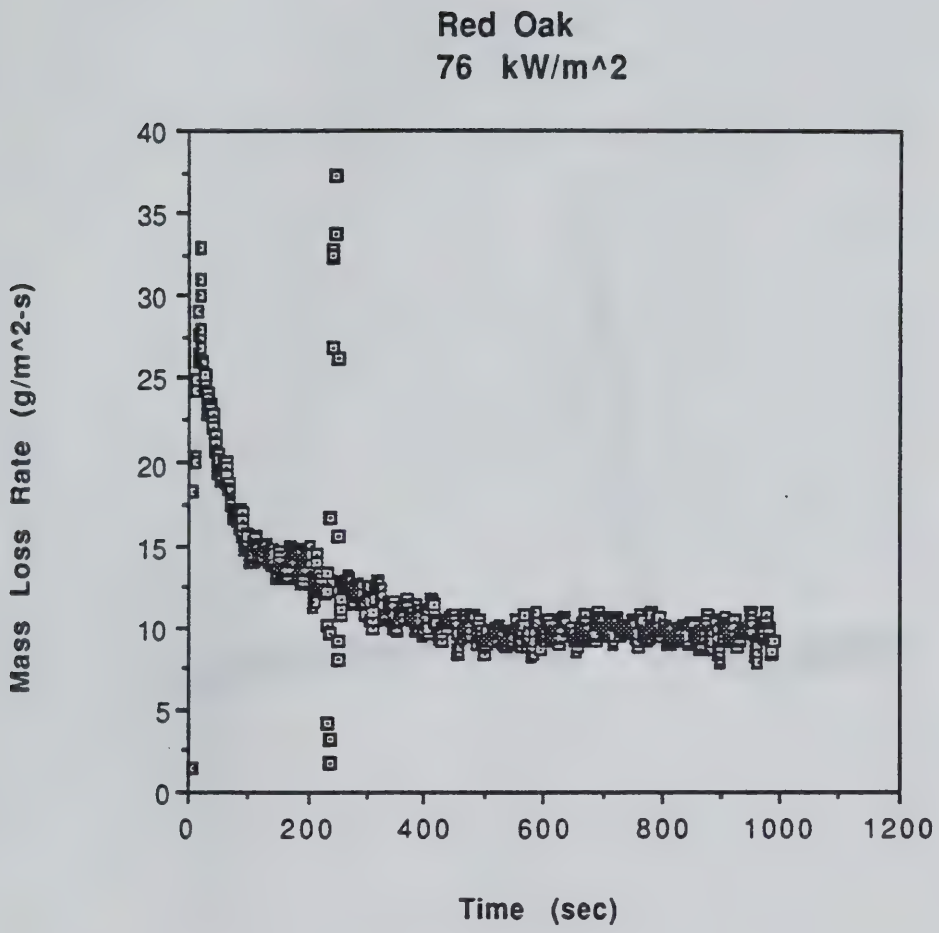

Figure J3 Mass loss rate results of Red Oak with a 76 kW/m^2 external irradiance.

APPENDIX K REDWOOD INCIDENT HEAT FLUX

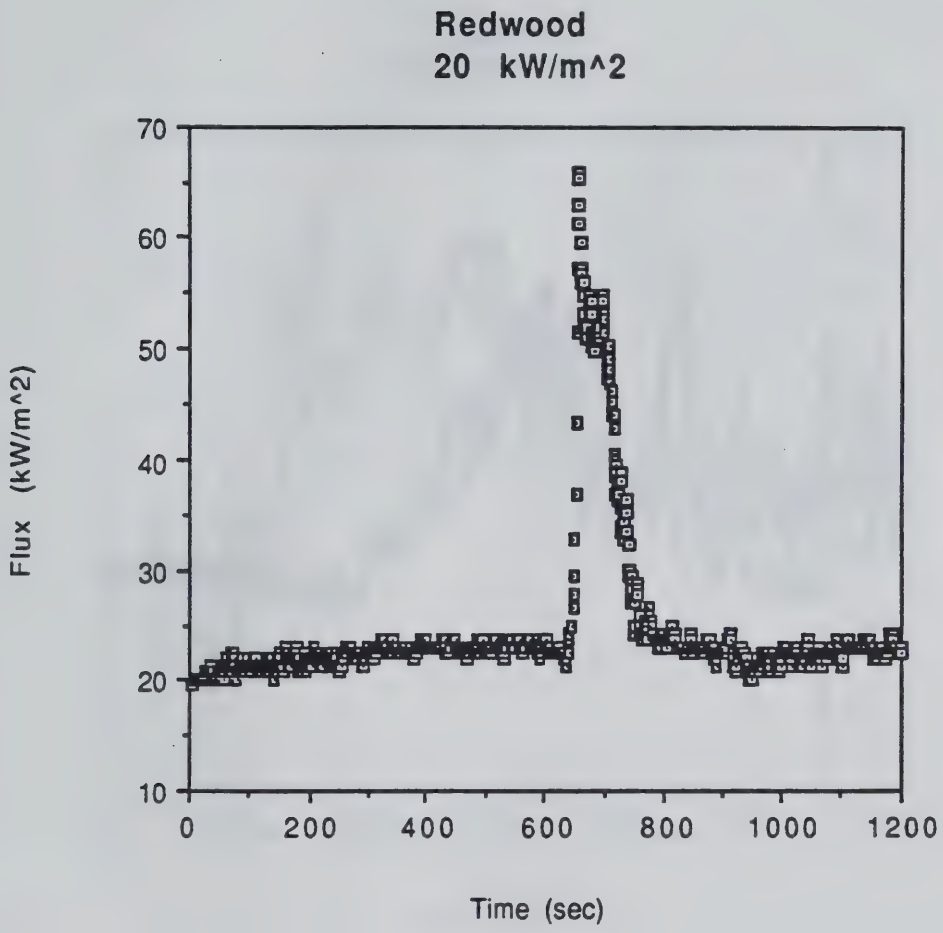

Figure K1 Incident heat flux results for Redwood with a 20 kW/m^2 external irradiance.

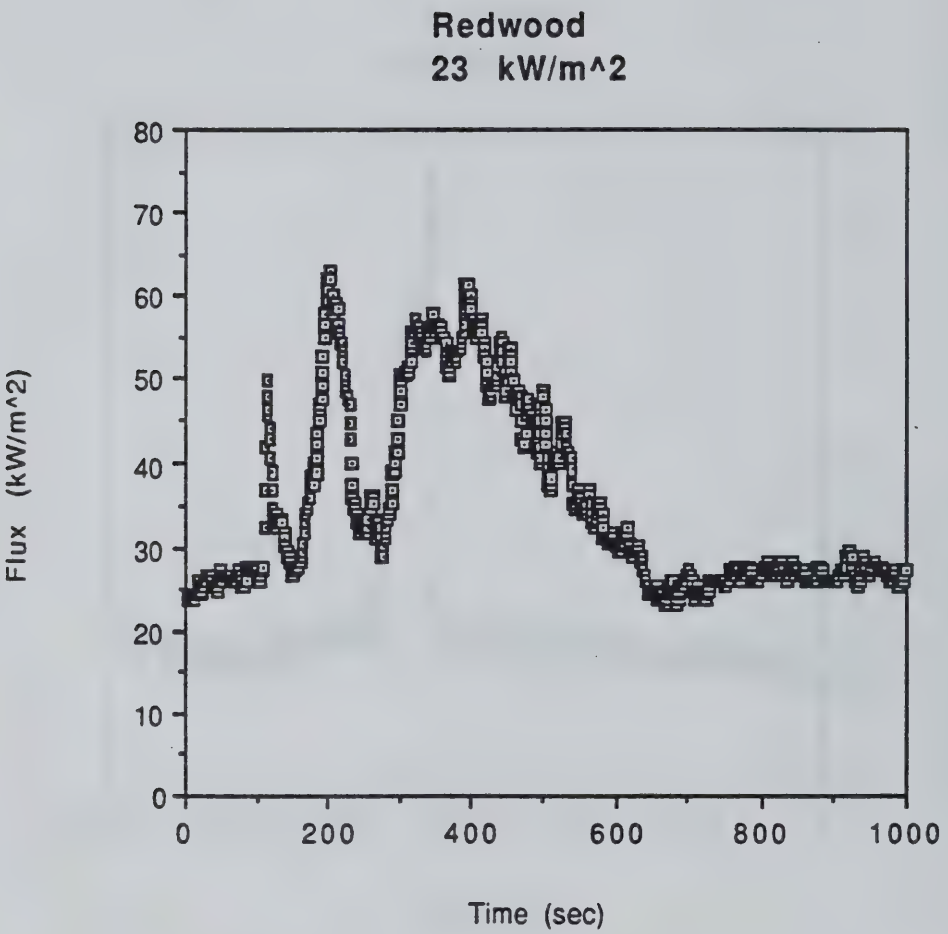

Figure K2 Incident heat flux results for Redwood with a 23 kW/m^2 external irradiance.

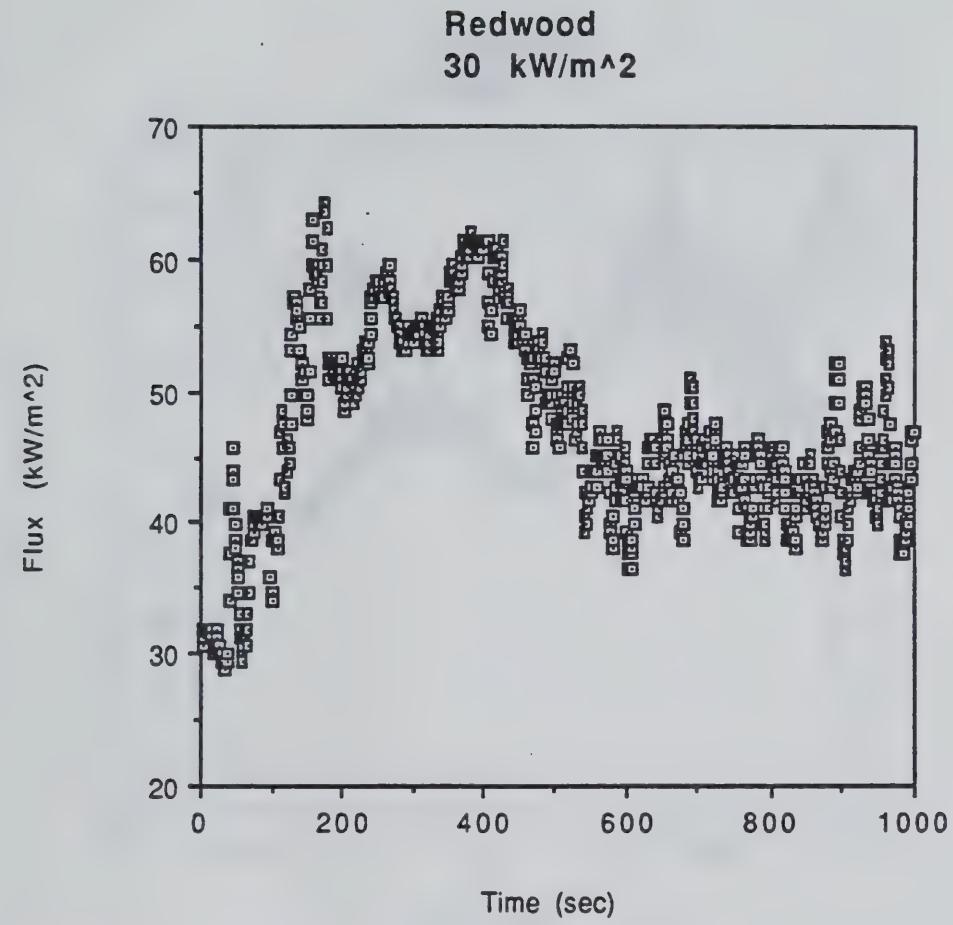

Figure K3 Incident heat flux results for Redwood with a 30 kW/m^2 external irradiance.

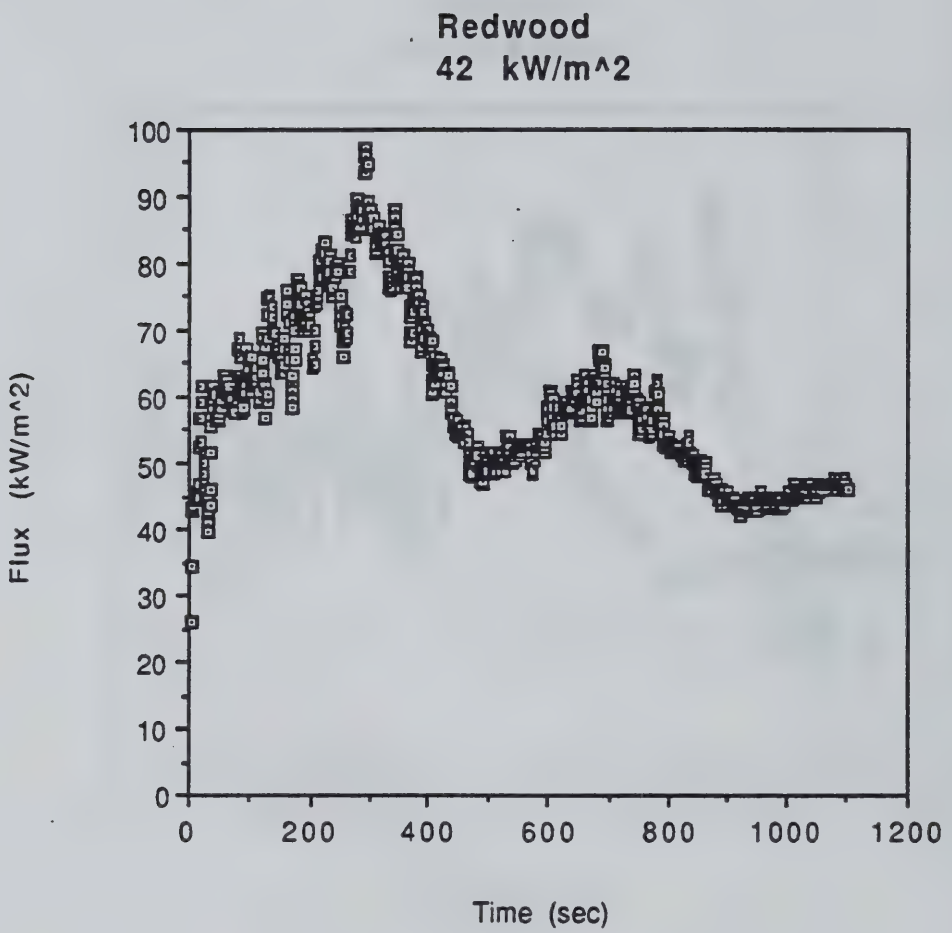

Figure K4 Incident heat flux results for Redwood with a 42 kW/m^2 external irradiance.

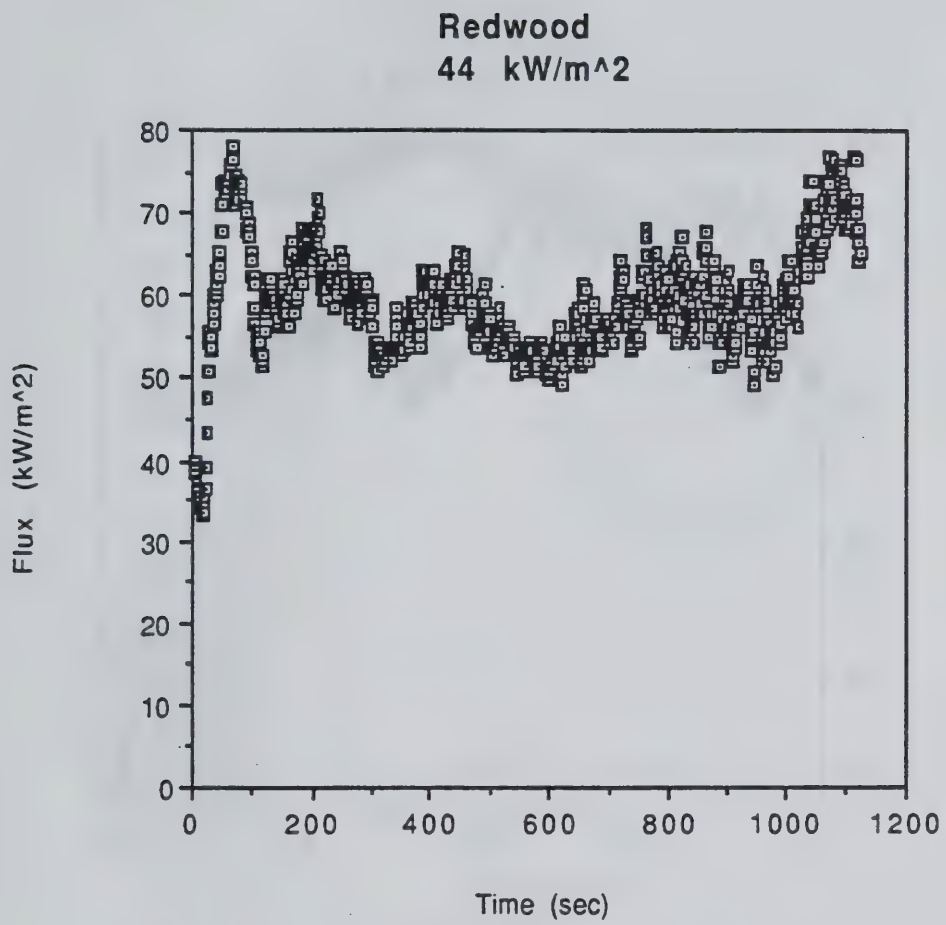

Figure K5 Incident heat flux results for Redwood with a 44 kW/m^2 external irradiance.

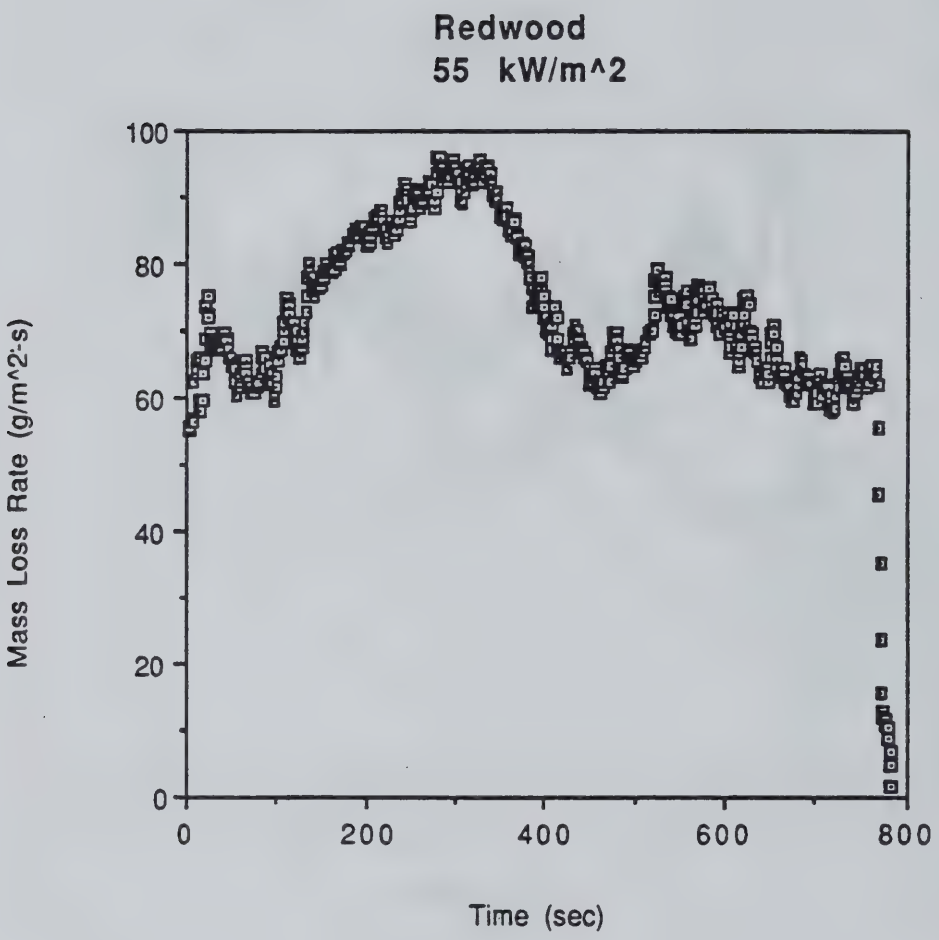

Figure K6 Incident heat flux results for Redwood with a 55 kW/m^2 external irradiance.

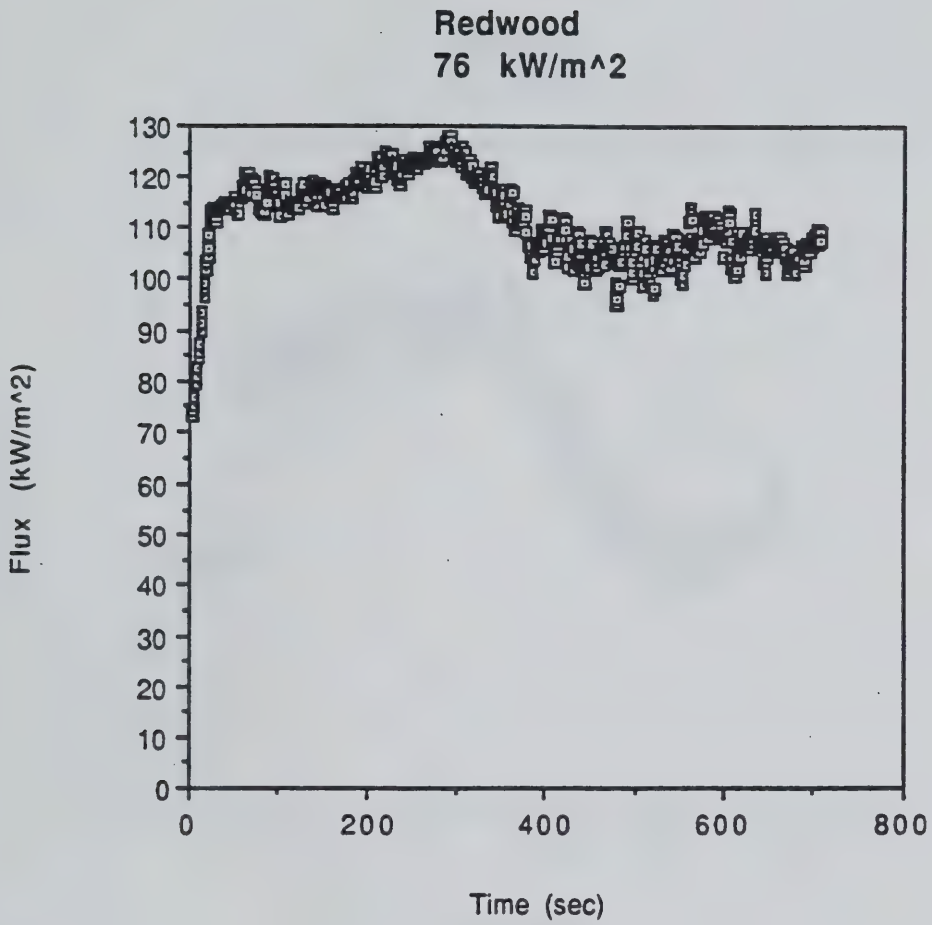

Figure K7 Incident heat flux results for Redwood with a 76 kW/m^2 external irradiance.

APPENDIX L RED OAK INCIDENT HEAT FLUX

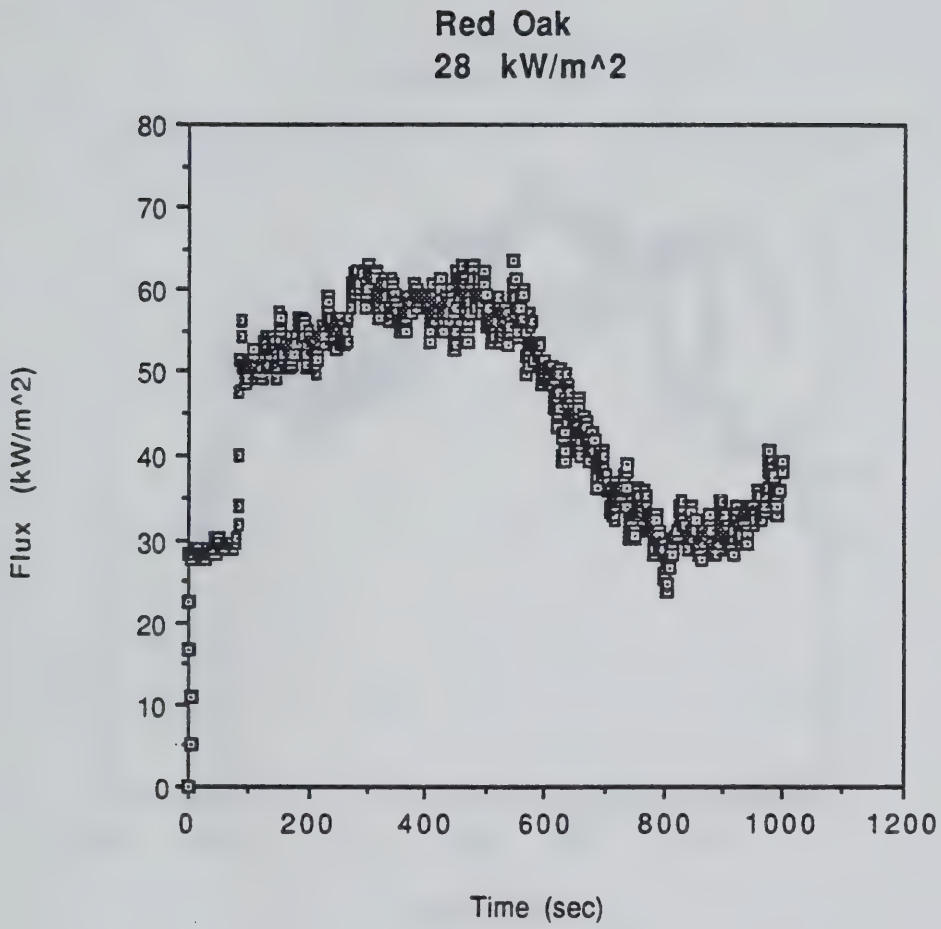

Figure L1 Incident heat flux results for Red Oak with a 28 kW/m^2 external irradiance.

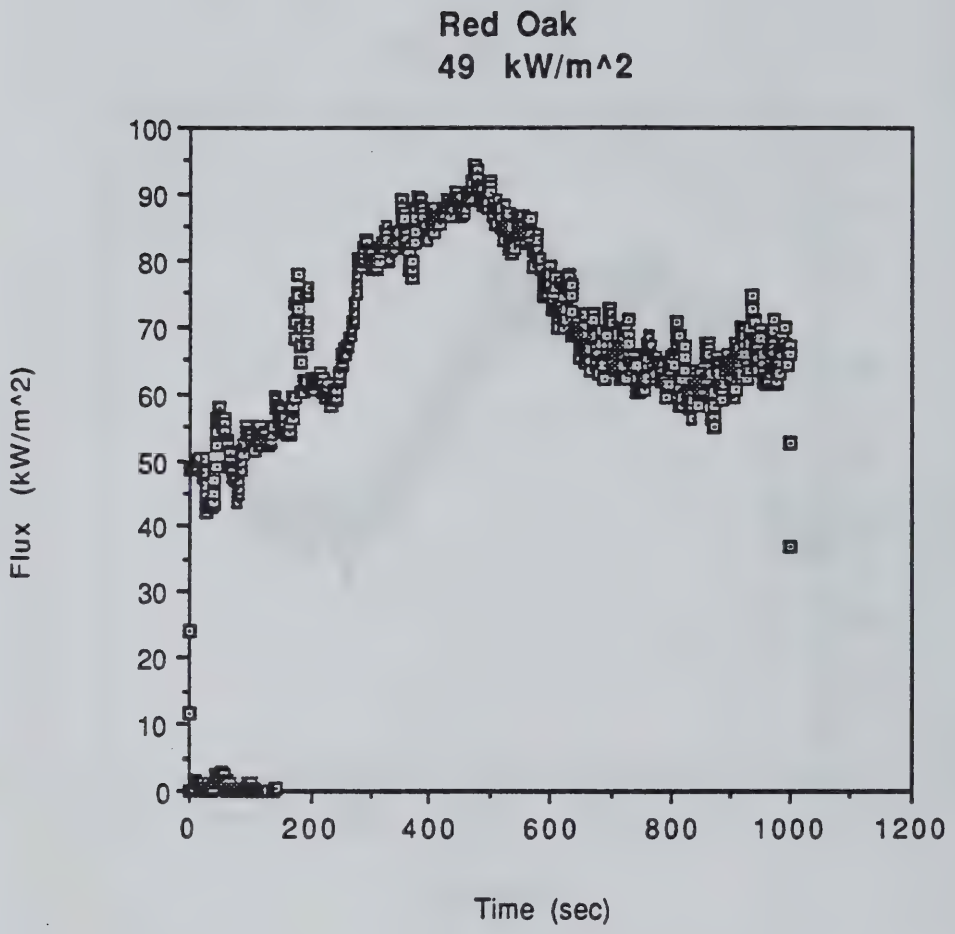

Figure L2 Incident heat flux results for Red Oak with a 49 kW/m^2 external irradiance.

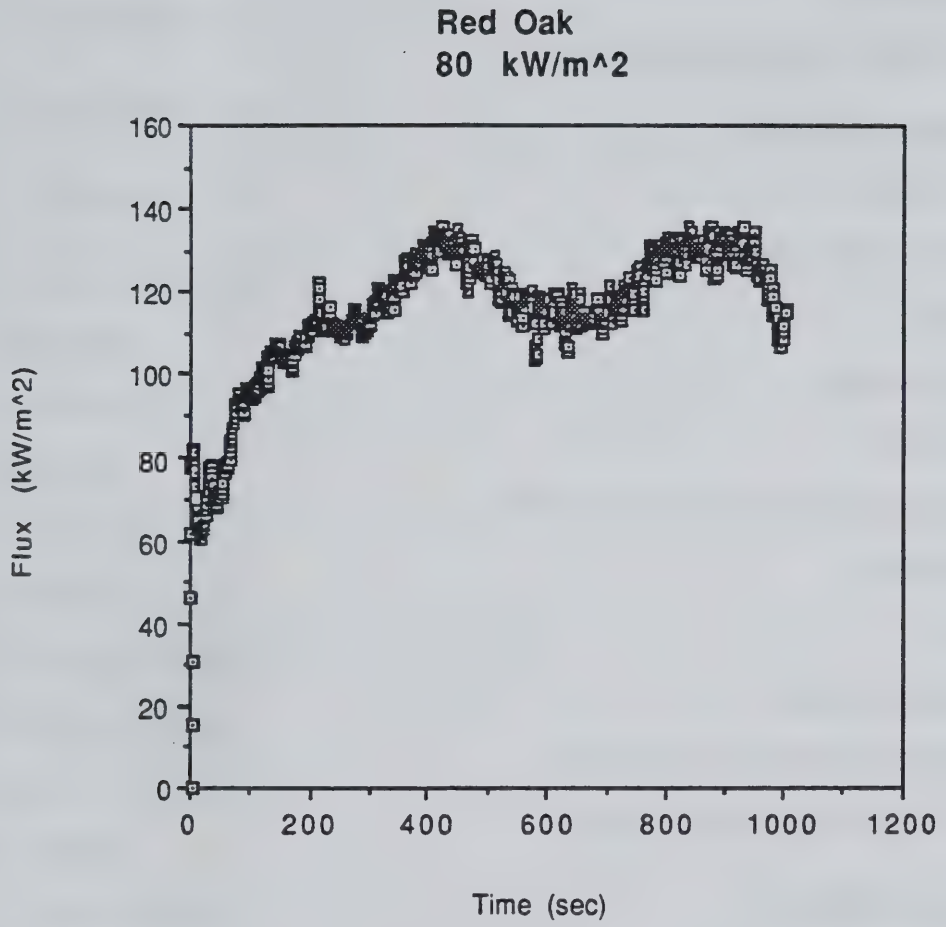

Figure L3 Incident heat flux results for Red Oak with a 80 kW/m^2 external irradiance.

NOMENCLATURE

c - specific heat

h_c - convective heat transfer coefficient

k - thermal conductivity

l - beam length

L - heat of gasification

m - mass

Q - power output

q - heat flow

r - stoichiometric oxygen to fuel mass ratio

T - temperature

t - time

y - space coordinate

y-dimensionless mass loss rate (ch. 6)

$Y_{ox,\infty}$ - ambient oxygen mass fraction

α - thermal diffusivity

δ - thermal penetration depth

ΔH_v - heat of vaporization

ΔH_c - heat of combustion

ε - emissivity

κ - absorption-emission coefficient

ρ - density

σ - Stefan Boltzmann constant

χ - heat fraction

ξ – variable (Eq. 4.16)

τ – dimensionless time

ϕ - variable (Eq. 6.2)

x - variable (Eq. 6.3)

Subscripts

c - convective

cr - critical

ext - external

fl - flame

fl,c - flame convection

fl,r - flame radiation

g - gas

ig - ignition

o - initial, ambient

m - mean

r - radiative

s - steady

v - vaporization

Superscripts

($\dot{}$) - per unit time

( )" - per unit area

REFERENCES

1. Quintiere, J. G., "A Semi-Quantitative Model for the Burning of Solid Materials", National Institute of Standards and Technology, NIST-4840, June, 1992.

2. Quintiere, J. G. and Iqbal, N., "A Burning Rate Model for Materials", accepted by Fire and Materials, July, 1993.

3. Standard Test Method for Heat and Visible Smoke Release Rates for Materials and Products Using Oxygen Depletion, (ASTM E 1354), American Society for Testing and Materials, Philadelphia, PA.

4. Wickstrom, U. and Goransson, U., "Prediction of Heat Release Rates of Surface Materials in Large-Scale Fire Tests Based on Cone Calorimeter Results", ASTM Journal of Testing and Evaluation, Vol. 15, No. 6, 1987.

5. Karlsson, B. "Modeling Fire Growth on Combustible Lining Materials in Enclosures", Report TVBB-1009, Lund University, Department of Fire Safety Engineering, Lund, Sweden, 1992.

6. Quintiere, J. G., "A Simulation Model for Fire Growth on Materials Subject to a Room-Corner Test", Fire Safety Journal, Vol. 18, 1992.

7. Quintiere, J. G., Haynes, G., and Rhodes, B. T., "Applications of a Model to Predict Flame Spread over Interior Finish Materials in a Compartment", International Conference for the Promotion of Advanced Fire Resistant Aircraft Interior Materials, FAA Technical Center, Atlantic City, NJ, March, 1993.

8. Quintiere, J. G. and Rhodes, B.T., "Fire Growth Models for Materials", Department of Fire Protection Engineering, University of Maryland at College Park, January, 1994.

9. Rhodes, B.T., "Burning Rate and Flame Heat Flux for PMMA in the Cone Calorimeter", Department of Fire Protection Engineering, University of Maryland at College Park, May, 1994.

10. Abu-Zaid, M. and Atreya, A., "Effect of Water on Piloted Ignition of Cellulosic Materials", National Institute of Standards and Technology, NIST-GCR-89-561, February, 1989.

11. Orloff, L. and deRis, J., "Froude Modeling of Pool Fires", 19th Symposium (International) on Combustion, pp. 885-895, The Combustion Institute, Pittsburgh, PA, 1982.

12. Modern Plastics Encyclopedia, Vol 48., No. 10A, Sidney Gross, ed., McGraw Hill, New York, October 1971.

13. Steckler, K. D., Kashiwagi, T., Baum, H. R., and Kanemaru, K., "Analytical Model for Transient Gasification of Non-Charring Thermoplastic Materials", Fire Safety Science Proceedings of Third (International) Symposium, pp. 895-904, G. Cox and B.

Landford, eds., Elsevier Applied Science, London, 1991.

14. Atreya A., Carpentier C., and Harkleroad, M., "Effect of Sample Orientation on Piloted Ignition and Flame Spread", Fire Safety Science Proceedings of First (International) Symposium, pp.97-109, Grant, C., and Pagni, P., eds., Hemisphere Publishing Corp., New York, 1986.

NIST-114
(REV. 6-93)
ADMAN 4.09

U.S. DEPARTMENT OF COMMERCE
NATIONAL INSTITUTE OF STANDARDS AND TECHNOLOGY

MANUSCRIPT REVIEW AND APPROVAL

(ERB USE ONLY)

ERB CONTROL NUMBER	DIVISION
PUBLICATION REPORT NUMBER	CATEGORY CODE
NIST-GCR-95-677	
PUBLICATION DATE	NUMBER PRINTED PAGES
September 1995	

INSTRUCTIONS: ATTACH ORIGINAL OF THIS FORM TO ONE (1) COPY OF MANUSCRIPT AND SEND TO THE SECRETARY, APPROPRIATE EDITORIAL REVIEW BOARD

TITLE AND SUBTITLE (CITE IN FULL)

Predicting the Ignition Time and Burning Rate of Thermoplastics in the Cone Calorimeter

CONTRACT OR GRANT NUMBER
60NANB2D1266

TYPE OF REPORT AND/OR PERIOD COVERED
Grant Report January 1995 - June 1995

AUTHOR(S) (LAST NAME, FIRST INITIAL, SECOND INITIAL)

Donald Hopkins, Jr.
Department of Fire Protection Engineering
University of Maryland
College Park, MD 20742

PERFORMING ORGANIZATION (CHECK (X) ONE BOX)

- [ ] NIST/GAITHERSBURG
- [ ] NIST/BOULDER
- [ ] JILA/BOULDER

LABORATORY AND DIVISION NAMES (FIRST NIST AUTHOR ONLY)

Building and Fire Research Laboratory, Fire Science Division

SPONSORING ORGANIZATION NAME AND COMPLETE ADDRESS (STREET, CITY, STATE, ZIP)

U.S. Department of Commerce
National Institute of Standards and Technology
Gaithersburg, MD 20899

PROPOSED FOR NIST PUBLICATION

- [ ] JOURNAL OF RESEARCH (NIST JRES)
- [ ] J. PHYS. & CHEM. REF. DATA (JPCRD)
- [ ] HANDBOOK (NIST HB)
- [ ] SPECIAL PUBLICATION (NIST SP)
- [ ] TECHNICAL NOTE (NIST TN)
- [ ] MONOGRAPH (NIST MN)
- [ ] NATL. STD. REF. DATA SERIES (NIST NSRDS)
- [ ] FEDERAL INF. PROCESS. STDS. (NIST FIPS)
- [ ] LIST OF PUBLICATIONS (NIST LP)
- [ ] NIST INTERAGENCY/INTERNAL REPORT (NISTIR)
- [ ] LETTER CIRCULAR
- [ ] BUILDING SCIENCE SERIES
- [ ] PRODUCT STANDARDS
- [X] OTHER NIST-GCR

PROPOSED FOR NON-NIST PUBLICATION (CITE FULLY) [ ] U.S. [ ] FOREIGN

PUBLISHING MEDIUM

- [X] PAPER
- [ ] CD-ROM
- [ ] DISKETTE (SPECIFY)
- [ ] OTHER (SPECIFY)

SUPPLEMENTARY NOTES

ABSTRACT (A 2000-CHARACTER OR LESS FACTUAL SUMMARY OF MOST SIGNIFICANT INFORMATION. IF DOCUMENT INCLUDES A SIGNIFICANT BIBLIOGRAPHY OR LITERATURE SURVEY, CITE IT HERE. SPELL OUT ACRONYMS ON FIRST REFERENCE.) (CONTINUE ON SEPARATE PAGE, IF NECESSARY.)

Ignition and burning rate data are developed for Nylon 6/6, Polyethylene, and Polypropylene in a Cone Calorimeter heating assembly. The objective is to examine a testing protocol that leads to the prediction of ignition and burning rate for thermoplastics from Cone data. The flame heat flux is not measured, but is inferred from Cone data. The constancy of the flame heat flux for thermoplastics in the Cone calorimeter is due to the geometry of the flame. The burning rate model is shown to yield good accuracy in comparison to measured transient values.

Ignition and burning rate data are developed for Redwood and Red Oak in a Cone Calorimeter heating assembly. Measurements of the flame plus external heat flux are presented. The data is intended to be used for future work to develop a testing protocol and burning rate model for charring materials.

KEY WORDS (MAXIMUM OF 9; 28 CHARACTERS AND SPACES EACH; SEPARATE WITH SEMICOLONS; ALPHABETIC ORDER; CAPITALIZE ONLY PROPER NAMES)

cone calorimeter; heat flux; nylon 6 (trademark); polyethylene; polypropylene; thermoplastics, wood.

AVAILABILITY

- [X] UNLIMITED
- [ ] FOR OFFICIAL DISTRIBUTION - DO NOT RELEASE TO NTIS
- [ ] ORDER FROM SUPERINTENDENT OF DOCUMENTS, U.S. GPO, WASHINGTON, DC 20402
- [X] ORDER FROM NTIS, SPRINGFIELD, VA 22161

NOTE TO AUTHOR(S): IF YOU DO NOT WISH THIS MANUSCRIPT ANNOUNCED BEFORE PUBLICATION, PLEASE CHECK HERE. [ ]

WORDPERFECT